The Pennsylvania State University

The Graduate School

REGULATION OF BRAIN IRON ACQUISITION AND MISAPPROPRIATION IN ALZHEIMER'S DISEASE

A Dissertation in

Biomedical Sciences and Clinical and Translational Sciences

by

Stephanie L. Baringer

Submitted in Partial Fulfillment
of the Requirements
for the Degree of

Doctor of Philosophy

December 2023

The dissertation of Stephanie Baringer was reviewed and approved by the following:

James R. Connor
Distinguished Professor of Neuroscience and Anatomy and Vice Chair for Research, Department of Neurosurgery
Dissertation Advisor
Chair of Committee

David J. DeGraff
Associate Professor, Department of Pathology and Laboratory Medicine

Xuemei Huang
Distinguished Professor of Neurology. Pharmacology, Neurosurgery, and Kinesiology

Yongsoo Kim
Associate Professor, Department of Neural and Behavioral Sciences

Elizabeth A. Proctor
Assistant Professor of Neurosurgery, Pharmacology, Biomedical Engineering, and Engineering Science & Mechanics

Lisa M. Shantz
Associate Professor, Department of Cellular and Molecular Physiology
Chair, Biomedical Sciences Graduate Program

ABSTRACT

Brain iron homeostasis is essential to proper neurological functioning, with high levels of brain iron being implicated as causative factors in neurodegenerative diseases and low levels leading to cognitive impairment and Restless Legs Syndrome. As such, uptake of iron in the brain is tightly regulated at the site of endothelial cells (ECs) of the blood-brain barrier (BBB). The working model is that as cells in the brain can signal their iron needs, based on their iron consumption, and control iron release from ECs in the form of apo (iron free)- and holo (iron bound)- transferrin (Tf). Our group has previously shown using *in vitro* models that apo-Tf indicates an iron deficient environment and stimulates iron release whereas holo-Tf indicates an iron saturated environment and suppresses iron release.

In Chapter 2, I determined if the delivery protein of iron or the sex of the organism could impact their regulatory mechanism by performing steady-state infusions of apo- and holo-Tf into the brain of male and female mice and then intraperitoneal injecting the mice with radioactive iron bound to Tf or H-ferritin, another iron delivery protein. I found that only iron delivered via Tf to the brain is influenced by brain side ratios of apo- and holo-Tf, while iron found to H-ferritin was not regulated by this mechanism. Additionally, I discovered a sex specific response to modulating the ratio of apo- and holo-Tf in the brain.

In Chapter 3, I investigated the molecular mechanism of apo- and holo-Tf's respective influence of iron release, and I found that holo-Tf incubation causes ubiquitination and subsequent degradation of ferroportin (Fpn), the only known iron exporter protein. Using orthogonal methods, I discovered that apo-Tf directly interacts with hephaestin, a ferroxidase that aims Fpn, and holo-Tf directly interacts with Fpn. Hepcidin is an inflammatory hormone peptide and long thought to be the primary iron release regulator. Thus, to understand how physiological and pathophysiological levels of hepcidin influence these protein-protein interactions, I

uncovered that only hepcidin levels consistent with disease interrupt the interaction between holo-Tf and Fpn, while no amount interrupts the interaction between apo-Tf and hephaestin. Furthermore, I found that the interaction disruption is due to hepcidin internalizing Fpn faster than holo-Tf. These data suggest that hepcidin may be deployed to abruptly stop iron release in systemic stress while holo-Tf is likely the primary regulator of iron release in homeostasis.

While numerous diseases display altered brain iron regulation, Alzheimer's disease (AD) exhibits excessive brain iron accumulation that can be used to predict cognitive decline. What's more, brain iron accumulation occurs early in the disease and prior to widespread amyloid-β (Aβ) deposition, suggesting an element of malfunction in the regulation of iron uptake. To explore iron release dysfunction is response to Aβ, in Chapter 4, I used induced pluripotent stem cell derived-ECs and astrocytes and I found that media collected from astrocytes exposed to low levels of Aβ stimulated iron release from ECs without damaging the cells. In response to low levels of Aβ, astrocytes increased their own iron uptake and mitochondrial activity, resulting in elevated levels of apo-Tf and iron deficient media. These data are the first to demonstrate how disease pathology can misappropriate iron release regulatory mechanisms and further disease dysfunction.

Taken together, the findings presented in this body of work aid in deciphering the important regulatory process of iron release from ECs of the BBB and present a novel interpretation of how the process can be misconstrued in disease. Furthermore, the findings shift the paradigm of conventional iron release regulation and suggest a novel mechanism in cells throughout the body.

TABLE OF CONTENTS

LIST OF FIGURES

ACKNOWLEDGEMENTS

To Dr. James Connor, thank you for being a phenomenal mentor; I am forever grateful to have joined your lab. Graduate students often grumble about their lab or PI, but I could only ever contribute, “Dr. Connor is a great and supportive guy.” You quickly saw my ambition to succeed and knew exactly the type of mentorship I needed. You stepped back to let me soar but were right there beside me when I stumbled and needed a helping hand. Thank you for cultivating an environment that has allowed me to flourish scientifically and personally. I cannot guarantee I am a more patient person than I was at the start of our journey together, but I can say that I am better at not making it everyone else’s problem. I would not be the scientist or communicator I am today had it not been for your guidance and leadership.

Thank you to all of the Connor lab members for laughing until we could barely breathe, commiserating over failed experiments, and answering all of my random questions that came out of nowhere. Specifically, Lisa Harman, I cannot tell you how much I apricated your constant defusing of my latest crisis. I truly could not have gotten a committee meeting scheduled, let along my defense, without your calendar wizardry. Becky, thank you for handling my manic ordering when every reagent I needed was backordered for 6+ months. Beth, thank you for being a fantastic lab manager and friend. I, of course, could never have manually perfused all of my radioactive mice alone, especially the one that tried to make a break for it! Beyond that, I could not have mentally survived over the years without our lunchtime chats. Any time I was stressed, distraught, or excited about lab, life, or dog agility scenarios, you were the first person I sought out. Thank you for handling every inconvenience, big and small, that I caused you over the years, including purchasing the espresso coffee maker within three months of me joining the lab – that was the best idea I have ever had. Palsa, thank you for your endless advice on experiments and broader scientific life. The new lab motto should be “Ask Palsa, he knows everything.” I would

have experienced a lot more self-inflicted failure had I not dropped into your office to chat about my latest hypothesis and experimental plan. My Ph.D. was more efficient and more fun with you around. Finally, a huge thank you to ProteinTech for saving my life more than once by producing the only working ubiquitinylated protein antibody on the market – I couldn't have finished my dissertation without you.

Thank you to my committee and other Penn State College of Medicine faculty for their support and pushing me to become a better scientist. Dr. David DeGraff, thank you for all of the "sorry for my ignorance, I just don't know" questions – they remind me to always explain the foundational information to an audience. Dr. Xuemei Huang, thank you for your infectious energy and boundless enthusiasm for both the science and the broader implications for patients. Dr. Yongsoo Kim, thank you for your tough but fair questions – they, without fail, always make me think more deeply about my data and my interruptions. Dr. Elizabeth Proctor, thank you for all of your thoughtful advice regarding both lab work and personal challenges. I always look forwarding to hearing your thoughts on my latest data and seeing your face in the crowd at my seminars. Dr. Ian Simpson, thank you for your meticulous feedback on all of my manuscripts, abstracts, and presentations. I know after a few rounds of edits with you, my work has explored all possibilities and is better for it. Dr. Ralph Keil, thank you for taking a chance on me by admitting me into the BMS program, even if I did have stellar mutual reference. I appreciate you always wanting what is best for me and all of the work you have done for my fellow graduate students. BMS will not be the same without you.

To my family back home in Ohio, thank you for your support in my unending pursuit of higher education. I know my drive takes me away from home, but I will always find my way back. Thank you to all of my friends that made Hershey home for four years. Specifically, thank you to Becca for always motivating me to be a better scientist and science communicator. You

are a valued colleague and friend, and I cannot wait to be your peer in the MSL world. To Gaelyn, thank you for being a great dog sitter and even better friend; it has been an amazing time exploring the vastness of Hershey with you…and then quickly exploring beyond Chocolate Town, USA when we ran out of things to do. Thank you to past and present Lions Talk Science editorial teams. It has been an honor to work with all of you for four years to disseminate science to the broader public. LTS has been one of my most constant joys during my time at PSCOM. Lastly, thank you to Katrina for being the greatest friend a blonde in the radiation room could have. I will always come visit you in Philly or wherever life takes both of us. You are a forever friend and I am forever grateful to have found you.

To Seth, thank you for always supporting my aspirations full-heartedly. Thank you for your patience and understanding that my journey has been anything but stress-free and supplying the emotional support and comfort food to get me through it. I cannot wait for our next adventure and I couldn't have asked for a better partner. Finally, to Atlas, my dream of giving you a yard is what keeps me going in my most difficult moments. Thank you for being everything I need in the exact moment I need it – furry cuddles when I am sad, trail runs when I am frustrated, and slobbery kisses when I am happy.

Funding: This work is supported by the National Institute on Neurological Disease and Stroke grant R01NS113912, National Institute on Aging grant R21AG064486, and National Center for Advancing Translational Sciences grant TL1TR002016.

Disclaimer: Findings and conclusions do not necessarily reflect the view of the above funding agencies

Chapter 1

Brain iron acquisition: An overview of homeostatic regulation and disease dysregulation

This work has been previously submitted as:

Baringer, S.L., Simpson, I.A., Connor, J.R. *Brain iron acquisition: An overview of homeostatic regulation and disease dysregulation*. Journal of Neurochemistry. (2023)

1.1 Abstract:

Brain iron homeostasis is crucial for neurological health, with pathological fluctuations in brain iron levels associated with a variety of neurological disorders. Low levels are connected to cognitive impairment and Restless Legs Syndrome, while high levels are connected to Alzheimer's disease, Parkinson's disease, and other neurodegenerative diseases. Given the detrimental effects unrestricted iron can have, regulated entry into the brain via transferrin and H-ferritin is critical. Endothelial cells of the blood-brain barrier are the site of iron transport regulation. The movement of iron through endothelial cells into the brain can be divided into three distinct processes: uptake, transcytosis, and release. Each process possesses external and internal influences to the regulation at each stage. This review will discuss the mechanisms of iron uptake, transcytosis, and release at the blood-brain barrier, as well as the elements that contribute to regulation. Additionally, we explore the dysregulation of brain iron in Alzheimer's disease, Parkinson's disease, and Restless Legs Syndrome.

1.2 Introduction

Iron plays an essential role in many important biological functions, including cognition and overall brain health. As an electron donator and acceptor, as well as a carrier of oxygen, iron is vital to the oxidation-reduction reactions that occur in cellular metabolism[1]. Furthermore, iron is utilized in the formation of myelin to insulate neuronal axons, which is crucial for proper signal transduction in the brain, and in the synthesis of many neurotransmitters, such as dopamine and norepinephrine[1]. As beneficial as iron is to the brain, a fluctuation in optimal iron levels can cause many neurological issues. Low levels of brain iron in adults are connected to Restless Legs Syndrome (RLS)[2,3], cognitive decline[4], and sleep disorders[5]. On the other hand, excessive iron in the brain is causatively linked to many neurodegenerative disorders[6], such as Parkinson's disease (PD)[7,8], amyotrophic lateral sclerosis[9], and Alzheimer's disease (AD)[10,11]. Thus, neurological health and proper functioning rely on the maintenance of iron homeostasis and requires tight regulation at the blood-brain barrier (BBB).

The BBB is the barrier that separates the vasculature from brain tissue and controls which molecules, ions, and nutrients are allowed to pass through to the brain[12], which calls for strict regulation to prevent the entry of toxic compounds. The first line of defense is endothelial cells (ECs) that encircle the blood vessels[12]. Next, are pericytes that are in close contact with ECs and aid in EC tight junction strength[12]. Lastly, astrocytes provide the signaling connection from the blood vessels to neurons[12] and vice versa. This interconnected network of cells allows for rapid cell to cell communication, allowing the brain to signal to the ECs to regulate BBB physiology and function[13], such as arteriole diameter[14], vascular blood flow rates[15], and iron transport[16].

The previous posited theory for brain iron uptake was that ECs served as passive conduits for iron, allowing it to flow through the ECs bound to transferrin (Tf) and be released into the brain. However, this theory did not consider the iron needs of the ECs nor did it acknowledge the

clear need for the brain to exert regulation. More recently, it has been demonstrated that apo (iron free)- and holo (iron loaded)-Tf have influence over the release of iron from ECs[16–20], and thus may be the source of brain iron uptake regulation the field has long ignored. Understanding the regulation of brain iron uptake has significant implications in the optimized harnessing of the brain iron uptake mechanisms for drug delivery and the treatment of iron uptake dysregulation in a variety of diseases. Here we will discuss the advancements in deciphering the regulation of brain iron uptake in homeostasis and its dysregulation in various neurological diseases (Figure 1-1).

Figure 1-1

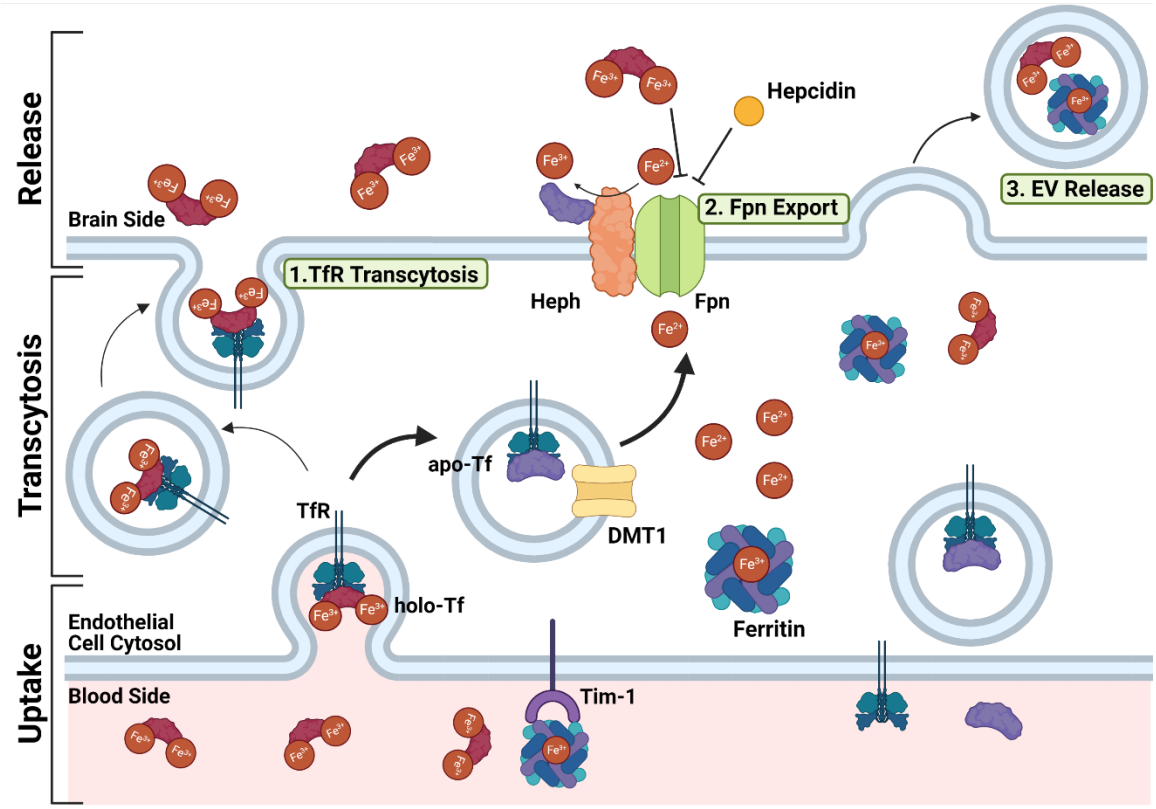

The process of brain iron acquisition can be split into three processes: uptake, transcytosis, and release. To start, holo (iron bound) – transferrin (Tf) binds to transferrin receptor (TfR) on the luminal membrane and is endocytosed. Once taken up into the endothelial cell (EC), the process of transcytosis can take two different routes. The first is **TfR transcytosis (1)**, in which the holo-

Tf and TfR complex are directly trancytosed to the abluminal membrane. Holo-Tf is then release into the extracellular fluid of the brain. Alternatively, the endocytosed TfR and holo-Tf can be sequestered in the EC. For this, within the endosome, the iron is reduced and detached from holo-Tf, resulting in apo (iron free) -Tf that is recycled back to the luminal membrane along with TfR. The intracellular iron can now be exported in two ways. In **ferroportin (Fpn) export (2)**, free intracellular ferrous (Fe2+) iron can be exported into the extracellular fluid through Fpn. Hephaestin (Heph) converts ferrous back to ferric (Fe3+), and apo-Tf binds the iron to become holo-Tf to be used by other cells. Fpn has a number of regulators, including hepcidin to control the release of free iron. In **extracellular vesicle (EV) release (3)**, iron can be bound to either Tf or H-ferritin (FTH1) and packaged for EV release to astrocytes. An exact proportion cannot yet be placed on each delivery pathway, but studies suggests that TfR transcytosis occurs scarcely compared to the other pathways of iron release. Figure made in Biorender.com.

1.3 Regulation in Homeostasis

1.3.1 Iron Uptake Processes

Brain iron uptake is largely mediated by Tf and the transferrin receptor (TfR). Circulating Tf is present in two forms: apo-Tf (iron free) and holo-Tf (iron bound). Differences in protein structure of apo- and holo-Tf[21] result in holo-Tf exclusively binding to TfR, whereas apo-Tf does not[22]. The overabundance of Tf in circulation makes the availability of TfR on the luminal membrane of ECs a key rate limiting step for brain iron uptake[23]. As such, intracellular iron levels regulate the translation of TfR protein via an iron response element and iron response protein, and equally important, other environmental conditions can regulate brain iron uptake. To this point, in

our *in vivo* studies, a intraventricular infusion of apo-Tf significantly increased the uptake of Tf-bound iron[17] by ECs, indicating that the iron status of brain transferrin in the extracellular fluid at the abluminal membrane of ECs can impact Tf-bound iron uptake from circulation.

In addition to Tf, H-ferritin (FTH1), which is typically considered an iron storage protein that binds much more iron than Tf[24], has also been shown to be a significant source of iron delivery to the brain[25–27] via the TIM-1 receptor and TfR[28,29]. Indeed, Chiou *et al*. reported that FTH1 is released as an iron delivery protein for ECs[18] and showed that basal apo- and holo-Tf affected the amount of FTH1-bound iron that was transported across the ECs in a similar manner as Tf-delivered iron[18]. However, our *in vivo* study found no change in FTH1 uptake when the levels of apo- and holo-Tf where manipulated via intraventricular infusion[17]. The differences between the results of these two studies is likely due to the complex dynamics of iron uptake *in vivo* including differences in signaling that regulates uptake of Tf and FTH1. Consistent with this notion is that other *in vivo* studies show that FTH1 broadly delivers iron to various organs regardless of iron status[25], suggesting that FTH1 uptake is not dependent on the same regulatory signals as Tf.

Because crossing the BBB presents such a challenge, drug studies have long focused on harnessing the TfR uptake pathway[30]. Work by Friden *et al.* was some of the first to show that TfR-targeted substances accumulate along brain capillaries and in the brain parenchyma[31–33]. However, the amount of a given TfR-targeted drug to accumulate in the brain typically does not surpass 1% of the injected dose[34]. This lack of accumulation is likely due to both the regulation of endogenous Tf-bound iron undergoes and the small amount of Tf transcytosis (see Transcytosis Mechanisms for details). Clinical findings of TfR-targeted biologics suggest that the admittedly small amounts of the drug that penetrates may be enough for functional changes in specific circumstances[35–38]. Additionally, drug developers are constantly modifying biologics to increase TfR affinity and brain penetrance[30].

1.3.1.1 Sex Contribution

Many processes in the brain that heavily rely on iron occur at different rates in males and females. Specifically, higher rates of myelin turnover[39], dopamine synthesis[40,41], and mitochondrial respiration[42] are reported in females and all are dependent on iron as a co-factor[43,44]. These observations would lead one to assume that females have higher brain iron content, however, numerous studies have shown that there is no difference in total brain iron content between males and females[45,46]. While iron content is not different, Duck *et al.* showed that five days after injecting mice with ^{59}Fe-Tf (radioactive iron bound to Tf), females display higher ^{59}Fe uptake into the brain than males[47]. This indicates that females meet their higher iron requirements by higher rates of uptake and presumably turnover than males. The constant utilization of iron for metabolic processes likely leads to an increased requirement of iron uptake into the brain. Our *in vivo* study supports this, where we found that, within 24 hours, brain iron uptake increased with apo-Tf infusions in males but not in females[17], potentially because the iron uptake signaling (apo-Tf) in females was already maximally elevated.

Aside from the contributions of metabolic differences between males and females, sex hormones could also impact the regulation of brain iron uptake[48–50]. Studies have identified estrogen response elements (ERE) on both hepcidin[51] and ferroportin (Fpn)[52]. The latter study found that treatment with 17β-estradiol reduced Fpn mRNA levels in various cancer cell lines[52]. The former study performed ovariectomies in mice and reported a decrease in serum iron levels and increase in hepcidin levels[51]. Similarly, Bajbouj *et al.* found that 17β-estradiol treatment of monocytes reduced hepcidin synthesis and increased iron release[53]. Shin *et al.* examined the influence of estrogen on brain iron and found that ferritin (a marker for total iron stores) and hepcidin were increased in aged female mice, and these levels were reduced when the mice were treated with 17β-estradiol[50], suggesting that estrogen decreases hepcidin. These results were

mirrored in neural cell cultures where 17β-estradiol upregulated Fpn[54,55]. Conversely, Ikeda *et al.* observed that ovariectomies in mice led to decreased hepcidin expression in hepatocytes and cells treated with 17β-estradiol had increased hepcidin expression[56]. Overall, the literature does not show a clear picture of how estrogen impacts the regulation of iron uptake. Most studies indicate that increases in estrogen lead to downregulation of hepcidin, and thus increases in Fpn and extracellular iron. Although the data are limited, they point in the direction that estrogen could be promoting iron export from the brain and supporting the notion of a more dynamic system in females for iron uptake and release.

1.3.1.2 Development and Aging Contributions

The development of the BBB requires the joint development of brain iron uptake mechanisms, and our laboratory and others have spent considerable effort on understanding the regulation of those mechanisms. In a study on the effects of dietary iron excess in rats, pups fed an iron loaded diet did not display increased brain iron content (unlike other organs)[57], suggesting that once the BBB is already formed by birth, so too is the ability to regulate iron uptake. Additionally, pups made iron deficient (ID) during prenatal development and then treated with dietary iron displayed lower brain iron content that was accompanied by behavioral and cognitive deficits compared to pups never made ID[58]. Pups made ID during postnatal development are more responsive to iron supplementation[59]. Clinical studies support that responsiveness of iron supplementation is dependent on the degree and timing of ID during development. Numerous studies show that infants born with ID but given iron-fortified diets by the age of 2-years-old recover the anticipated cognitive deficits[60]. However, the question remains: does prenatal ID change the formation of iron uptake regulatory signals or does ID change the brain's perception of it's on iron needs? Studies suggest the latter showing that a developmentally ID brain has

altered metabolic processes, including inefficient ATP production, altered neurotransmitter synthesis, particularly dopamine, and reduced myelin synthesis[61]. Limited availability of iron negatively impacts the establishment of these processes, resulting in long lasting consequences that then influence the regulation of iron uptake.

Even with regulation intact, the process of brain iron uptake differs during organism development. A number of studies in rodents have shown that the rate of transferrin-bound iron uptake increases rapidly from birth to postnatal day (PND) 15 and then decreases until a plateau at adulthood[26,62,63]. Interestingly, Chiou *et al.* found that ^{59}Fe-Tf uptake peaked at PND 14 yet ^{59}Fe-FTH1 uptake peaked later at PND 21, indicating the brain may rely on a differently regulated form of iron uptake during the later stages of brain development[26]. The rapid uptake of Tf-bound iron in early development corresponds to the physiological development of the BBB itself in rodents. Around PND 15 (equivalent to a 2-year-old human), the astrocytes start to make contact with the EC of the BBB in the developing brain and stimulate iron release[64]. After PND 15, the astrocytic end feet are fully developed and in communication with the ECs, resulting in tightening of the cell-to-cell tight junctions and reduction of iron efflux and reliance of regulatory signals to release iron[64].

The staging of iron uptake regulation is supported transcriptionally as well. Key iron regulatory proteins, such as Fpn, TfR, and divalent metal transporter (DMT1), are all differentially expressed at PNDs 7, 14, 21, and 70 in different brain tissue[26,65,66]. However, none of these studies examined the changes in iron regulatory proteins at the BBB. Interestingly, the iron status of the developing brain seems to have long lasting consequences to regulation. Many groups have shown that if rodent pups are made ID from birth, later iron replenishment cannot fully correct changes to iron regulatory proteins[59,67,68]. This suggests that the regulation of brain iron is solidified during development and lack of nutrient acquisition can have lasting impacts.

At the other end of an organism's lifespan, aging also can contribute to iron uptake regulation, or more accurately, its dysregulation. Brain iron accumulation is a sex-dependent hallmark of aging, with menopause and alterations to estrogen levels believed to be the main cause[69]. It remains unknown if dysregulation with age is due to an inability of the ECs to respond to regulatory signals, a dysfunction in regulatory signals, or BBB permeability. The ability of ECs to properly transport labeled serum proteins was examined and found that in an aged brain there is an increase in non-specific caveolar transcytosis[70]. Yang *et al.* also found that while EC TfR levels decreased, brain iron content was increased[70], further pointing to the dysregulation. A few different groups have explored the changes in hepcidin levels during aging and have found in mice that hepcidin levels increase and Fpn levels decrease with age[71,72], possibly due to increases of inflammation in the aging brain[73]. Lastly, a recent study examined BBB permeability in aged mice and found that brain iron content increases correlated with BBB permeability increases as measured by decreased tight junction protein levels[71]. Taken together, these studies suggest that brain iron uptake may be dysregulated through multiple means. Improper transport and neuroinflammation increase brain iron content, which damages the BBB and further exacerbates iron uptake dysregulation.

1.3.2 Iron Transcytosis Mechanisms

During routine Tf-bound iron transport at the BBB, holo-Tf binds to TfR on the luminal (blood-side) membrane of ECs, resulting in endocytosis of the complex[74]. In the endosome, the iron is released from Tf and subsequently reduced from ferric (Fe^{+3}) to ferrous (Fe^{+2}) by ferrireductases. The free iron is then transported into the cytosol by DMT1, a transmembrane protein[16]. The resulting apo-Tf and TfR within the EC endosome are recycled back to the luminal membrane, where the apo-Tf is released and the receptor is ready to bind to more holo-Tf and

start the process over again[16]. The free iron now within the EC can enter the labile iron pool to be used by the cell, stored within ferritin, a major iron storage protein, for future use, or transported out the EC via Fpn, the only known exporter of iron[75] to be utilized by the brain. Fpn is aided by hephaestin (Heph), a ferroxidase that converts Fe^{+2} back to Fe^{+3}, during iron efflux[76–78]. In the abluminal (brain-side) space, brain-produced apo-Tf will bind the exported Fe^{+3} molecules to carry iron to neural and glial cells in need of iron.

As an alternative to Fpn export, iron bound to Tf can be directly transcytosed from the luminal to the abluminal membrane. EM-immunocytochemistry on rat brain microvessels has shown the distribution of TfR on both membranes as well as the intracellular space[16]. Fishman *et al.* first demonstrated the transcytosis of Tf and TfR in rat microvessels using ^{125}I-Tf and saw the accumulation of Tf in both the microvessels and brain homogenate[79]. Importantly, twice the amount of ^{125}I-Tf accumulated in the microvessels than in the brain homogenate. This observation has been repeated by numerous groups[17,80,81]. TfR targeting antibodies injected intravenously have been shown to be deposited in the brain parenchyma, indicating they were trancytosed at the BBB, though at fairly low proportions of what was injected[30,82,83]. The kinetics of Tf-TfR transport have been modeled and experimentally found to be consistently lower than predicted[84]. Further complicating the process, studies have suggested that TfR transcytosis is regulated by intracellular tubules that can control the destination (degradation or exocytosis) of TfR and its cargo[85,86]. Collectively, these studies suggest that Tf can be directly transcytosed to deliver iron to the brain, however, this amount is minute compared to the amount recycled back to the blood.

An additional alternative to direct transport of Tf bound iron across ECs comes from recent reports of release of extracellular vesicles from ECs[87–89] and their ability to transport Tf and FTH1 bound iron[90]. While the release of these vesicles from ECs is regulated intracellularly by iron concentrations[90], it is unclear if there is additional regulatory signaling coming from the brain to control iron release. These findings add to the exciting prospect that the brain has

multiple mechanisms for iron transport across the BBB and knowing the proportion of iron delivered by each would be greatly beneficial to the field.

1.3.2.1 IRE/IRP System Contribution

Iron response elements (IRE) and iron response proteins (IRP) further regulate numerous proteins involved in the transcytosis of iron at the translational level in response to labile iron pool levels[91,92]. IREs are stem-loops in the untranslated region (UTR) of mRNAs. When intracellular iron levels are low, IRPs bind to these regions. In the presence of excess iron, the IRE binding site is blocked on IRP, preventing it from binding to the IRE. When an IRE is present on the 5'-UTR, as is the case with ferritin, IRP binding (low iron levels) blocks the translation of the protein. When an IRE is present on the 3'-UTR, as is the case with TfR, IRP binding stabilizes the transcript and increases translation of the protein. Fpn's transcript contains a 5'-IRE, in order to block translation in low intracellular iron conditions, however, groups have reported two isoforms of Fpn – 1a and 1b – with the latter found in duodenal cells of the intestine[93] and in whole brain tissue[94]. Fpn-1b lacks the 5'-IRE that is present in Fpn-1a, and thus avoids labile iron pool regulation. This absence of intracellular regulation emphasizes the need for extracellular regulation of Fpn in order to preserve homeostatic iron release. Overall, the presence of translational modification of iron transport proteins within ECs further demonstrates that iron undergoes a regulated release from the cells rather than simply passing through without regulation.

1.3.3 Iron Release Regulation

As the evidence grows suggesting that ECs are reservoirs for iron, it is important to specifically investigate the process of iron release. Our *in vivo* studies have shown that rates of iron uptake and release are correlated, but they differ in value, with iron uptake into the microvessels being significantly more than what is initially release into the brain parenchyma[17]. If TfR is the rate limiting step for iron uptake, Fpn, the only known iron exporter in all barriers, is the rate limiting step for free iron export. As such, regulation of iron release focuses on the regulation of Fpn protein presence on the abluminal membrane.

One source of iron release regulation may be apo- and holo-Tf (Figure 1-2). As cells, such as neurons or astrocytes, need iron, they endocytose holo-Tf[95]. Once in the cell, the iron is used and the resulting apo-Tf is exocytosed[95]. This concept suggests that cells in the brain are able to signal to the ECs of the BBB their iron needs based on their iron consumption. For example, Simpson *et al.* demonstrated that cerebrospinal fluid (CSF) from iron deficient monkeys and conditioned media from iron chelated astrocytes resulted in increased iron release from cultured bovine retinal ECs (BRECs), while iron loaded biological samples resulted in decreased iron release[16]. This model also provides an explanation for regional iron uptake differences, as demonstrated by a number of studies[67,96,97] – areas with higher iron needs have higher iron consumption.

This apo- and holo-Tf regulation hypothesis is supported by a number of studies. Simpson *et al.* replicated their conditioned media results by directly exposing ECs to apo- and holo-Tf, and this increased and decreased iron release respectively[16]. Duck *et al.* expanded on these findings and demonstrated that the increase of iron release from ECs due to apo-Tf was independent of hepcidin[98]. These studies were further supported and extended by Chiou *et al.* who demonstrated differences in the release of protein-bound iron and free iron from induced

pluripotent stem cell (iPSC) derived-ECs in response to apo- and holo-Tf[18]. More recently, we have shown via intraventricular infusion *in vivo* that apo-Tf significantly increased brain iron levels[17], suggesting more iron was released from the ECs.

Figure 1-2

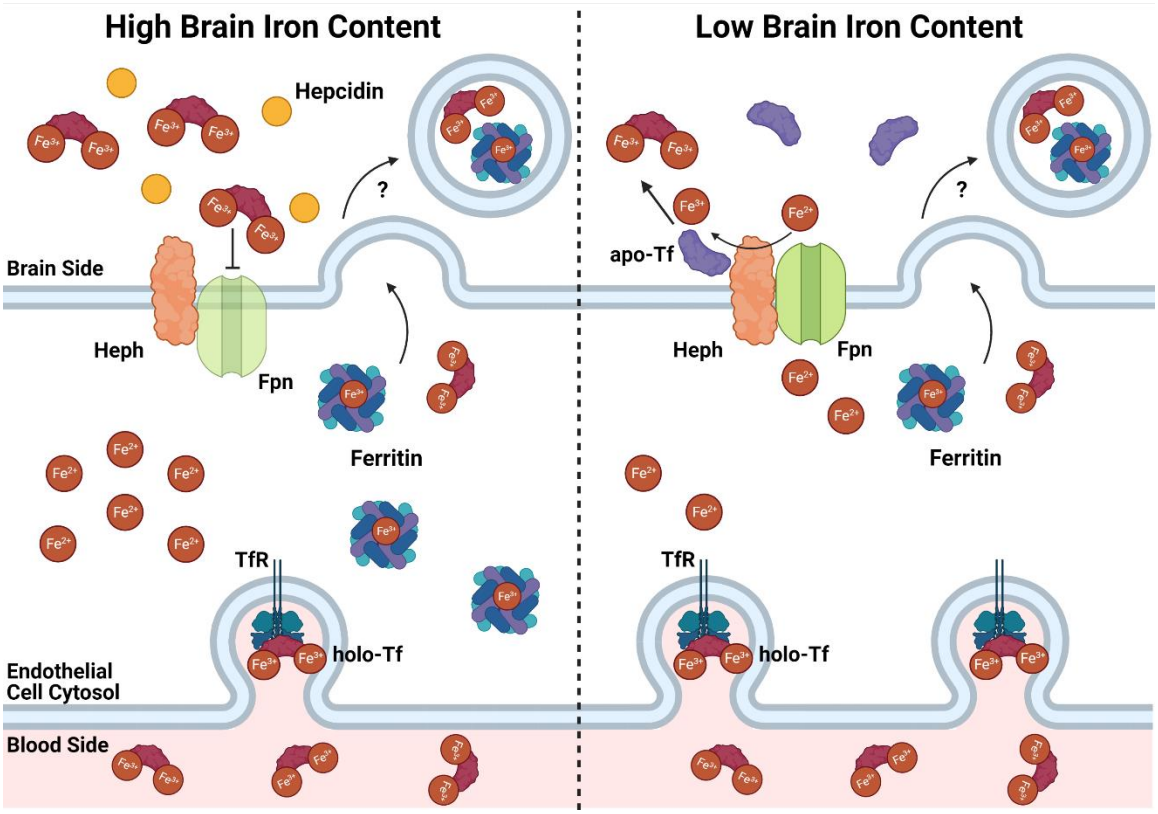

Brain iron status is the driving force of iron release regulation. **When brain iron content is high**, excess brain-derived holo (iron bound) -transferrin (Tf) suppresses iron release by decreasing ferroportin (Fpn) levels. If brain iron levels reach a pathological threshold, hepcidin production is upregulated and can rapidly reduce endothelial cell Fpn levels to halt free iron release. **When brain iron content is low**, excess brain-derived apo (iron free) -Tf stimulates iron release possibly by increasing hephaestin (Heph) activity and promotion of Fpn membrane stability. Intracellular iron levels impact extracellular vesicle (EV) release, however, it is not yet known the regulatory effects brain iron status has on EV release. It can be expected that the iron content of

the endothelial cells have some influence on release of iron into the brain although we postulate that signals from the cells within the brain are the driving force. Figure made in Biorender.com.

Having observed the functional effects of apo- and holo-Tf on iron release, the mechanism by which this is achieved has not been resolved. It has been suggested that apo-Tf modulates iron release through protein interactions with ceruloplasmin (Cp) and Heph. Both Cp and Heph are homologous ferroxidases that aid Fpn in the export of iron from cells, with Heph most commonly found in barrier cells such as ECs[78]. On the other hand, Cp is in a glycosylphosphatidylinositol-anchored form present in astrocytes[99] but still vital to brain iron acquisition[100]. It has been implicated in the stimulation of iron release from ECs[101,102]. Whether Cp is also found in extracellular fluid is not clear. Ha-Duong *et al.* demonstrated using fluorescence emission spectroscopy and cell-free recombinant protein that apo- and holo-Tf interact with Cp, though in slightly different ways[103]. The same research group expanded on these findings and showed that Tf binds to oxidized Fe^{+3} and is then transferred to a different binding site as holo-Tf[104]. However, Hudson *et al*. found no stable interaction between Tf and Cp or Heph using native polyacrylamide gel electrophoresis and surface plasmon resonance[105]. Sokolov *et al.* attempted to shed light on discrepancies in the literature regarding Tf and Cp binding and found that an interaction appeared to be present, though not stable at physiological concentrations[106]. Further contradicting previous studies, Sakajiri *et al.* used a variety of biological methods and computational modeling to show that apo-Tf and Cp did bind at physiological levels and zinc mediated this interaction[107].

A parallel mechanism of iron release regulation seen in the brain may be present in the intestine. The enterocytes of the intestine present a barrier for molecules to cross and iron status of crypt cells can influence iron accumulation[108]. Furthermore, enterocytes are similarly polarized, as ECs are, with Fpn exclusively expressed on the abluminal membrane[109]. Alvarez-

Hernandez *et al*. cultured Caco-2 intestinal cells in bicameral chambers to examine iron transport and discovered that apo-Tf stimulated the release of iron at very low concentrations, with a K_m of 0.078 μM[110,111]. Another study replicated these data in Caco-2 cells and found that basal apo-Tf stimulated ^{59}Fe release from prelabeled cells at a rate double than the control[112]. Taken together, these studies suggest that the regulatory mechanism for iron uptake may be the same in both ECs and enterocytes and urge the larger iron biology field to reexamine the hepcidin regulatory dogma.

1.3.3.1 Hepcidin Contribution

Hepcidin, a pro-inflammatory hormone peptide secreted by the liver, has long been the primary focus of Fpn regulation and cellular iron export (Figure 1-3). The majority of systemic hepcidin is produced by hepatocytes of the liver[113]; however, hepcidin is also expressed in astrocytes[114,115] and the choroid plexus[116,117], though in much smaller amounts[117,118]. Hepcidin was discovered in 2000 independently by a number of groups[119], however, the role hepcidin played in iron regulation was not identified until years later. Nemeth *et al.* found that hepcidin induced the internalization and subsequent degradation of Fpn *in vitro*[120]. In line with these data, functional studies in HEK293 cells showed a decrease in iron export when exposed to hepcidin[120]. Both Nemeth *et al.* and others have shown that hepcidin exerts this influence by binding directly to Fpn[120–122]. Later studies demonstrated that hepcidin results in the ubiquitination of Fpn, tagging it for endocytosis and lysosomal degradation[75]. Furthermore, the inhibition of ubiquitination prevents this process[123]. The ubiquitination of Fpn occurs within 10 minutes of hepcidin exposure[123] and internalization follows shortly within 30 minutes[124].

The effects of hepcidin on iron release at the BBB has received less direct investigation. McCarthy and Kosman used two cell lines, human brain microvascular endothelial cells

(hBMVEC) and C6 glioma astrocytes, to model the BBB *in vitro*[101] and found that exogenous hepcidin and co-culture with astrocyte both resulted in the internalization of EC Fpn[101]. Blocking of Fpn internalization by the compound fursultiamine increased iron release from ECs[101]. As previously mentioned, Simpson *et al.* replicated the findings that hepcidin reduces both Fpn protein levels and iron release in BRECs but also found that holo-Tf basal incubation had a similar result[16]. Chiou *et al.* added by using iPSC-derived ECs to illustrate hepcidin decreased the release of free ^{59}Fe but had no impact on Tf-bound ^{59}Fe transport[18]. *In vivo* studies that examined how astrocytic hepcidin impacted brain iron uptake by using hepcidin knockdown and overexpression mice found that a lack of hepcidin leads to iron accumulation and increased Fpn protein levels in the brain parenchyma[125].

Given the important task of regulating membrane-bound Fpn, and thus iron export, hepcidin levels must also participate in a system of checks and balances. Hepcidin has two primary regulators: iron levels and inflammation. Primary hepatocytes increase hepcidin mRNA and circulating hepcidin in the blood increases proportionally to Tf saturation when animals are fed a high iron diet[126]. This iron sensing regulation is mediated through the BMP pathway to stimulate hepcidin transcription[127], though the exact molecular interactions remain unknown. This mechanism allows the regulating cells (hepatocytes and possibly astrocytes) to sense extracellular iron levels and increase or decrease hepcidin production accordingly to ensure optimal iron transport at barriers, such as enterocytes and the BBB. Inflammation is another regulator of hepcidin production. Infections often correlate with increased circulating hepcidin[128]. In humans injected with IL-6, blood levels of hepcidin significantly increased[129], suggesting that pro-inflammatory signals are responsible for increased hepcidin levels. In both hepatocytes and astrocytes, inflammatory stimuli increase hepcidin production and secretion[130]. Specifically, this upregulation is mediated by the IL-6/STAT3 pathway[131]. This regulation by inflammation is likely a defense mechanism to subject pathogens to hypoferremia conditions to prevent survival.

Figure 1-3

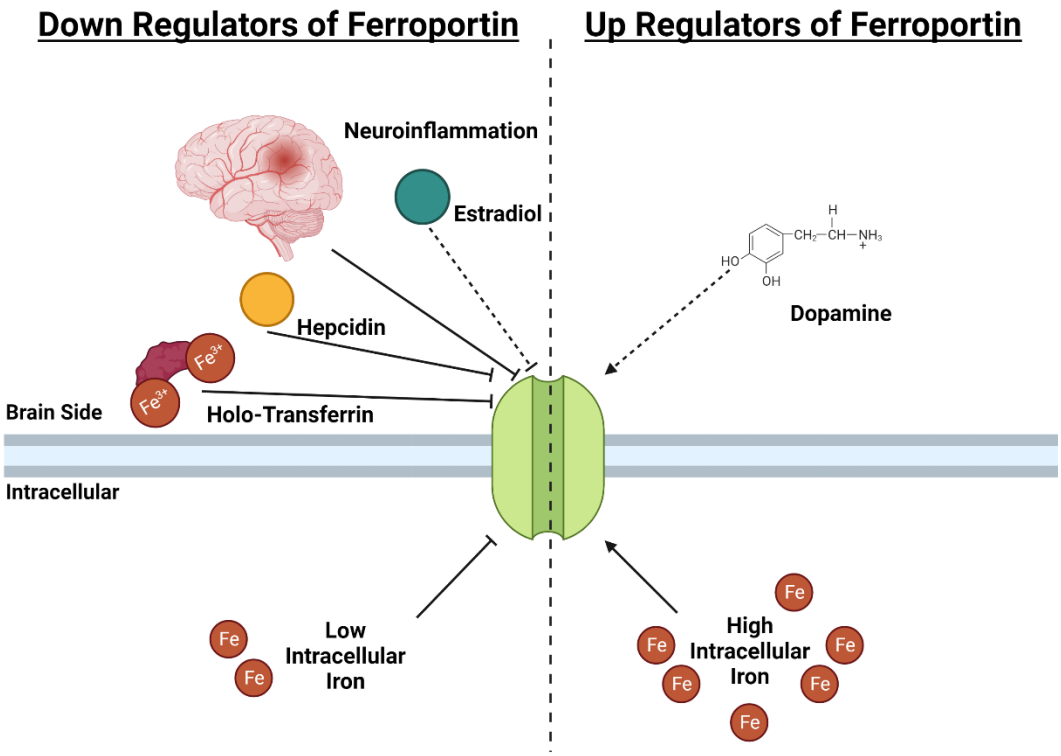

Ferroportin (Fpn) has numerous up- and down-regulators in an effort to control iron release from endothelial cells (ECs). The 5'- iron response element (IRE) present the Fpn transcript dictates that low intracellular iron levels downregulate Fpn translation in an effort to conserve iron stores. Conversely, high intracellular iron levels upregulate Fpn translation in order to remove excess iron from the cell. From the brain, there are a number of extracellular factors that down regulate Fpn on the EC membrane. These include holo (iron bound) – transferrin (Tf) and hepcidin, which is upregulated due to high extracellular iron levels and neuroinflammation. While less concrete, estradiol may also downregulate Fpn levels. In terms of extracellular upregulators, dopamine has been suggested to increase Fpn levels, though it too is not solidified. Figure made in Biorender.com.

The nuances in the literature about hepcidin's role in iron release regulation at the BBB suggest there may be another factor involved. Enculescu *et al.* designed a mathematical model to simulate iron content in various conditions ranging from dietary changes, inflammatory states, and genetic manipulations[132]. When comparing experimental results to the model, the study found that while hepcidin control over iron uptake was essential, it was not sufficient to explain the results[132]. It was only after the researchers included a secondary mechanism were they able to model their observed data[132]. Furthermore, recent work from our group shows that exosomal iron release is independent of hepcidin[90]. Overall, the literature suggests that hepcidin may play an integral role in iron uptake during a systemic emergency, such as iron overload or inflammation, in which a rapid reduction of Fpn is needed.

1.4 Dysregulation in Disease

The dysregulation of brain iron uptake- both excessive and inadequate- is a key pathology in numerous diseases. Here we examine potential causes and manifestations of this dysregulation, as well as treatment strategies, in three of the more prominent examples: Alzheimer's disease, Parkinson's disease, and Restless Legs Syndrome.

1.4.1 Alzheimer's disease

Alzheimer's disease (AD) is the most common form of dementia. Pathologically, AD is characterized by amyloid-β (Aβ) plaques and neurofibrillary tau tangles (NFTs); however, increasing evidence shows that brain iron accumulation is an emerging hallmark of AD[10,11] that occurs prior to the widespread formation of Aβ plaques and NFTs[133], as well as clinical symptoms in the form of cognitive decline and memory loss[10]. Various MRI studies have

identified iron accumulation patterns in AD that can even differentiate between early- and late-onset AD[134–136].

AD exemplifies the link between brain iron and degenerative pathology, where pathology contributes to iron accumulation which in turn exacerbates pathology. Translation of amyloid precursor protein (APP), the precursor to Aβ, increases in the presence of iron[137]. This increase in translation is due to the presence of a 5'-iron responsive element (IRE) in the mRNA 5'-untranslated region of APP[138] and iron regulatory protein 1 (IRP1) exerting control on APP translation[139]. IRP1 normally binds to the 5'-IRE of a given gene mRNA and blocks its translation; however, in a high iron environment, iron binds to IRP1, preventing it from inhibiting 5'- IREs, thus increasing the expression of the 5'-IRE containing gene. The increase in APP translation provides the opportunity for β-secretase to cleave APP more frequently, resulting in Aβ peptide formation. Additionally, iron aids in the formation of Aβ plaques by participating in reduction reactions that lead to Fe^{+2} directly interacting with Aβ peptides, resulting in the peptides forming a complex around the iron molecules in the core of the plaques[140]. The relationship between iron and Aβ plaque formation is supported by *in vivo* studies showing strong co-localization of iron and Aβ plaques in mice[141,142] and patients[143,144]. While the association between iron and disease status is established, the mechanism of iron accumulation in AD remains unknown.

The excessive iron accumulation seen in AD can most likely be attributed to dysfunctions at the BBB, which has been well characterized in AD[145,146] and has recently been shown to be an early biomarker of the disease that can predict cognitive decline in patients[147]. High concentrations of Aβ peptides reduce EC viability and overall BBB integrity *in vitro*[148] and can infiltrate and damage the brain blood vessels[149]. This can lead to cerebral amyloid angiopathy (CAA), which is present in 90% of AD patients and often results in stroke or bleeding[149].

Neuroinflammation, another hallmark pathology of AD[150], may play a role in iron uptake dysregulation. Cytokines released from activated microglia and astrocytes decrease the integrity of the BBB[151–153]. Furthermore, inflammation is connected to increased iron accumulation in neurons, astrocytes, and microglia *in vitro*[130] and *in vivo*[154]. Activation of astrocytes and the release of inflammatory cytokines in response to Aβ exposure has been demonstrated with both *in vitro*[155] and *in vivo* models[156]. Given the close signaling coordination between astrocytes and ECs at the BBB[14,15], the increased release of cytokines has the fastest opportunity to give rise to BBB dysfunction[157]. De Vries *et al.* demonstrated that both IL-6 and TNF-α, both elevated in AD patients[158], reduce EC monolayer integrity by about 60%, as measured by trans epithelial electrical resistance (TEER), in rat cerebral ECs; TEER reduction was then prevented with treatment of indomethacin, a cyclooxygenase (COX) inhibitor[151].

However, the release of cytokines does not only reduce BBB integrity. Zhang *et al.* found that brain ECs isolated from mice that were intracranially injected with $A\beta_{25\text{-}35}$, displayed increased Fpn and TfR expression, indicative of increased iron release into the brain[159]. Similar results were obtained when neural cells were exposed to inflammatory stimuli in culture[130]. These combined data indicate that inflammatory cytokines may contribute to increased iron accumulation in the brain by both impairing BBB integrity and modulating the expression of key iron regulatory proteins. Both dysregulations would lead to increased iron release by the ECs of the BBB into the brain, resulting in iron accumulation.

Dysregulation of iron creates a vicious cycle of Aβ pathology and iron accumulation in AD. A number of therapies have attempted to neutralize the excessive iron in the brain through iron chelators. Clioquinol prevented amyloid deposition in the brain of Tg2576 transgenic mice[160] and was tested in a Phase 2 clinical trial in 2003. PBT2 improved synaptic spine density and protein levels, indicating improve synaptic health, in Tg2576 transgenic mice[161]. However, a 2007 clinical trial of PBT2 reported no change in cognitive decline despite reduced $A\beta_{42}$ levels in

CSF[162]. Deferiprone lessened Aβ deposition and mitigated cognitive impairment in rats treated with scopolamine[163] and reduced iron and aggregated tau in P301L tau transgenic mice[164]. A Phase 2 trial for deferiprone was initiated in 2018. While none of the mentioned therapeutics to remove excessive iron have proven successful in mitigating cognitive impairment thus far, the argument can be made that these attempts to curb iron accumulation are too late. Recent findings show that iron accumulation manifests prior to widespread pathology[10,133], which spreads long before cognitive symptoms begin. Further investigation of how iron transport is dysregulated in early AD may be the key to targeting iron accumulation pathology in the disease.

1.4.2 Parkinson's disease

Parkinson's disease (PD) is the second most common neurodegenerative disease that affects those over the age of 65. Clinical symptoms of PD include motor dysfunction and bradykinesia, as well as cognitive decline and dementia in later stages[165]. Pathologically, PD is characterized by 1) the loss of dopaminergic neurons in the substantia nigra (SN) pars compacta (SNpc), the region of the brain that controls bodily movement, and early loss of noradrenergic neurons that control alertness[166], 2) the accumulation of aggregates of the protein α-synuclein within inclusions termed Lewy bodies, and 3) excessive iron accumulation exclusively in the SN[165,167,168]. In fact, increased iron levels in the SN have been correlated with disease severity in both post-mortem studies[169] and MRI imaging studies[170] and can be at least in part attributed to an increase in iron uptake[171] rather than simple increased iron usage in processes such as dopamine synthesis or cellular metabolism.

There are many similarities between AD and PD iron pathology. The relationship between iron and Aβ mirrors the relationship between iron and α-synuclein. The α-synuclein transcript contains an IRE[172], indicating that increased iron content in cells will lead to increased

translation of the protein. Furthermore, α-synuclein deposits has been shown to lead to increased neuroinflammation[173]. Neuromelanin within the SN has been shown to bind iron similarly to Aβ[174,175]. Many have reported alterations in iron regulatory proteins in PD, indicating dysregulation of iron metabolism and transport. Ayton *et al.* found that the SN of PD patients contains nearly 35% less Tf than healthy controls[176], and Loeffler *et al.* observed a lower Tf to iron ratio in PD patients, indicating a disrupted mobilization capacity of iron[177]. Others have reported that early PD patients actually have less iron in the SN[178], suggesting that PD may start as an issue of brain iron deficiency that facilitates disease progression. This is further supported by the recent clinical trial data that deferiprone, an iron chelator, worsened symptoms in early PD patients[179]. However, it remains unclear if iron dysregulation is a secondary or primary pathological disturbance in PD and what could cause the later accumulation seen as the disease progresses.

Unlike AD, PD exhibits increased cell death of dopaminergic (DAergic) neurons in the SNpc, leading to a reduction of dopamine (DA) and PD's unique motor deficits. The relationship between iron and DA is an active area of research but can be summarized in one word: toxic[180–182]. Santiago *et al.* perfused combinations of DA and iron into the brain of rats and only saw a neurotoxic effect to the DAergic system when the two were co-perfused[183]. The study also found that while the number of DA transporters (DAT) was unchanged, DA uptake was decreased[183]. DA may even facilitate this destructive effect. It has been shown in macrophages[184] and in astrocytes[185] that DA promotes iron uptake. Dichtl *et al.* found that treatment of DA increased free iron uptake, but not Tf-bound iron uptake[184]. The study also discovered that DA increased both the transcription and translation of key iron transport proteins: TfR and Fpn[184].

BBB breakdown in PD has been characterized in a number of studies[186,187]. Fujita *et al.* specifically examined BBB permeability in PD patients with a special focus on whether the patient had dyskinesia[187]. Dyskinesia is an extremely common side effect of long term treatment

with levodopa (L-DOPA), a DA precursor that crosses the BBB and is used to replenish DA in the brain. Using rubidium-82 and PET imaging, the group demonstrated that BBB permeability was unchanged between PD patients with or without dyskinesia[187]. However, another study found that PD patients with dyskinesia had higher iron levels in the SN using quantitative susceptibility mapping (QSM) MRI imaging[188]. These studies suggest that the elevated iron levels in PD patients with dyskinesia, following L-DOPA use, may be due to a mechanistic dysregulation of brain iron uptake instead of BBB leakage.

The question of L-DOPA's influence on iron uptake in living early PD patients was explored by Du *et al.* using QSM MRI in PD-drug treated and PD-drug naïve patients[178]. The researchers found that PD-drug treated patients had higher iron levels in the SN compared to the PD-drug naïve, L-DOPA use was positively correlated with iron levels in a regression analysis, and drug use duration was a significant contributor to iron levels[178]. Interestingly, PD-drug naïve patients had lower iron levels in the SN compared to controls, suggesting that low iron levels are a risk factor for a pathology cascade that results in increased iron accumulation[178]. It is possible that L-DOPA traffics iron across the BBB, leading to increased iron uptake[171] and accumulation[169]. A number of D2 and D4 antagonists have been shown to facilitate an increase in iron transport at the BBB[189], and DA itself can complex with Fe^{+3} at physiological pH[190]. Alhassen *et al.* mirror these data and discovered that, at concentrations even lower than treatment peaks, L-DOPA binds to Fe^{+3} and then forms a stable complex with siderocalin, an iron chelating protein[191]. These data suggest that it is possible for L-DOPA to carry iron across the BBB and this could explain the patterns of iron accumulation and subsequent symptoms in PD patients before and after modern day medical intervention.

Taken together, a new hypothesis for the contribution of iron dysregulation in PD can be presented that suggests PD starts as iron deficiency in the SN that promotes dysfunction in the highly iron dependent DAergic systems. The treatment of L-DOPA to combat the loss of DA

facilitates excessive brain iron uptake. The co-increase of DA and iron lead to toxic effects on neurons and glia that further contribute to the dysregulation of brain iron uptake and worsening of motor symptoms, including dyskinesia. Furthermore, excess iron propagates α-synuclein and BBB breakdown in a vicious cycle. The most common treatment for PD may enable disease progression. Conformation of these hypotheses could dramatically improve the treatment regimen for those suffering from PD.

1.4.3 Restless Legs Syndrome

Restless legs syndrome (RLS) is a chronic sensorimotor neurological disorder with notable primary pathologies of inadequate brain iron levels and DA dysfunction[44], as first described by Nordlander[192]. Clinically, RLS patients display an unrelenting urge to move their legs, particularly at night and thus disrupting sleep. RLS affects approximately 9.8% of the population, with women accounting for roughly two-thirds of all RLS patients[193]. The exact pathological mechanisms at play are poorly understood, however, the improvement of RLS symptoms in response to iron supplementation and DA agonists points to dysregulation in these two processes[194].

Approximately 31% of those suffering from iron deficiency (ID) develop RLS, however, it is not uncommon for RLS patients to have normal iron but low serum ferritin levels[44]. Studies have shown that while RLS patients are frequently clinically ID, it is not a requirement for the symptoms to develop. In a cross-sectional study, Berger *et al.* found that serum iron measures, including ferritin levels, Tf levels, transferrin saturation percentage, and transferrin iron binding capacity, were no different between RLS patients and healthy controls[193]. Regardless of peripheral iron status, brain iron levels have been consistently reported as low in RLS patients[195]. MRI studies have shown decreased iron in the SN and putamen of RLS patients compared to

control, and this decease of iron was proportional to the severity of the RLS symptoms[196]. These findings suggest that the brain ID in RLS is not due to peripheral ID but instead may be a dysfunction in the regulation of iron uptake at the BBB.

The precise cause of low levels of brain iron in RLS remains largely unknown. Numerous post mortem studies have shown changes in iron regulatory proteins in the brain that are consistent with low iron availability[2,197,198]. In line with these findings, Connor *et al.* proposed the hypothesis that RLS is a disorder of dysfunction of iron acquisition by the brain and investigated if mutations in iron regulatory pathway genes contributed to increased risk of developing RLS, however, they found no such risk mutations[199]. The same group isolated ECs from RLS brains post mortem and found they had decreased levels of FTH1, Tf, and TfR and no change in Fpn levels[197], and these results were replicated in whole brain tissue[2]. However, when ECs were exposed to RLS CSF to determine if the CSF of RLS patients contained different iron release signals from the brain, there was no change in iron transport compared to control[200]. Currently used models may not be able to replicate the complex miscommunication of iron dysregulation in this disease. Taken together, these data support that RLS is associated with decreased brain iron uptake and the decrease begins at the regulation in the BBB.

RLS patients who also have ID are often treated with IV iron treatments which can prove to be beneficial[201]. However, these IV iron formulation do not cross the BBB to directly supplement the inadequate iron in the brain[202]. Instead, the benefit is likely due to the IV iron going to macrophages that convert the iron to a formulation that can be delivered to the brain. This is supported by a meta-analysis of pharmacological treatments for RLS that found that iron supplementation was only effective in RLS patients with peripheral ID[194]. Even the benefits seen in ID RLS patients are moderate and this is expected because both IV iron formulations and circulating iron are subject to the same regulation at the BBB. Thus, if iron uptake is dysregulated on the brain side, iron supplementation can only help to a certain point. Given the evidence that

L-DOPA could increase iron uptake in PD, it would be of interest to further investigate if combined treatment of L-DOPA and iron supplementation could increase brain iron levels, and thus reduce clinical, symptoms of RLS. Although current clinical data suggest that L-DOPA treatment of RLS patients is problematic.

1.5 Conclusions

The regulation of brain iron uptake is clearly essential for proper brain functioning. This is evident by the havoc dysregulation, whether it be in timeliness of delivery or amount, can bring to neurological health. Excessive iron accumulation is intricately connected to neurodegenerative diseases, such as AD and PD[165]. On a microscale, high levels of intracellular iron can result in oxidative stress, damage to the plasma membrane, and ferroptosis cell death[203]. Brain iron deficiency can lead to impaired cognitive functions in children and disorders such as RLS in adults[204]. The effects of cellular iron deficiency vary based on the cell type but overall result in reduced functioning.

Due to the numerous complications that arise when brain iron is dysregulated, it is crucial to thoroughly understand how iron uptake is regulated. Hepcidin has long thought to be the ultimate regulator of iron release from ECs of the BBB, but there are some concerns with the hypothesis that should be considered. First, such regulation would be inherently inefficient as hepcidin is a pro-inflammatory hormone peptide that is upregulated in times of inflammation and high iron levels. This broad response does not account for the regional differences in brain iron uptake nor does it explain regulation in times of adequate iron levels. Our recent studies have made a case for apo- and holo-Tf as regulators of iron release from the ECs locally. Apo- and holo-Tf regulation allows cells to communicate their iron needs based on their iron consumption to ECs of the BBB. Iron depleted regions, where apo-Tf would be elevated, would be able to

locally increase iron release and fulfil the iron requirements. However, many questions remain regarding the potential of sex and age differences, mechanistic interactions, the interplay with hepcidin, and the precise dysregulation in various diseases.

A thorough grasp of this regulatory feedback loop has great clinical implications. By better understanding how brain iron uptake is regulated in homeostasis, the mechanisms of dysregulation in numerous diseases can be teased out, leading to targeted therapeutics to address brain iron status and its role in disease progressions. Numerous pharmaceutical companies are currently attempting to harness the Tf-TfR uptake pathway to deliver agents into the brain. However, if the mechanism of brain iron uptake is dysregulated in a particular disease, attempts to use the iron uptake pathway for drug delivery may face additional challenges beyond the normal regulatory mechanisms. Advances in studying the regulation of both the Tf and FTH1 pathways will lead to optimized and more effective delivery strategies, as well as overall brain health.

Chapter 2

Regulation of brain iron uptake by apo- and holo-transferrin is dependent on sex and delivery protein

This work has been previously submitted as:

Baringer, S.L., Neely, E.B., Palsa, K., Simpson, I.A., Connor, J.R. *Regulation of brain iron uptake by apo- and holo-transferrin is dependent on sex and delivery protein*. Fluids and Barriers of the CNS. (2022)

2.1 Abstract:

The brain requires iron for a number of processes, including energy production. Inadequate or excessive amounts of iron can be detrimental and lead to a number of neurological disorders. As such, regulation of brain iron uptake is required for proper functioning. Understanding both the movement of iron into the brain and how this process is regulated is crucial to both address dysfunctions with brain iron uptake in disease and successfully use the transferrin receptor uptake system for drug delivery. Using *in vivo* steady state infusions of apo- and holo-transferrin into the lateral ventricle, we demonstrate the regulatory effects of brain apo- and holo-transferrin ratios on the delivery of radioactive ^{55}Fe bound to transferrin or H-ferritin in male and female mice. In discovering sex differences in the response to apo and holo Tf infusions, ovariectomies were performed on female mice to interrogate the influence of circulating estrogen on regulation of iron uptake. Our model reveals that both sex and type of iron delivery protein have significant effects on the regulation of iron uptake into the microvasculature and subsequent release into the brain. Furthermore, we show that cells of the microvasculature act

as significant reservoirs of iron and release the iron in response to cues from the interstitial fluid of the brain. These findings extend our previous work to demonstrate that the regulation of brain iron uptake is influenced by both the mode in which iron is delivered and sex. These findings further emphasize the role of the microvasculature in regulating brain iron uptake and the importance of cues regarding iron status in the extracellular fluid.

2.2 Background:

Due to iron's important role in neurological health, through its utilization in cellular metabolism, myelination, and neurotransmitter synthesis, there is a clear need for strict regulation of brain iron uptake at the blood-brain barrier (BBB). Previously it was posited that endothelial cells (ECs) of the BBB, which make up approximately 2% of the brain[205], passively transport iron from blood to brain. The premise was that holo-transferrin (Tf) (iron rich) bound to its receptor, on the luminal membrane and was transcytosed to the abluminal space. However, this model did not consider the iron needs of the ECs nor did it acknowledge the clear need for regulation of iron access to the brain.

Our laboratory and others have since demonstrated regulation of iron uptake by ECs[16,18,20,62,64,98]. Specifically, our group has shown that apo-Tf (iron poor) in the basal space increases both iron transport and release from ECs *in vitro*[18]. Furthermore, H-ferritin (Fth1), which has gained increasing interest as an iron delivery protein[25–27], has been shown to deliver iron to the brain and remains unaccounted for in the Tf transcytosis theory. Overall, Chiou *et al.* have suggested that iron uptake into the brain is regulated by ECs, which control uptake into the cells, storage of iron therein, and subsequent release into the brain[18].

While these studies shed light on how brain iron uptake is regulated on a cellular level by apo- and holo-Tf, they do not address if there is regulation of iron uptake *in vivo*. Particularly,

animal models allow us to determine the presence of sex differences, which have been shown to be prominent in brain iron acquisition[26,47,201], as well as the movement of iron from microvasculature into the brain parenchyma. Our primary hypothesis was that similar to previous work, apo-Tf would increase brain iron uptake, particularly when bound to Tf. Ultimately, the data presented herein serve to add physiological context to established data, decipher sex differences in the regulation of brain iron uptake, and track the movement of iron from ECs to the brain.

2.3 Methods:

2.3.1 Experimental Design

Mini osmotic pumps were inserted subcutaneously connected to a cannula inserted in the lateral ventricle (Figure 2-1). After 48 hours of infusion, animals were injected intraperitoneally with either ^{55}Fe-Tf or ^{55}Fe-Fth1. Twenty-four hours later, brains were harvested and separated into microvessel and brain parenchyma fractions. The tissue was then solubilized and counted using liquid scintillation counting. Researchers were blinded to infusion pump contents but not to injections.

Figure 2-1

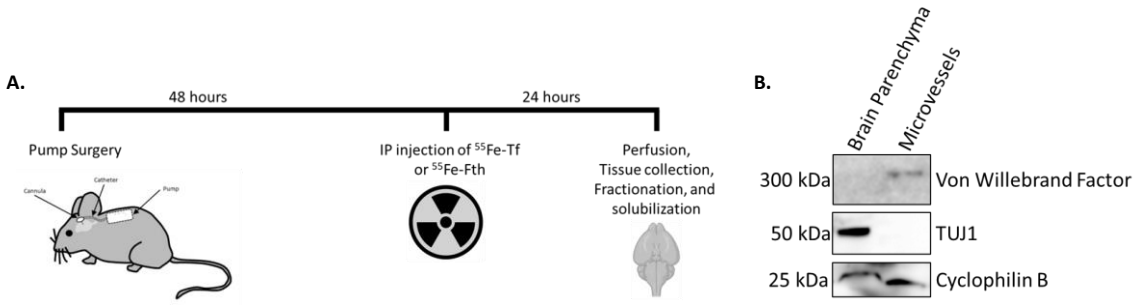

Experimental setup. Mini osmotic pumps were inserted subcutaneously in three-month-old male and female mice (**A**). Pumps contained nothing (sham), aCSF, 1 mg/ml apo-Tf, or 1 mg/ml holo-Tf. Forty-eight hours after the surgery, mice were injected IP with radioactive ^{55}Fe-Tf or ^{55}Fe-Fth1. Twenty-four hours later the mice were euthanized and perused. Brains were collected and homogenized. Microvessels (MV) were isolated from the brain parenchyma using centrifugation. Both fractions of MVs and brain parenchyma were further solubilized. Radioactivity in each fraction was determined using liquid scintillation counting. Western blotting was performed on brain parenchyma and MV fractions (**B**). The blots show von Willebrand factor, an endothelial cell specific marker, present in the MV fraction and not in the brain parenchyma fraction. TUJ1, a neuronal marker, is shown in the brain parenchyma fraction and not the MV fraction. Cyclophilin B was used as a loading control for samples.

2.3.2 Pump Surgery

Forty-eight hours prior to the surgery, osmotic pumps (infusion rate 0.25 µl/hour, Alzet, model 2004) were filled according to manufacturer instructions with nothing (sham), artificial cerebrospinal fluid (aCSF, 125 mM NaCl, 2.5 mM KCl, 1 mM MgCl-6H_2O, 1.25 mM NaH_2PO_4, 2 Mm CaCl-2H_2O, 25 Mm $NaHCO_3$, 25 mM glucose, pH 7.3), 1 mg/ml apo-Tf in aCSF, or 1 mg/ml holo-Tf in aCSF. Three-month-old wildtype (B6;129X1-Hfetm1Jrco/J background) mice were subjected to pump insertion under isoflurane anesthesia (1%-2%). A power analysis revealed n=5 was required for 80% at alpha 0.05. Briefly, the pump with attached tubing was placed subcutaneously and the cannula was placed 1 mm lateral to Bregma and 0.5 mm posterior to deliver the pump contents directly to the lateral ventricle. This placement was considered sufficient to influence iron uptake by the microvasculature given that the well-established

dynamic equilibrium of CSF and interstitial fluid, allowing the pump contents to distribute throughout the brain parenchyma[206]; similar to endogenous Tf produced by the choroid plexus[207]. The inclusion of aCSF as an experimental condition allows us to exclude the vehicle to be the cause of changes and informs us of general infusion effects and to determine any dilution effect of the endogenous Tf on the iron uptake. The incision was then sutured with nylon sutures. The mice were then placed in a heated recovery chamber until they regained consciousness, and accordingly, they were returned to their cages. Mice were maintained under normal housing conditions. They were given ad libitum access to rodent chow pellets and water. Both males and females were included in experiments. This study complies with the ARRIVE 2.0 guidelines. All procedures were conducted according to the NIH Guide for the Care and Use of Laboratory Animals and were approved by the Pennsylvania State University College of Medicine Institutional Animal Care and Use Committee.

2.3.3 Iron Protein Preparation

Wild-type human Fth1 containing a poly-His tag was subcloned into pET30a(+), to be produced in BL21 *Escherichia coli*[25]. Isopropyl-β-D-thio-galactoside (IPTG) was used to induce expression. Following this, bacteria were lysed, and Fth1 protein was purified on a nickel column using standard techniques (GE Healthcare Bio-Sciences). Transferrin was purchased commercially (Sigma).

2.3.4 Radiolabeling

^{55}Fe (Perkin Elmer) was complexed with 1 mM nitrilotriacetic acid (NTA), 6 mM ferric chloride ($FeCl_3$), and 0.5 M sodium bicarbonate ($NaHCO_3$) at a ratio of 100μL NTA: 6.7μL

$FeCl_3$: 23.3µL $NaHCO_3$: 50µCi $^{55}FeCl_3$ to form the ^{55}Fe-NTA complex[18]. After complexing, ^{55}Fe-NTA was incubated with apo-Tf (Sigma) or Fth1 for 30 minutes to allow for iron loading. Unbound iron was separated from the total complex using PD midiTrap-G25 columns following manufacturer's instructions (GE Healthcare Bio-Sciences).

2.3.5 Uptake Studies

Mice received a single intraperitoneal injection of 3.4 mg/kg body weight ^{55}Fe-Tf or ^{55}Fe-Fth1. 24 hours after injection, blood was drawn and mice were transcardially perfused with 0.1M phosphate-buffered saline (PBS, pH 7.4). Brains were collected, weighed immediately, and homogenized on ice using disposable tissue grinders (VWR) and MVB Buffer (0.147 M NaCl, 0.4 mM KCl, 0.3 mM CaCl2, 0.12 mM MgCL2, 15 mM HEPES, 0.5% BSA, 5 mM glucose). Homogenates were transferred to microcentrifuge tubes and spun at 1000 x g for 10 minutes at 4°C. The supernatant was collected, and the pellet was resuspended in buffer and spun again. The resulting supernatant was combined with the previous collection and termed brain parenchyma. The pellet was resuspended again and termed microvessels (MVs). Validation of these fractions can be found in Figure 2-1. This separation allowed us to determine the amount of ^{55}Fe that entered the brain or was sequestered in the MVs. Tissue was solubilized using 1 mL Solvable (Perkin Elmer) according to manufacturer's instructions. After solubilization, 10 mL Hionic-Fluor scintillation cocktail (Perkin Elmer) was added. Samples were counted using the Hidex 300 SL (LabLogic) for three minutes each. Blank tube values were subtracted from final counts to correct for background counts.

2.3.6 Protein Detection

Brain homogenates were spun at 1000 x g for 10 minutes at 4°C[47]. The supernatant (cortical fraction) was spun at 14000 x g for 10 minutes. The resulting cell pellet was resuspended and digested in RIPA buffer (Sigma) containing protease inhibitor cocktail (PIC, Sigma) for 1 hour on ice. The MV pellet was resuspended and digested in a mixture of RIPA buffer (Sigma) and protease inhibitor cocktail (PIC, Sigma) for 1 hour on ice. All homogenates were sonicated on ice for 90 seconds and spun at 14000 x g for 10 minutes at 4°C for final collect of the protein lysate. Total protein was quantified by bicinchoninic assay (BCA, Pierce) and 25 μg was loaded onto a 4-20% Criterion TGX Precast Protein Gel (Bio-Rad). Protein was transferred onto a nitrocellulose membrane and probed for the neuronal marker TUJ1 (Abcam, 1:1000, ab18207) or the brain MV marker von Willebrand factor (Abcam, ab174290, 1:1000) and cyclophilin B as a loading control (Abcam, ab16045, 1:1000). Corresponding secondary antibody conjugated to HRP was used (1:5000, GE Amersham) and bands were visualized using ECL reagents (Perkin-Elmer) on an Amersham Imager 600 (GE Amersham).

2.3.7 Ovariectomy

Two-month-old female mice were subjected to aseptic bilateral surgical ovariectomy (OVX) via a dorsal incision under isoflurane anesthesia (1%-2%). After surgery, the skin was sutured with nylon sutures. These mice were then placed in a heated recovery chamber until they regained consciousness, and accordingly, they were returned to their cages. After two weeks, blood was collected from OVX mice and four equally aged intact mice to act as a control.

2.3.8 Serum Molecule Detection

Blood was collected via submandibular cheek blood collection in heparin-coated tubes. Serum was separated from whole blood fractions by centrifugation at 2000 x g for 15 minutes. Serum levels of estradiol were measured by enzyme-linked immunosorbent assay (Cayman Chemical, 501890) according to the manufacturer's protocol. Total iron binding capacity (TIBC), transferrin percent saturation, and serum iron were measured using an assay kit (Abcam, ab239715).

2.3.9 Statistical Analysis

Statistical analyses were performed using Prism 9.2 software (Graphpad Software Inc.). Data from at least five independent biological replicates were averaged and are expressed as the mean ± standard error of the mean (SEM). One-way ANOVA with Tukey post-hoc analysis or unpaired t-tests were used to evaluate for statistical significance where appropriate. A p-value <0.05 was considered significant.

2.4 Results:

2.4.1 ^{55}Fe-Tf uptake is responsive to apo- and holo-Tf in a sex-dependent manner

The aim of the first study was to examine the regulatory effects of apo- and holo-Tf on ^{55}Fe-Tf uptake. In males, both ^{55}Fe-Tf uptake (Figure 2-2A) and release (Figure 2-2B) were significantly increased with apo-Tf infusions ($*p<0.05$) by nearly 41%. In contrast, infusion of holo-Tf resulted in levels of ^{55}Fe-Tf uptake and release significantly lower than observed with apo-Tf infusion ($*p<0.05$ and $**p<0.01$). When the MV and brain parenchyma fractions were

pooled together to examine whole brain uptake, the effect of apo-Tf on ^{55}Fe-Tf uptake is further exemplified (Figure 2-2C, ***p<0.001). The infusion of aCSF increased ^{55}Fe-Tf uptake and release, though not statistically significant or to the same level as apo-Tf. However, in females, ^{55}Fe-Tf uptake into MVs (Figure 2-2D), release into the brain (Figure 2-2E), and total whole brain uptake (Figure 2-2F) were unaltered in response to apo- and holo-Tf infusions. There appears to be a bimodal distribution in the ^{55}Fe-Tf total uptake sham condition in females (Figure 2-2F), whoever the data passed the Shapiro-Wilk test for normality. Notably, about 50% more ^{55}Fe-Tf was sequestered in the MVs than was released into the brain, supporting the regulator role of the MVs regardless of sex.

Figure 2-2

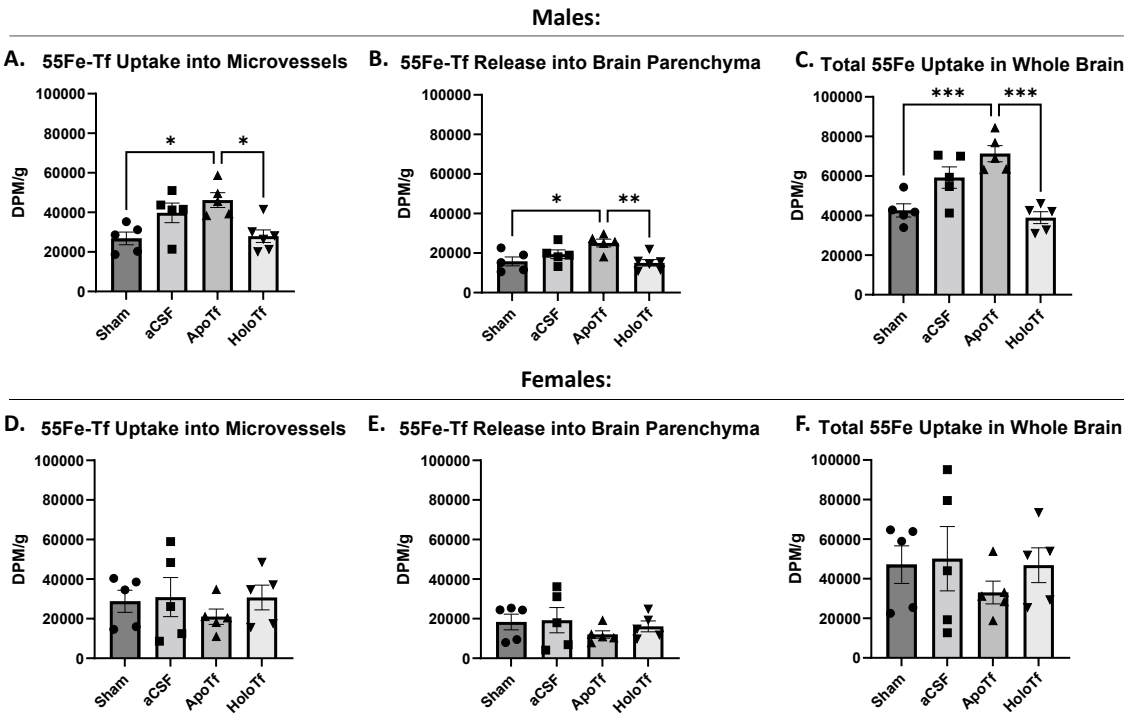

^{55}Fe-Tf brain uptake in males and females. Samples are reported as DPM per gram of brain tissue. In males, increasing levels of apo-Tf in the brain significantly increases ^{55}Fe-Tf uptake into MVs (**A**) and release into the brain (**B**). Additionally, increasing levels of holo-Tf results in significantly reduced ^{55}Fe-Tf uptake compared to infusions of apo-Tf. This difference is further

demonstrated when MV and parenchyma fractions were pooled for total uptake in the whole brain (**C**). However, in females, the ratio of apo- to holo-Tf in the brain has little regulatory effect on ^{55}Fe-Tf uptake into MVs (**D**), release into the parenchyma (**E**), and total uptake in the whole brain (**F**). n= 5 for all conditions, means of biological replicates ± SEM were evaluated for statistical significance using one-way ANOVA with Tukey's posttest for significance. * $p<0.05$, ** $p<0.01$, *** $p<0.001$

2.4.2 ^{55}Fe-Fth1 uptake is not responsive to apo- or holo-Tf

The regulation of ^{55}Fe-Fth1 uptake and release by apo- and holo-Tf infusion was examined next. In male mice, ^{55}Fe-Fth1 uptake into MVs (Figure 2-3a), release into the parenchyma (Figure 2-3b), and total whole brain uptake (Figure 2-3c) were not significantly different in response to either holo or apo Tf infusion. Similarly, in female mice, ^{55}Fe-Fth1 uptake into MVs (Figure 2-3d) or whole brain (Figure 2-3f) was unaltered with the respective infusions, however, release into the brain (Figure 2-3e) increased with infusion of apo-Tf by about 43% compared to sham but with considerable variability. Thus, the results were not statistically significant. As was the case with Tf delivered iron, uptake of Fth1 into the MVs was 50% higher than that released into the brain for both sexes.

Figure 2-3

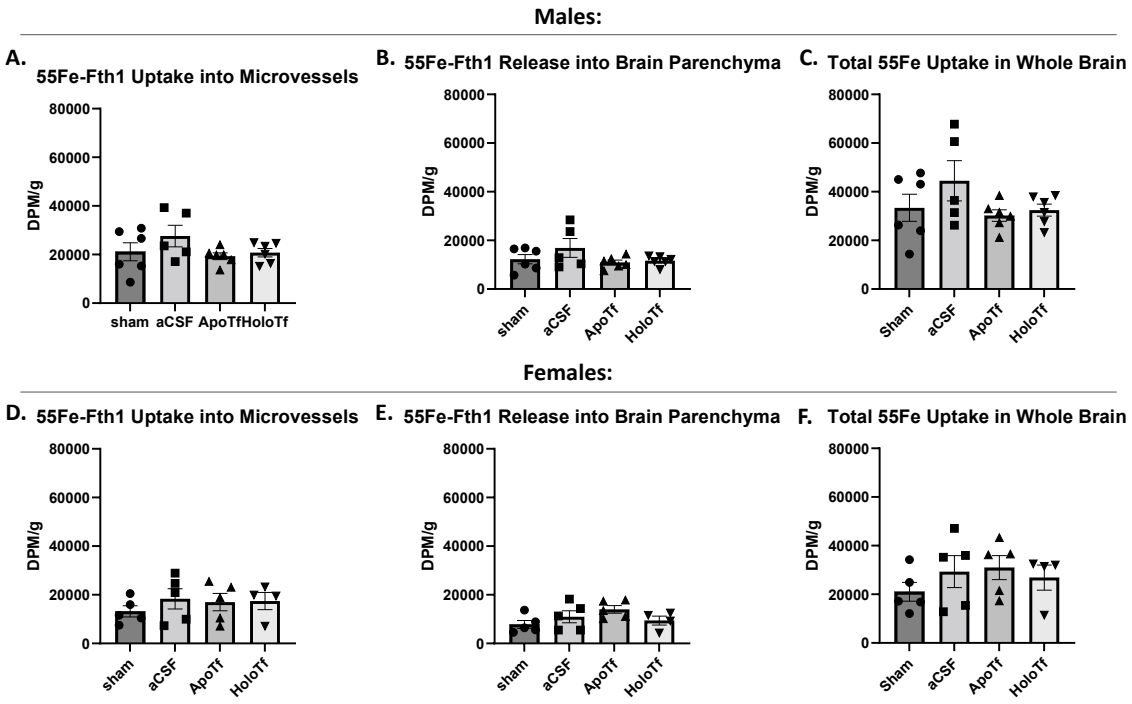

^{55}Fe-Fth1 brain uptake in males and females. Samples are reported as DPM per gram of brain tissue. In males, the ratio of apo- to holo-Tf in the brain has little regulatory effect on uptake into MVs (**A**), release into the parenchyma (**B**), or uptake into the whole brain (**C**). In females, the ratio of apo- to holo-Tf in the brain has little regulatory effect on uptake into MVs (**D**) or whole brain (**F**) but increased ratio of apo-Tf increases release into the brain (**E**). Notably, the MVs contain substantially more ^{55}Fe than the entirety of the brain, supporting the role of MVs in regulating iron release. n= 5 to 6 for all conditions, means of biological replicates ± SEM were evaluated for statistical significance using one-way ANOVA with Tukey's posttest for significance.

2.4.3 Iron uptake is strongly carrier protein- and sex-dependent

Next, baseline differences in total iron uptake between sexes and carrier proteins were established by pooling the ^{55}Fe uptake into the MVs and release into the brain parenchyma (Figure 2-4a) from the sham control group. Males had little difference in total ^{55}Fe uptake whether bound to Tf or Fth1, whereas females took up 55% more iron when bound to Tf compared to Fth1 (*$p<0.05$). On completing this analysis, it became apparent that there was a noticeable difference in variability of ^{55}Fe-Tf total uptake between males and females. Therefore, the coefficient of variation, which is the ratio of the standard deviation to the mean, was determined for ^{55}Fe-Tf uptake in sham groups in both sexes. The coefficient of variation was 17.43% in males and 45.09% in females. This level of variance in females suggested the existence of a confounding variable. The proportion of ^{55}Fe released into the brain parenchyma to the ^{55}Fe taken up by the MVs was also compared between the sexes. In females, compared to males, the proportion of ^{55}Fe-Tf released to ^{55}Fe-Tf taken up into the MVs was significantly higher (Figure 2-4b, *$p<0.05$). When bound to Fth1, the proportion of ^{55}Fe released was not different between males and females (Figure 2-4c).

Figure 2-4

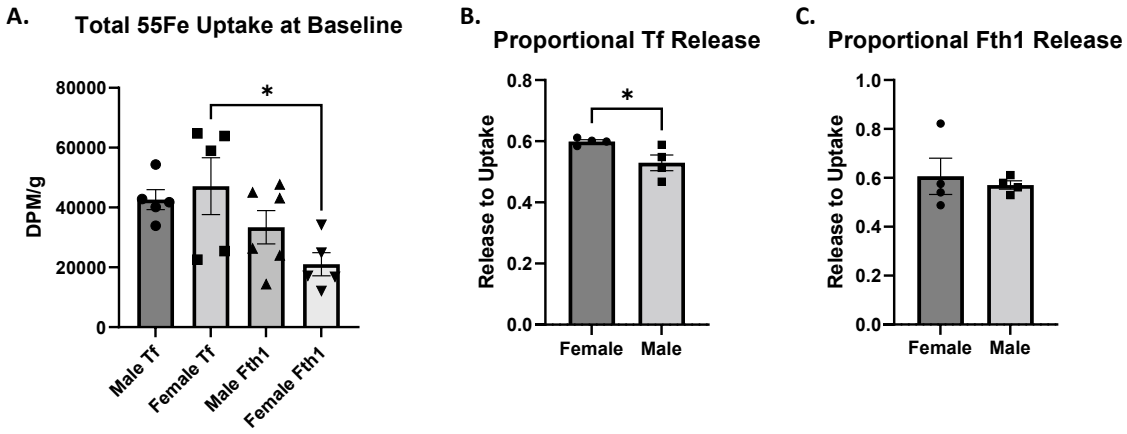

Differences in baseline iron uptake. When pooling the ^{55}Fe present in both MV and brain parenchyma fractions (**A**), females take up significantly more ^{55}Fe when bound to Tf than Fth1.

Of note, the variability of ^{55}Fe-Tf uptake and release in females is substantial. The coefficient of variability of the sham condition in females is 45.09%. The corresponding coefficient of variability of this condition in males is 17.43%. When further exploring the proportion of ^{55}Fe-Tf that is released into the brain to the amount that is taken up into the MVs, females release significantly more of the iron the MVs take up compared to males (**B**). There was no difference between males and females on the proportion of ^{55}Fe-Fth1 release to uptake (**C**). n= 5 to 6 for all conditions, means of biological replicates ± SEM were evaluated for statistical significance using one-way ANOVA with Tukey's posttest for significance for A. Proportions of release to uptake for each infusion condition were calculated and plotted, means ± SEM were evaluated for statistical significance using unpaired t-test for significance for B and C. * $p<0.05$

2.4.4 Reduction of circulating estrogen does not impact ^{55}Fe-Tf uptake regulation

To determine whether the variation within the female dataset was related to the estrus cycle, circulating estrogen was removed by performed ovariectomies (OVX) on 2-month-old female mice. We hypothesized that removal of estrogen would reduce variability and result in female ^{55}Fe-Tf uptake and regulatory pattern similarly to the males. Two weeks after the OVX surgery, serum was isolated from the blood of the mice and confirmed their reduced estradiol levels (Figure 2-5d). Three-month-old OVX mice displayed ^{55}Fe-Tf uptake by MVs (Figure 2-5a) and release into the brain (Figure 2-5b) that was unaltered by any infusion compared to sham, as observed in the intact female mice. Intact female mice were included to demonstrate that ^{55}Fe was taken up in similar amounts to the intact mice. However, the coefficient of variation of the total ^{55}Fe uptake in sham conditions was 16.15% for the OVX group, which was more comparable to male variance (17.43%) than intact females (45.09%). In order to better understand the systemic

iron status of the OVX mice, we further analyzed the serum isolated from the mice by examining the total iron binding capacity (TIBC) and serum iron levels (Figure 2-5e). TIBC was higher in OVX mice (427.5 µmol/L) compared to intact control mice (341.2 µmol/L). Serum iron was lower in OVX mice (90.6 µmol/L) compared to the control (110.0 µmol/L). Lastly, Tf saturation percentage was decreased in OVX (23.0%) compared to control (32.4%). These measures indicate reduced systemic iron levels, but not enough to be deemed iron deficient.

Figure 2-5

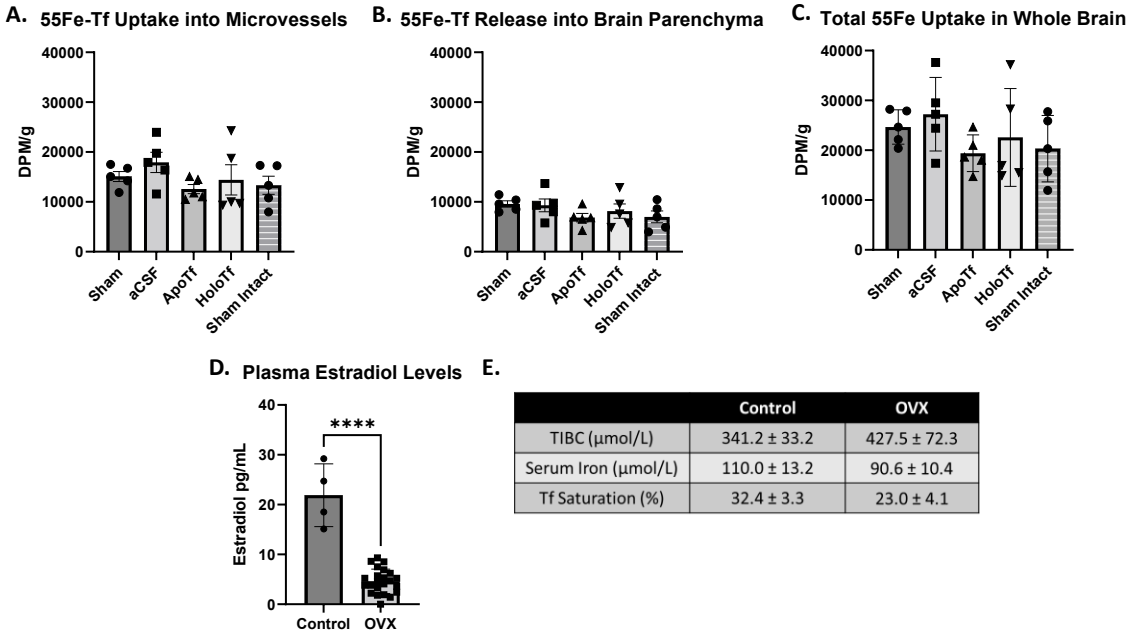

E.

	Control	OVX
TIBC (µmol/L)	341.2 ± 33.2	427.5 ± 72.3
Serum Iron (µmol/L)	110.0 ± 13.2	90.6 ± 10.4
Tf Saturation (%)	32.4 ± 3.3	23.0 ± 4.1

OVX on ^{55}Fe-Tf brain uptake in females. Samples are reported as DPM per gram of brain tissue. After removing circulating estrogen via OVX, female mice still do not show changes in ^{55}Fe-Tf uptake (**A**), release (**B**), or total uptake (**C**) across infusion conditions. Intact sham mice were included as a control. The coefficient of variability of ^{55}Fe-Tf uptake in sham conditions was 16.15%. The levels of plasma estradiol levels were determined to confirm the success of the OVX in all mice used (**D**). The TIBC of plasma is higher in OVX mice while the Tf saturation percentage and serum iron are lower when compared to control. (**E**). n= 5 for all conditions, means of biological replicates ± SEM were evaluated for statistical significance using one-way

ANOVA with Tukey's posttest for significance for A and B. Means ± SEM were evaluated for statistical significance using unpaired t-test for significance for C and D. **** $p<0.0001$

2.5 Conclusions:

The objective of this study was to determine the regulation of Fth1- and Tf-bound iron uptake into the brain by apo- and holo-Tf *in vivo.* In pursuit of this aim, we discovered significant sex differences in the regulation of iron uptake mediated by these two proteins. The results of this study have demonstrated that the ratio of apo- to holo-Tf in the CSF regulates Tf-bound iron uptake in males, but not in females in this model. However, there was significant variation in ^{55}Fe-Tf uptake in females. To address these differences, we performed ovariectomies aimed to determine if reducing circulating estrogen would enable the regulatory response to apo- and holo-Tf infusions that were seen in males. We found that reducing peripheral estrogen did not change the lack of response of ^{55}Fe-Tf uptake into MVs and release into the brain following infusion of apo- or holo-Tf. However, the variability that had been seen in the intact females was significantly reduced to that seen in males after removal of circulating estrogen. Additionally, delivery of Fth1 bound iron was not responsive to the ratio of apo- to holo-Tf in the CSF of either males or females. A particularly notable finding in this study was that MVs contained significantly more of the injected iron regardless of the delivery protein than the brain parenchyma even though the MVs account for only 2% of the total brain cells[205]. This finding further establishes our position that the ECs serve as a reservoir for iron for subsequent regulated release into the brain. Previous studies reporting on uptake of iron or other nutrients have rarely differentiated what is in the microvasculature versus what has entered the brain parenchyma.

Furthermore, our data demonstrate that acquisition of brain iron is dependent on carrier protein and sex.

Previously, we and other have postulated the concept of regulation of iron release to the brain by endothelial cells of the BBB in cell culture models[16,18–20,98,208]. For example, Simpson *et al.* demonstrated that CSF from iron deficient monkeys, as well as conditioned media from iron chelated astrocytes, increased iron release from bovine retinal endothelial cells[16] in a bi-chamber model of the BBB. Moreover, our group previously showed, using iPSC-derived ECs in a simulated BBB model, that exposure to apo-Tf resulted in increases in both ^{59}Fe-Tf and ^{59}Fe-Fth1 transport from apical to basal chambers, whereas incubation with holo-Tf decreased their transport[18]. *In vitro* conditions simulating iron deficient environments have repeatedly resulted in increased iron transport across the BBB[16,200,209]. However, until now, the demonstration of *in vivo* regulation was lacking. Our *in vivo* data from male mice support regulated release of iron from ECs forming the MV and suggest that the brain uses apo- and holo-Tf to relay its iron status to ECs, which in turn release more or less iron in response. An example of how this feedback can occur *in situ* is that, following iron uptake by neurons and astrocytes, these cells release apo-Tf into the extracellular fluid[95,210]. Thus, areas of greater energetic activity can regionally signal for increased iron release from MVs. Thus, our data address for the first time local regulation of brain iron uptake in response to iron utilization and help explain the findings of Beard *et al.* who demonstrated that brain iron uptake differs in various regions[211].

The role of Fth1 as an iron delivery protein to the brain is a relatively new concept with great implications as it binds nearly 2000 times more iron than Tf[24]. It has been reported that Fth1 can replace Tf as the iron delivery protein for oligodendrocytes[212] and ECs[18]. Fth1 is a substantial iron contributor to the brain during development, as up to postnatal day 22, mice take up significantly more Fth1 bound iron than Tf bound iron into the brain[26]. In previous *in vitro* studies, the iron status of Tf in the basal compartment of the BBB model impacted the amount of

Fth1-bound iron that was transported across the ECs[18]. However, in this *in vivo* study, we did not see any significant differences in Fth1 bound iron uptake into MVs or release into the brain following infusion of apo- or holo-Tf. In females, the infusion of apo-Tf did result in a two-fold increase in iron release into the brain compared to sham control. Although this difference did not reach statistical significance, the Cohen's *d* effect size between sham control and apo-Tf is 0.65, indicating a moderate effect. The absence of statistical significance was likely due to the variability in the different groups. Thus, the data suggest that Fth1 delivered iron is responsive to CSF iron deficiency in females.

Intracerebroventricular (ICV) injection of iron transporter proteins has been well established by a number of foundational studies[213–216]. Moos and Morgan demonstrated that 24 hours after a single ICV injection of [^{125}I]Tf, up to 10% is present in the brain and 5% is still present in the CSF, while ^{59}Fe was deposited past the ependyma cells near the injection site[213]. Moos further demonstrated that labeled transferrin diffused in the vicinity of the injection, reaching past the ependyma cells to neurons and glia, as well as areas along the subarachnoid space[214]. Similarly, Brightman observed the rapid diffusion of ferritin after ICV injection in as little as 10 minutes, with further distribution into the brain tissue as time increased. More contemporary studies have reported similar ICV protein dynamics[215,216]. Iliff *et al.* infused various tracer molecules into the lateral ventricle to map their distribution into the brain. Within 30 minutes, a 3 kDa molecule and a 2000 kDa molecule penetrated 50% and 25%, respectively, of the brain near CSF compartments[217]. Given that our model uses a steady state infusion that continuously delivers apo- or holo-Tf along with the turnover of CSF, we have little doubt that our infused apo- and holo-Tf has the ability to interact with the endothelium, even if only in the vicinity of CSF compartments, and produce robust changes in ^{55}Fe brain uptake.

In a few experiments conducted, infusion of aCSF increased iron uptake into MVs and release into the brain. Based on our calculations, the 0.25 µl/hour infusion rate would have

resulted in an approximately 1% dilution of total CSF and, thus, should have minimal effect on endogenous Tf signals with complete turnover every 1.8 hours in the mouse[218]. It is possible that in the less than 1 µl volume of the mouse lateral ventricle[219] this initial dilution is locally greater and results in a more regional iron uptake and release. Regardless, the observation that apo-Tf or aCSF increases the uptake of transferrin-bound iron to the brain and release by the microvasculature underscores how exquisitely fined tuned the signaling from the brain to the MVs regarding iron status is.

Significant sex differences were detected in baseline (sham control group) iron uptake between Tf and Fth1. Female mice took up significantly more iron bound to Tf than to Fth1, while there was no statistically significant difference in iron uptake by either delivery protein in males. What's more, baseline Tf-bound iron uptake in females appears to follow a slight bimodal distribution, further suggesting a biological influence. There was an increased proportion of Tf-bound iron released into the brain in females relative to males, indicating that iron was more rapidly released to the brain. The differences in baseline uptake would suggest differences in iron levels in the brain but studies have shown there is little to no difference in total brain iron levels between males and females[45,46]. These studies, however, largely fail to examine the process of iron accumulation. Brain iron accumulation was addressed by Duck *et al.,* who showed that 24 hours after injecting mice with ^{59}Fe-Tf, males and females had the same amount of iron uptake; however, after five days post injection, females took up significantly more ^{59}Fe than males[47]. Combined with our data presented herein, these findings indicates that females have more iron uptake over time than males. More iron accumulation by females compared to males would be consistent with increased in myelin turnover[39] and dopamine synthesis[40,41] reported in females; both processes are dependent on iron as a co-factor[43,220]. The constant utilization of iron for these metabolic processes likely leads to an increased requirement of iron uptake into the brain which seems to be predominantly met by regulation of Fth1. This idea is also consistent with the lack of

Tf delivered iron response by females to the infusion of apo- and holo-Tf. Future studies to decipher how differences in metabolic needs impact female brain iron uptake are needed.

Literature suggests that estrogen plays an important role in iron homeostasis[48–50]. Our experiments aimed to determine if reducing circulating estrogen would diminish the variability to brain iron uptake and perhaps allow the regulatory effects of apo- and holo-Tf to change iron uptake. We found that reducing peripheral estrogen significantly reduced the variability of iron uptake by the females but did not impact the regulation of iron uptake into the brain via apo- and holo-Tf. It should be noted that others have found that serum and CSF levels of estrogen are only weakly correlated[221] and the brain can produce its own estrogen[222]. Nonetheless, we did see a dramatic decrease of the variability within the data, indicating that circulating estrogen may still play a role in iron uptake regulation. The effect of OVX did reduce serum iron levels and increase TIBC, but this was not enough to induce an iron deficiency in our mice.

In conclusion, this study is the first demonstration of *in vivo* regulation of brain iron uptake into MVs and subsequent release into the brain by apo- and holo-Tf. Moreover, we have identified striking sex differences in the baseline uptake and regulation of iron uptake for both Tf and Fth1. Understanding the sex differences and differences in Tf versus Fth1 delivered iron is crucial for clinical translation of these studies for the treatment of brain iron dysregulation and use for drug delivery efforts.

Chapter 3

Apo- and holo- transferrin differentially interact with hephaestin and ferroportin with minimal hepcidin influence

This work has been previously submitted as:

Baringer, S.L., Palsa, K., Spiegelman, V.S., Simpson, I.A., Connor, J.R. *Apo- and holo-transferrin differentially interact with hephaestin and ferroportin in a novel mechanism of cellular iron release regulation*. Journal of Biomedical Sciences. (2023)

3.1 Abstract:

Apo- (iron free) and holo- (iron bound) transferrin (Tf) participate in precise regulation of brain iron uptake at endothelial cells of the blood-brain barrier. Apo-Tf indicates an iron-deficient environment and stimulates iron release, while holo-Tf indicates an iron sufficient environment and suppresses additional iron release. Free iron is exported through ferroportin, with hephaestin as an aid to the process. Until now, the molecular mechanisms of apo- and holo-Tf influence on iron release was largely unknown. Here we use a variety of cell culture techniques, including co-immunoprecipitation and proximity ligation assay, in iPSC-derived endothelial cells and HEK 293 cells to investigate the mechanism by which apo- and holo-Tf influence cellular iron release. Given the established role of hepcidin in regulating cellular iron release, we further explored the relationship of hepcidin to transferrin in this model. We demonstrate that holo-Tf induces the internalization of ferroportin through the established ferroportin degradation pathway. Furthermore, holo-Tf directly interacts with ferroportin, whereas apo-Tf directly interacts with

hephaestin. Only pathophysiological levels of hepcidin disrupt the interaction between holo-Tf and ferroportin, but similar hepcidin levels are unable to interfere with the interaction between apo-Tf and hephaestin. The disruption of the holo-Tf and ferroportin interaction by hepcidin is due to hepcidin's ability to more rapidly internalize ferroportin compared to holo-Tf. These novel findings provide a molecular mechanism for apo- and holo-Tf regulation of iron release from endothelial cells. They further demonstrate how hepcidin impacts these protein-protein interactions, and offer a model for how holo-Tf and hepcidin cooperate to suppress iron release. These results expand on our previous reports on mechanisms mediating regulation of brain iron uptake to provide a more thorough understanding of the regulatory mechanisms mediating cellular iron release in general.

3.2 Background:

Precise regulation of iron uptake at the blood-brain barrier (BBB) is crucial for proper brain function. Our group has shown that iron release from endothelial cells (ECs) of the BBB is modulated by levels apo (iron free)- and holo (iron bound)- transferrin (Tf)[16–18,20,98] in extracellular fluid. Using both *in vitro*[16,18,98] and *in vivo*[17] models, we have shown that increasing the ratio of apo- to holo-Tf, reflecting an iron deficient environment, stimulates iron release from ECs, whereas elevated holo-Tf relative to apo-Tf, reflecting an iron-replete environment, suppresses iron release. This feedback mechanism allows for regional specificity of iron uptake based on regional iron consumption and metabolic needs[97,211]. A commonly held hypothesis in the iron field is that hepcidin, a pro-inflammatory peptide hormone, primarily secreted by the liver[126] and in small amounts by astrocytes[125], is the sole regulator of iron release at barrier cells. However, this theory lacks the regulatory precision that apo- and holo-Tf offer.

Free iron is released from cells, including ECs, through ferroportin (Fpn), the only know iron exporter. Fpn function is aided by a number of proteins, including hephaestin (Heph)[76,223], a ferroxidase that converts released ferrous (Fe^{2+}) to ferric (Fe^{3+}) iron. Heph is required for both the stability of Fpn in the plasma membrane and the efflux of iron through Fpn[76,223]. Inversely, Fpn can be inhibited by hepcidin[120]. When hepcidin binds to Fpn, Fpn is ubiquitinated for internalization and subsequent degradation[75,120]. Hepcidin is upregulated in response to systemic inflammation and high serum iron levels[128], with baseline physiological levels[224] and pathophysiological levels[225] differing by nearly 10-fold.

Simpson *et al.* found that, in addition to iron release, holo-Tf also decreases Fpn protein in EC culture models of the BBB[16] but the mechanism is unclear. Conversely, it has been proposed that apo-Tf participates in interactions with ferroxidases such as Heph and ceruloplasmin to facilitate iron release[104,106,107]. In the present study, we have determined the differential interactions that apo- and holo-Tf have with Fpn and Heph to control iron release. Moreover, we demonstrate the impact that hepcidin can have on these interactions. These results provide significant novel insights not only into the regulatory mechanism of iron release into the brain but are likely relevant to cellular iron release in general.

3.3 Methods:

3.3.1 Cell Culture

Human endothelial-like cells (ECs) were differentiated from ATCC-DYS0100 human iPSCs as described previously[90,226]. Briefly, iPSCs were seeded onto a Matrigel-coated plate in E8 medium (Thermo Fisher Scientific, 05990) containing 10 μM ROCK inhibitor (Y-27632, R&D Systems, 1254) at a density of 15,000 cells/cm^2. The iPSCs differentiation was initiated by

changing the E8 medium to E6 medium (Thermo Fisher Scientific, A1516401) after 24 hours seeding. E6 medium was changed daily up to 4 days before switching to human endothelial serum free medium (hESFM) (Thermo Fisher Scientific, 11111) supplemented with 10nM bFGF (Fibroblast growth factor, Peprotech, 100-18B) and 10 μM all-trans retinoic acid (RA, Sigma, R2625) and 1% B27 (Thermo Fisher Scientific, 17504-044). After 48 hours of no medium changes, cells were harvested and replated onto Transwell filters coated with collagen IV and fibronectin. Twenty-four hours after replating, bFGF and RA were removed from the medium to induce barrier phenotype. HEK 283 cells were maintained in Dulbecco's modified Eagle's medium (DMEM, Gibco, 11965-084) and supplemented with 10% FBS and 1% penicillin-streptomycin (Gibco, 15070063).

3.3.2 Plasmid and Transfection

HEK 293 cells were seeded at a density of 7 x 10^4 cell/cm^2 in a 6-well plate. The following day, the cells were transfected with 1 μg/well of the HA-tagged Fpn plasmid (Vector Builder, VB220407-1185gaa, Figure 3-1) using Lipofectamine™ 3000 Transfection Reagent (Invitrogen, L3000001).

Figure 3-1

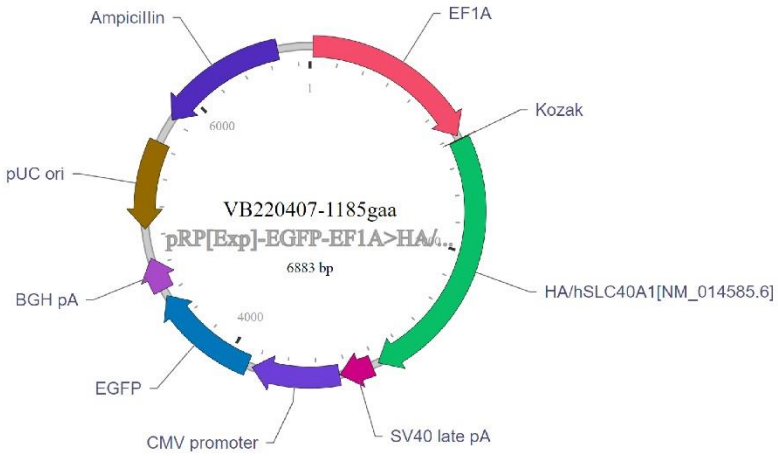

HA-tagged Fpn plasmid map. HEK 293 cells were transfected with an HA-tagged Fpn plasmid to enable effective pull down of Fpn in co-IP experiments. The plasmid was designed using Vector Builder. The full sequence, as well as purchasing options, are available online https://en.vectorbuilder.com/vector/VB220407-1185gaa.html.

3.3.3 Proximity Ligation Assay (PLA)

PLA is a technique that precisely demonstrates if two proteins directly interact with one another. When two proteins are in close enough proximity to be interacting, the secondary oligomer probes ligate together, allowing for the amplification of the oligomers and resulting in a fluorescent signal. PLA was performed using a Duolink assay kit (Sigma-Aldrich, DUO92013) according to the manufacturer's instructions[227]. Chamber slides (Falcon, 354108) were coated with poly-D-lysine 2 hours before HEK 293 cells were culture on the slides at a density of 15,000 cell/cm^2. In order to remove an exogenous Tf, 24 hours later the media was replaced with DMEM containing no FBS. Cells were exposed to apo- or holo-Tf (Sigma, T1147 and T4132) for 10 minutes and then washed to procced with PLA. Primary antibodies used were the following: myelin basic protein 1 (MBP1, Abcam, ab22460, 1:500), ferritin (Abcam, ab77127, 1:500), Tf (ProteinTech, 66161-1, 1:500), TfR (Cell Signaling, 13208S, 1:500), Tf (Abcam, ab82411, 1:500), Fpn (gift from M. Knutson, 1:500), and Heph (Santa Cruz, SC-365365, 1:500). Positive and negative controls used for assay optimization can be found in Figure 3-2. Imaging and analysis were performed using Revolve R4 microscope (Echo). The integrated density was calculated by summing the pixels from PLA signal and dividing by the field of view area. The integrated density of background from negative controls were subtracted from these values. To

determine the integrated density per cell, this was then divided by the number of cells in the field of view. A minimum of three images were taken in different regions of the slides and then averaged for a single biological replicate. Image brightness was uniformly increased for the purposes of publication but not for quantification.

Figure 3-2

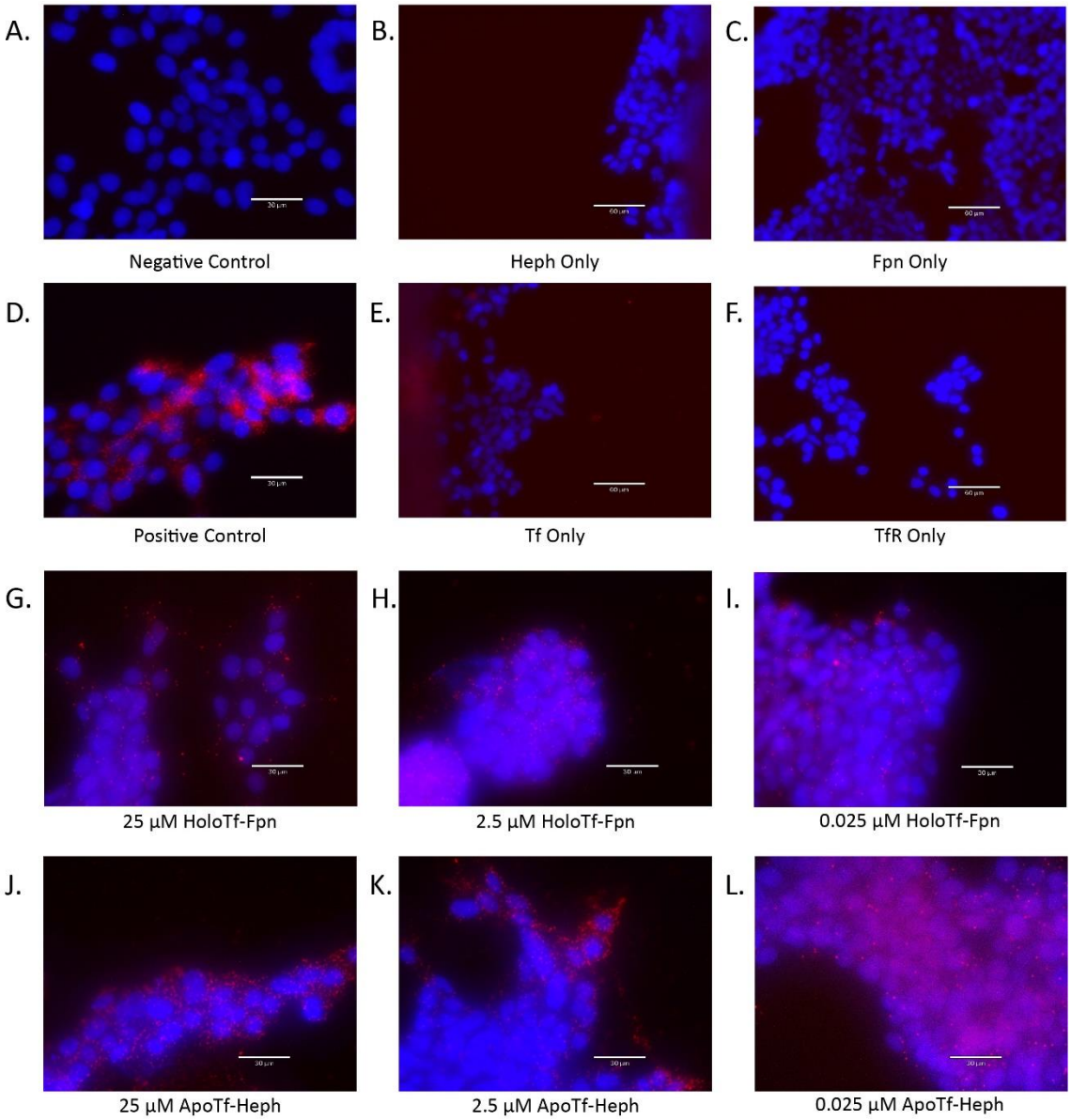

PLA controls A number of controls were employed while optimizing the use of PLA to determine the interactions apo- and holo-Tf had with Heph and Fpn respectively. The negative

control consisted of probing for two proteins known to not interact – here MBP and ferritin (**A**). The positive control consisted of probing for two proteins known to interact – here exogenous Tf and TfR (**D**). Furthermore, each antibody used to probe for Fpn, Heph, Tf, and TfR was assessed for nonspecific binding by performing solo incubations and ensuring the antibody alone did not produce PLA signal (**B-C, E-F**). In order to determine the best concentration of apo- and holo-Tf to use, we tested 0.025 μM, 2.5 μM, and 25 μM along with 0.25 μM (which was used for experiments) (**G-L**). All additional concentrations of apo- and holo-Tf show similar amounts of PLA puncta as the used 0.25 μM.

3.3.4 Co-immunoprecipitation

In order to remove an exogenous Tf, the media was replaced with DMEM containing no FBS 24 hours before the start of experiments. Cells were exposed to apo- or holo-Tf (Sigma, T1147 and T4132) for 10 minutes and then washed on ice with cold PBS twice. Chilled 100 μl Co-IP lysis buffer (20 mM Tris HCl, pH 8, 137 mM NaCl, 10% glycerol, 1% Triton x-100, and 2 mM EDTA) was added to each well. Cells were collected and incubated with rotation for 30 minutes at 4°C. Cell solutions were centrifuged at 14,000 x g for 20 minutes at 4°C. Supernatant was collected, and protein estimation was performed using Pierce BCA Protein Assay Kit (Thermo, 23227). Approximately 1 mg of protein was used for Co-IP using anti-HA magnetic beads (Thermo, 88837) or Protein G magnetic beads (Thermo, 10003D) complexed with anti-Heph antibody (Santa Cruz, SC-365365) according to manufacturer's instructions[212]. Briefly, magnetic beads were washed twice with PBS before adding lysates. The bead and lysate solutions were incubated with rotation for 30 minutes at room temperature. After washing with PBS, protein was eluted from beads by resuspending in non-reducing sample buffer and boiling at

90°C for 10 minutes. A magnet was used to isolate the magnetic beads from the protein solution, which was then reduced using 2 M DTT and then loaded for immunoblotting.

3.3.5 Membrane Protein Isolation

Cells were washed with PBS three time before incubating with 200µl digitonin buffer (20mM Tris-HCl, 250 mM sucrose, 0.007% digitonin, 1x protease inhibitor cocktail)[228]. Cells were gently lifted from the plate and collected in chilled glass mini homogenizers. Once homogenized, samples were spun at 1,500 x g for 10 minutes. The pellet was reserved and the supernatant was spun again at 10,000 x g for 10 minutes. The resulting pellet was combined with the pervious pellet and resuspended in RIPA buffer and 1x protease inhibitor cocktail. After immunoblotting was performed on the samples, the membranes were stained for total protein content using Ponceau S staining solution (Thermo, A40000279) to use as a loading control.

3.3.6 Immunoblotting

Samples were loaded onto a 4-20% Criterion TGX Precast Protein Gel (Bio-Rad)[17]. Protein was transferred onto a nitrocellulose membrane and probed for Fpn (Alpha Diagnostics, MTP11-S, 1:1000), DMT1 (Millipore, ABS983, 1:1000), Heph (Santa Cruz, SC-365365, 1:1000), TfR (Santa Cruz, sc-65882, 1:250), Tf (Abcam, ab82411, 1:1000), HA tag (Invitrogen, MA5-27915, 1:1000), ubiquitin (Protein Tech, 10201-2-AP, 1:1000) or cyclophilin B (Abcam, ab16045, 1:1000) as a loading control. Corresponding secondary antibody conjugated to HRP was used (1:5000, GE Amersham) and bands were visualized using ECL reagents (Perkin-Elmer) on an Amersham Imager 600 (GE Amersham). Cellular lysate samples were normalized to cyclophilin B protein as a loading control, and then subsequently normalized to an untreated

control sample within each experiment. Membrane protein samples were stained with Ponceau S and normalized to total protein as a loading control.

3.3.7 Statistical Analysis

Statistical analyses were performed using Prism 9.2 software (Graphpad Software Inc.). Data from at least three independent biological replicates were averaged and are expressed as the mean ± standard error of the mean (SEM). One-way ANOVA with Tukey post-hoc analysis, two-way ANOVA with Sidak's post hoc analysis, or unpaired t-tests were used to evaluate for statistical significance. A p-value <0.05 was considered significant. For each experiment, n indicates 2-3 wells of cells pooled together for one replicate and a different passage of cells per n.

3.4 Results:

3.4.1 Holo-Tf decreases Fpn levels through Fpn's degradation pathway

In the first series of experiments, we examined the effects of apo- and holo-Tf on the cellular levels of Fpn by incubating iPSC-derived ECs with increasing concentrations of either apo- or holo-Tf in hESFM for 8 hours. ECs were cultured onto Transwell inserts and apo- or holo-Tf was placed in the basal chamber to represent the brain-side. The ECs were collected and probed for various iron transport proteins. Incubations with holo-Tf decreased Fpn protein levels by 50% at concentrations as low as 0.1 μM (*$p<0.05$, Figure 3-4A) whereas apo-Tf had no impact on Fpn (Figure 3-4A). Other iron transport proteins, such as Heph, DMT1, and TfR, were relatively unchanged with incubations of apo- or holo-Tf (Figure 3-3).

Figure 3-3

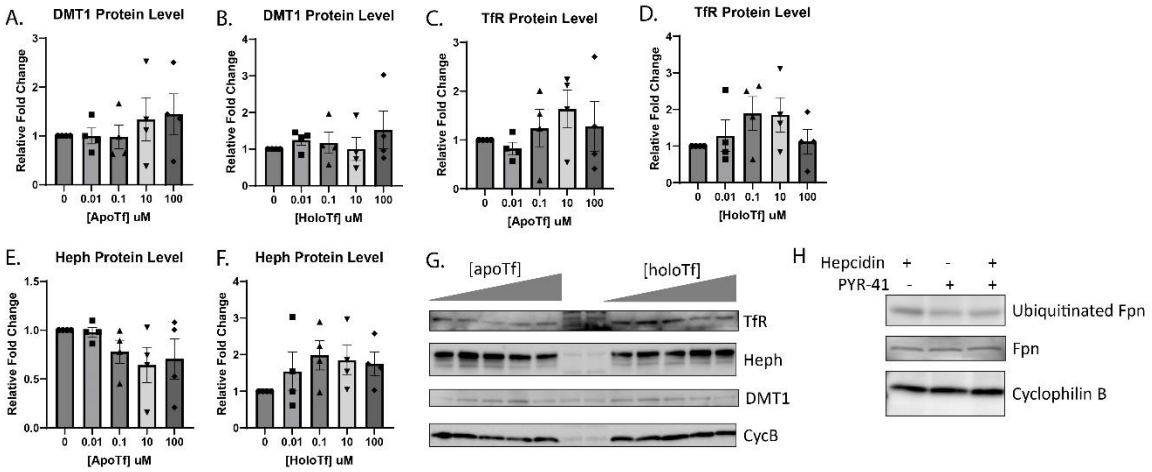

Additional iron regulatory proteins with holo-Tf incubation and PYR-41 validation. iPSC-derived ECs were incubated with holo-Tf in the basal chamber of Transwell inserts. The cells were collected and additional iron regulatory proteins were probed for using immunoblotting. Neither apo- nor holo-Tf incubations resulted in significant changes to DMT1, Heph, or TfR protein levels (**A-G**). PYR-41's inhibition of ubiquitination was validated using hepcidin to trigger Fpn ubiquitination (**H**). Exposure to hepcidin alone for 30 minutes increases ubiquitination of Fpn. When pretreated with PYR-41 for 30 minutes, the increased ubiquitination of Fpn is blocked. Total Fpn levels are unchanged. n=3 to 4 for all experiments, means of biological replicates ± SEM were evaluated for statistical significance using one- way ANOVA with Tukey's posttest for significance.

The degradation pathway for Fpn involves ubiquitination by E1 ubiquitin ligase, resulting in the internalization and degradation of Fpn[75,123]. To determine if this established degradation pathway was the cause of the decreased Fpn induced by holo-Tf, we pretreated ECs with 50 μM PYR-41, an E1 ubiquitin ligase inhibitor, before exposure to either apo- or holo-Tf. The use of 50 μM PYR-41 to prevent Fpn ubiquitination has been demonstrated previously[123]. The inhibition of Fpn ubiquitination resulted in a mitigation of holo-Tf's decrease of Fpn (Figure 3-4D), while apo-

Tf continued to have no impact on Fpn levels (Figure 3-4D). In order to confirm the ubiquitination inhibition by PYR-41, we exposed ECs to 500 nM of hepcidin (standard concentration in the literature[75,120,123]) following pretreatment with 50 μM PYR-41 for 30 minutes (Figure 3-3). Controls were either solely exposed to hepcidin or PYR-41. As expected, hepcidin alone increased Fpn ubiquitination and PYR-41 pretreatment prevented this increase (Figure 3-3). To further confirm that holo-Tf induces the ubiquitination of Fpn and observe the timing of Fpn degradation, we incubated ECs in Transwell inserts with 0.25 μM holo-Tf (physiological level in CSF[229]) in the basal chamber for intervals of 1 hour before collecting the cells and probing for ubiquitinated protein and Fpn. In a time-dependent manner, Fpn levels decrease over time with incubation of holo-Tf (Figure 3-4G). After 5 hours of holo-Tf incubation, Fpn levels have decreased to about 50% (***$p<0.001$, Figure 3-4H). Furthermore, The levels of ubiquitinated Fpn increase over time, with a maximal effect at 3 hours (*$p<0.05$, Figure 3-4I). Because Fpn is degraded over time, we further calculated the extent of ubiquitination relative to the amount of Fpn (Figure 3-4J). The level of ubiquitination per Fpn is elevated after 1 hour and remains constant over time, suggesting Fpn is continuously ubiquitinated during holo-Tf-exposure.

Figure 3-4

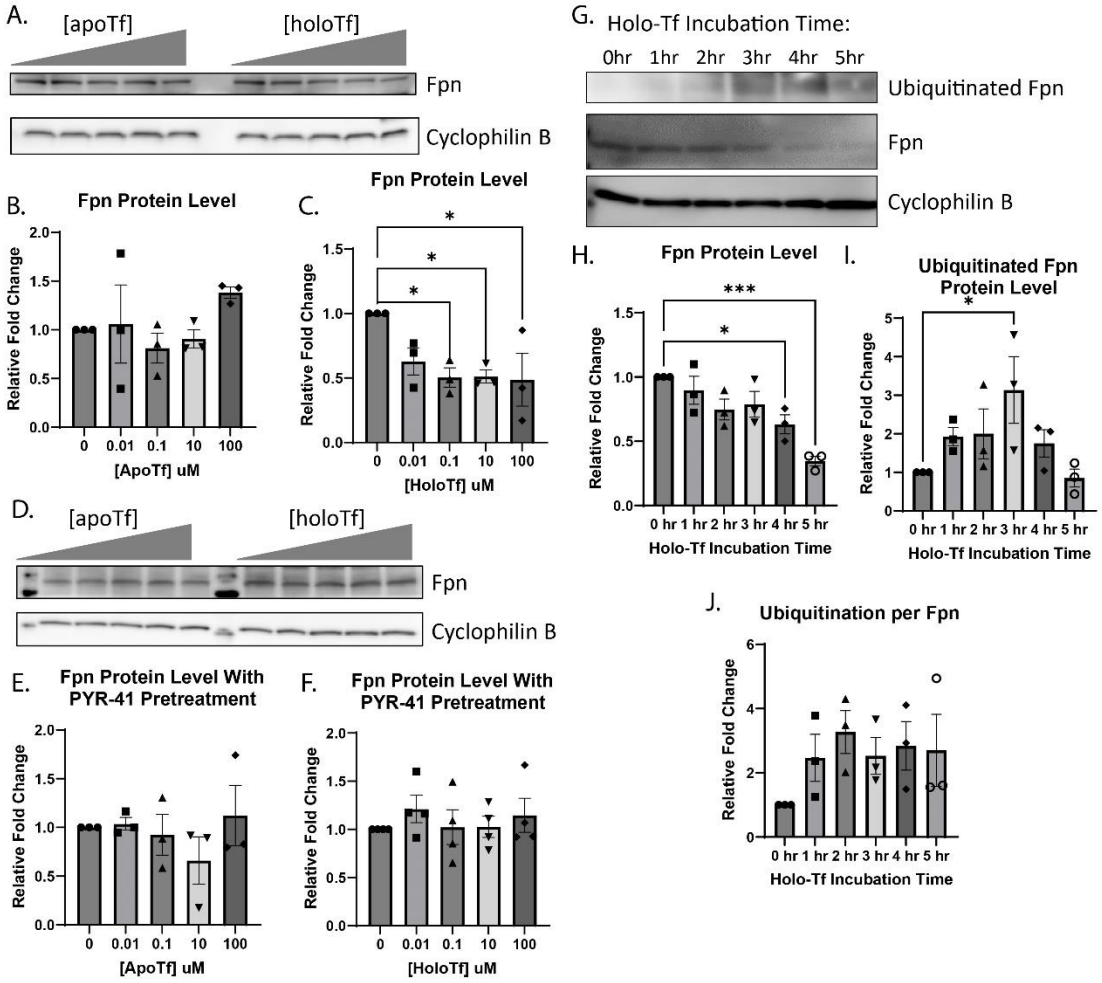

Modulation of Fpn protein levels in ECs by holo-Tf. iPSC-derived ECs were cultured on bi-chamber plates, incubated with apo- or holo-Tf in the basal chamber, and collected after 8 hours for immunoblotting. Fpn protein levels were normalized to cyclophilin B as a loading control. All quantifications were further normalized to untreated control to account for cell count variability. Holo-Tf decreased Fpn protein levels by 50% at concentrations as low as 0.1 μM, while apo-Tf did not (**A-C**). Holo-Tf-mediated internalization and degradation of Fpn was inhibited by a ubiquitination inhibitor, PYR-41, (**D-F**) confirming that holo-Tf's decreases Fpn through the established degradation pathway. ECs were incubated with 0.25 μM holo-Tf to observe the ubiquitination and internalization of Fpn over time. After 1 hour, ubiquitination of Fpn was

detected, with a maximal effect at 3 hours (**G-J**). By 5 hours, 50% of Fpn is internalized with continuous ubiquitination per Fpn present. n=3 to 4 for all experiments, means of biological replicates ± SEM were evaluated for statistical significance using one- way ANOVA with Tukey's posttest for significance. *p<0.05, ***p<0.001

3.4.2 Apo- and holo-Tf differentially interact with Fpn and Heph

We next aimed to determine if holo-Tf interacted directly with Fpn. Due to their transfectability[230] and wide use for foundational biochemical studies[231,232], as well as their universal iron export mechanism[123,233,234], we used HEK 293 cells transfected with an HA-tagged Fpn plasmid to selectively pull-down HA-Fpn. We incubated the cells with 0.25 μM of either apo- or holo-Tf (physiological level in CSF[229]) in media containing no FBS for 10 minutes prior to co-immunoprecipitation (co-IP). Regardless of whether the cells were incubated with either apo- or holo-Tf, Tf was co-immunoprecipitated with HA-Fpn (Figure 3-5A). This indicates that apo- and holo-Tf bind to the Fpn complex of proteins. Because Heph aids Fpn in the export of iron[223], we hypothesized that apo-Tf could bind to Heph, leading to its co-immunoprecipitation with HA-Fpn. To confirm this, we incubated ECs, which have greater Heph expression than HEK 293 cells, with either apo- of holo-Tf, and performed co-IP with Heph antibody. Again, in cells incubated with either apo- of holo-Tf, Tf was co-immunoprecipitated (Figure 3-5B) further confirming that Fpn, Heph, and Tf complex together.

Because co-IP precipitates the entire complex of Fpn, Heph, apo-Tf, and holo-Tf, we aimed to better differentiate if apo- and holo-Tf directly interact with Fpn and Heph by employing proximity ligation assay (PLA), a highly sensitive method of detecting protein-protein interactions. ECs are highly polarized and exclusively express Fpn on the basolateral

membrane[226,235] that is adherent to the plate or slide surface, making it difficult to study protein interactions in this location. For this reason, we used HEK 293 cells for the PLA studies. Because the physiological concentration of Tf in the CSF is 0.25 μM[229], we chose this concentration for our studies. However, a range of concentrations of Tf were tested and no difference in PLA signal were found (Figure 3-2). All Tf incubations were in media containing no FBS for 10 mins. Cells incubated with holo-Tf showed PLA signal when probing for a Tf and Fpn interaction (Figure 3-5D), while cells incubated with apo-Tf showed PLA signal when probing for a Tf and Heph interactions (Figure 3-5F). A small amount of PLA puncta just above background signal was detected when cells were treated with apo-Tf and probing for the Tf-Fpn interaction, however, this is likely due to apo-Tf binding to iron in the media and being converted to holo-Tf. Thus, holo-Tf directly interacts with Fpn while apo-Tf does not (***$p<0.001$, Figure 3-5D-E). Conversely, apo-Tf directly interacts with Heph, while holo-Tf does not (****$p<0.0001$, Figure 3-5F-H).

Figure 3-5

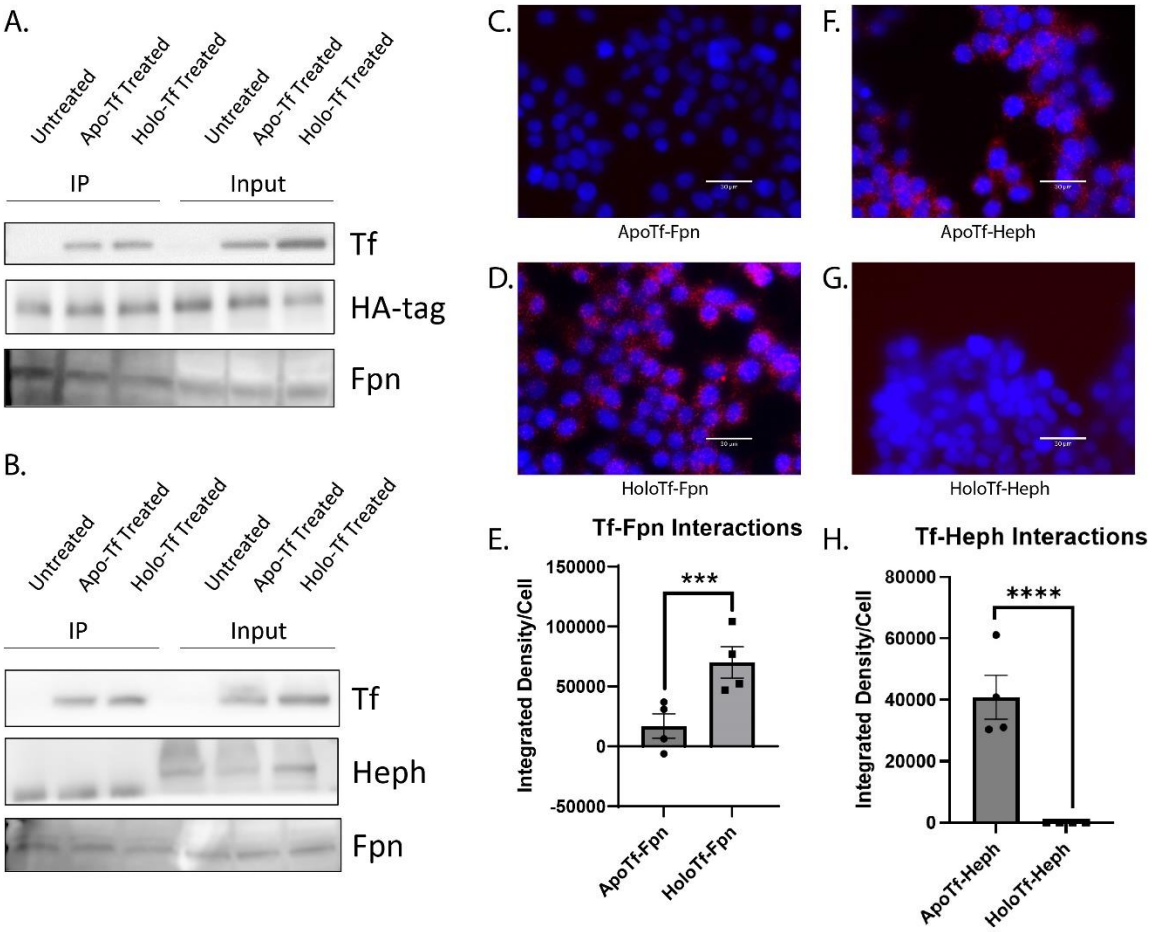

Apo- and holo-Tf interactions with Fpn and Heph. HEK 293 cells were transfected with HA-tagged Fpn and subsequently incubated with 0.25 μM apo- or holo-Tf for 10 minutes. Immunoprecipitate (IP) and 50% of cell lysate (input) was processed for immunoblotting. Co-IP of HA-Fpn shows that both apo- and holo-Tf are pulled down along with the Fpn complex (**A**). Co-IP of Heph in iPSC-derived ECs replicated these data (**B**). HEK 293 cells were used to determine direct protein interactions using PLA, reported as integrated density per cell in the field of view per image. Holo-Tf interacts with Fpn (**D**), while apo-Tf does not (**C**). Alternatively, apo-Tf interacts with Heph (**F**), while holo-Tf does not (**G**). n=4 for all experiments, means of biological replicates ± SEM were evaluated for statistical significance using unpaired t test. ***p<0.001, ****p<0.0001

3.4.3 High levels of hepcidin interrupt the interaction between holo-Tf and Fpn

Hepcidin is a well-known regulator and binding partner of Fpn, therefore we aimed to understand how the novel interaction between holo-Tf and Fpn could be impacted by physiological conditions that contribute to iron release. To do so, we used PLA to examine if hepcidin competed with holo-Tf for binding to Fpn. HEK 293 cells were co-incubated with 500 nM hepcidin (standard concentration in the literature[75,120,123]) and varying concentrations of holo-Tf (Figure 3-6A-F) for 10 minutes. All co-incubation conditions were compared to the incubation with 0.25 μM holo-Tf (Figure 3-6A). Hepcidin interrupted the interaction between 0.25 μM holo-Tf and Fpn (Figure 3-6D), resulting in an 75% reduction of PLA signal (*$p<0.05$) compared to no hepcidin treatment. Hepcidin was able to reduce the PLA signal by nearly 90% when the concentration of holo-Tf was only 0.025 μM (**$p<0.01$, Figure 3-6E). When holo-Tf was present in higher concentrations (25 μM and 2.5 μM), hepcidin did not interrupt the interactions between holo-Tf and Fpn (Figure 3-6B, C,F) but these concentrations of holo-Tf are likely pathophysiological[225].

To determine if the amount of hepcidin was crucial to the interruption of the holo-Tf and Fpn interaction, we performed the reverse competition experiment and co-incubated HEK 293 cells with 0.25 μM holo-Tf and varying concentrations of hepcidin (Figure 3-6G-K) for 10 minutes. Hepcidin interrupted the interaction between holo-Tf and Fpn in a dose dependent manner. The highest concentration of 500 nM significantly interrupted the interaction between holo-Tf and Fpn (*$p<0.05$, Figure 3-6G). However, the physiological concentration of hepcidin[224], 25 nM, had no impact on the holo-Tf-Fpn interaction (Figure 3-6J).

Figure 3-6

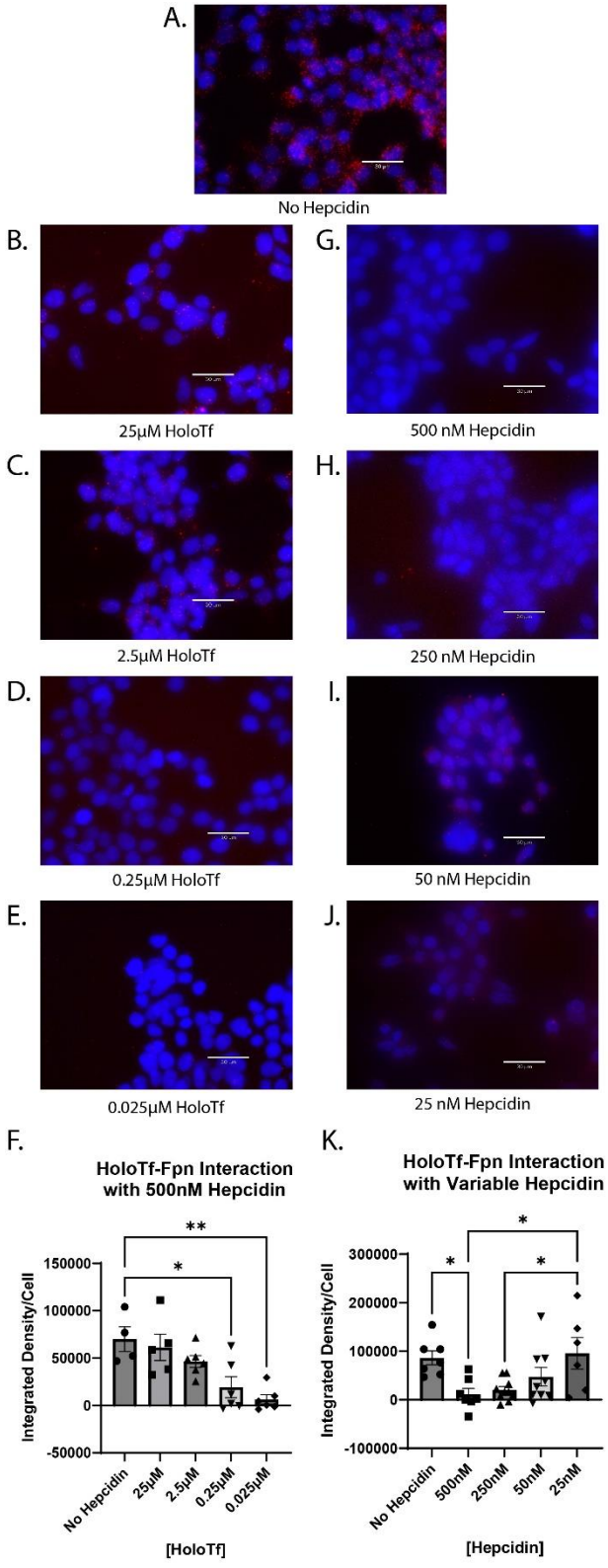

Hepcidin impact on interaction between holo-Tf and Fpn. HEK 293 cells were used to

determine the impact of hepcidin on holo-Tf and Fpn interactions using PLA, reported as integrated density per cell in the field of view per image. The level of disrupted interaction was compared to a 0.25 μM holo-Tf and no hepcidin treatment control (**A**). Cells were co-incubated with holo-Tf and hepcidin for 10 minutes. The highest concentrations of hepcidin (500 nM) interrupt the interaction between holo-Tf and Fpn when holo-Tf is present at physiological (0.25 μM) levels (**D and G**), but not at the higher concentrations of holo-Tf concentrations (25 and 2.5 μM) (**B and C**) or when hepcidin concentrations are closer to physiological baseline of 25 nM (**H-J**). n=4 to 6 for all experiments, means of biological replicates ± SEM were evaluated for statistical significance using one- way ANOVA with Tukey's post-test for significance. *$p<0.05$, **$p<0.01$

3.4.4 Hepcidin does not interrupt the interaction between apo-Tf and Heph

Apo-Tf has been shown to stimulate iron release despite the presence of hepcidin[98], thus we hypothesized that hepcidin would have no impact on the interaction between apo-Tf and Heph using PLA. HEK 293 cells were co-incubated with 500 nM hepcidin and varying concentrations of apo-Tf (Figure 3-7B-F) for 10 minutes. Unlike with holo-Tf, 500 nM hepcidin did not interrupt the interaction between apo-Tf and Heph (Figure 3-7B-E), as indicated by the unchanged PLA signal. In the reverse competition experiment, we co-incubated HEK 293 cells with 0.25 μM apo-Tf and varying concentrations of hepcidin (Figure 3-7G-K). No concentration of hepcidin was sufficient to alter the interaction between apo-Tf and Heph (Figure 3-7G-J). These data are consistent with previous findings that apo-Tf stimulates iron release from ECs even when co-incubated with hepcidin.

Figure 3-7

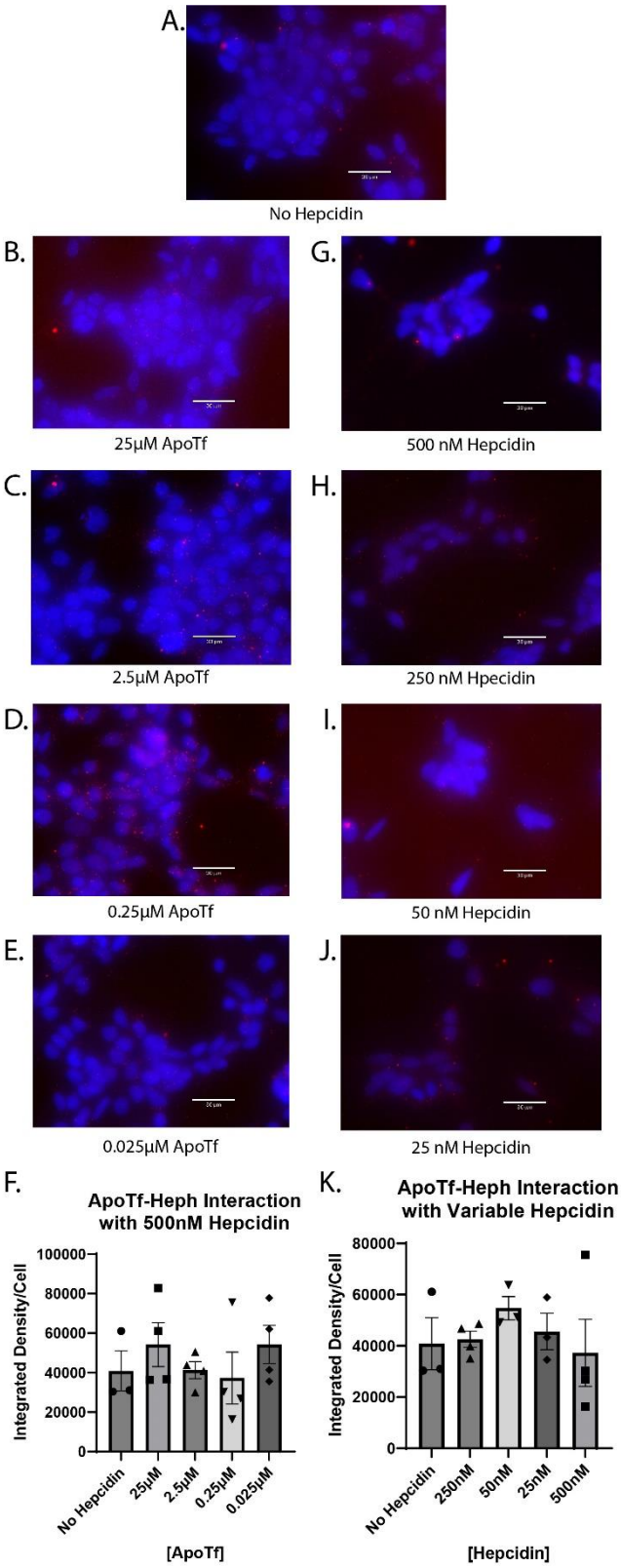

Hepcidin impact on interaction between apo-Tf and Heph. HEK 293 cells were used to

determine the impact of hepcidin on apo-Tf and Heph interactions using PLA, reported as integrated density per cell in the field of view per image. Cells were co-incubated with apo-Tf and hepcidin for 10 minutes. The level of disrupted interaction was compared to a 0.25 μM apo-Tf and no hepcidin treatment control (**A**). Hepcidin has no impact on the interaction between apo-Tf and Heph at any apo-Tf concentrations (**B-E**) or at any hepcidin concentrations (**G-J**). n=3 for all experiments, means of biological replicates ± SEM were evaluated for statistical significance using one- way ANOVA with Tukey's post-test for significance.

3.4.5 Hepcidin internalizes Fpn faster than holo-Tf

The PLA experiments showed there was competition between holo-Tf and hepcidin, but did not differentiate between the possibility that hepcidin was directly competing with holo-Tf for a binding site on Fpn or that hepcidin was internalizing Fpn faster than holo-Tf. To answer these questions, we utilized pretreatment with PYR-41, which prevents the degradation of Fpn and thus removes internalization dynamics as a factor in the binding of holo-Tf and hepcidin to Fpn. We performed PLA on HEK 293 cells exposed to 0.25 μM holo-Tf alone (Figure 3-8A), 0.25 μM holo-Tf and 500 nM hepcidin for 10 minutes (Figure 3-8B), and pretreatment of 50 μM PYR-41 for 30 minutes and then 0.25 μM holo-Tf and 500 nM hepcidin for 10 minutes (Figure 3-8C). As reported in the experiments shown in Figure 2-3D, hepcidin interrupts the interaction between holo-Tf and Fpn (*$p<0.05$), however, this decreased interaction is prevented by PYR-41 pretreatment (***$p<0.001$). This finding indicates that hepcidin decreases the interaction between holo-Tf and Fpn due to the ability of hepcidin to rapidly internalize Fpn. To further confirm a decrease of Fpn membrane presence by holo-Tf and hepcidin, we isolated membrane bound proteins following co-incubation of 0.25 μM holo-Tf and 500 nM hepcidin and found a

significant decrease of membrane Fpn protein (*p<0.05, Figure 3-8E). This decrease in membrane Fpn is prevented when cells are pretreated with PYR-41 (*p<0.01, Figure 3-8E). These data align with the PLA results and suggests that hepcidin prevents holo-Tf from binding to Fpn by inducing the rapid internalization of Fpn.

The rate of Fpn internalization induced by holo-Tf or pathophysiological levels of hepcidin was further examined by incubating HEK 293 cells with either 0.25 μM holo-Tf or 500 nM hepcidin over time and subsequently isolating the membrane bound proteins. After only 5 minutes of 500 nM hepcidin incubation, membrane Fpn levels were decreased by nearly 50% compared to holo-Tf treatment (*p<0.05, Figure 3-8G). The trend continues at incubation times of 15 minutes (***p<0.001), 30 minutes (*p<0.05), and 60 minutes (*p<0.05, Figure 3-8G). By 60 minutes, hepcidin has internalized 70% of membrane Fpn compared to holo-Tf (*p<0.05, Figure 3-8G). By 60 minutes holo-Tf internalized 20% of Fpn compared to control (Figure 3-8G).

Figure 3-8

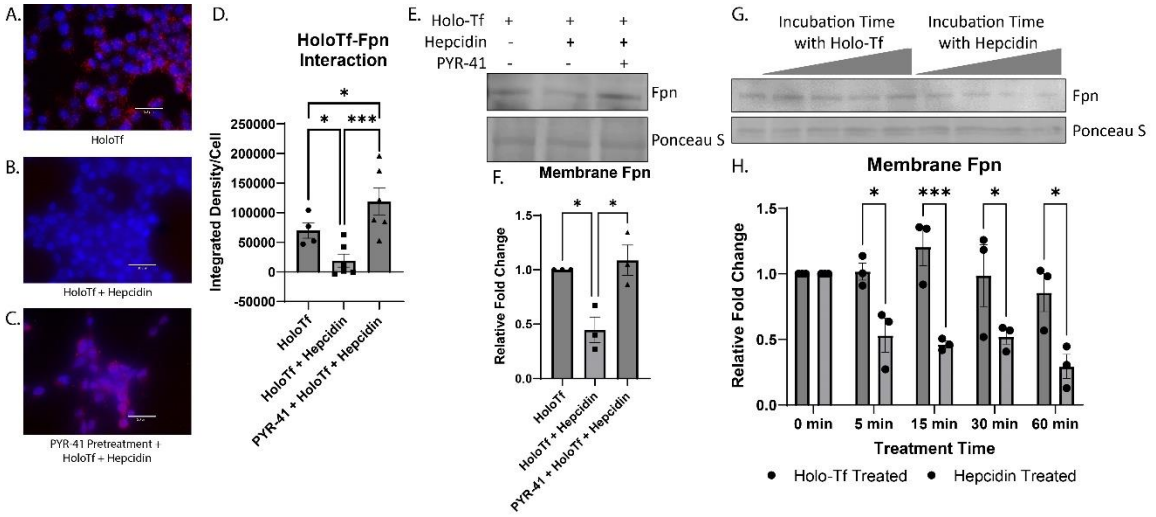

Modulation of Fpn internalization by hepcidin and holo-Tf. HEK 293 cells were used to determine the dynamics of holo-Tf and hepcidin on Fpn internalization using PLA, reported as integrated density per cell in the field of view per image (**A-D**). Pretreatment with PYR-41 (**C**) prevented the hepcidin induced reduction of interaction between holo-Tf and Fpn (**B**). The

isolation of membrane bound Fpn confirms that hepcidin and holo-Tf co-incubation greatly reduces membrane Fpn levels, and this is prevented with PYR-41 (**E-F**). Hepcidin reduces membrane Fpn at a faster rate than holo-Tf (**G-H**). n=3 to 5 for all experiments, means of biological replicates ± SEM were evaluated for statistical significance using one- way ANOVA with Tukey's posttest for significance (**D**) and (**F**) or two-way ANOVA with Sidak's post-test for significance (**H**). *p<0.05, ***p<0.001

3.5 Discussion:

This study addresses the molecular mechanisms by which apo- and holo-Tf regulate iron release from cells and provide insights to our previous findings at the BBB. More specifically, this study demonstrates that apo- and holo-Tf differentially interact with Heph and Fpn. Through its interaction with membrane bound Fpn, holo-Tf induces ubiquitination of and subsequent reduction in Fpn protein levels through the established Fpn degradation pathway. Holo-Tf directly interacts with Fpn as shown by orthogonal techniques of co-IP and PLA. Furthermore, when incubated together, high levels of hepcidin, that might correspond with inflammation or high systemic iron levels, can interrupt this interaction but not at baseline levels. The disruption in the holo-Tf and Fpn interaction by high concentrations of hepcidin appears to be due to hepcidin's ability to internalize Fpn faster than holo-Tf and not due to direct competition for the same binding site. On the other hand, hepcidin does not interrupt the interaction between apo-Tf and Heph. These findings provide insights into the mechanism of free iron release into the brain and from cells in general. The discovery of the novel Tf protein interactions using both ECs and HEK 293 cells suggests that the mechanism may be applicable to general cellular iron export regulation, specifically for cells expressing hephaestin, which is most abundant in barrier cells[236].

Fpn is the only known iron exporter, thus control of the amount of membrane bound Fpn controls release of free iron. The internalization and subsequent degradation of Fpn has been extensively studied in the context of hepcidin[75,120,123,124]. Briefly, once hepcidin binds to Fpn, it promptly triggers the ubiquitination of the Fpn, thus signaling for its internalization and lysosomal degradation. Simpson *et al.* showed that by incubating bovine retinal ECs (BRECs) with 12.5 μM holo-Tf, the levels of Fpn decreased[16]. Here, we have replicated those findings in iPSC-derived ECs but with physiological concentrations of transferrin, which is found in CSF at about 2 mg/dL, or 0.25 μM[229]. We demonstrate that a concentration of holo-Tf as low as 0.1 μM results in a 50% decrease of membrane Fpn. These data provide a mechanistic explanation for why we have reported holo-Tf suppresses iron release from ECs[16,18]. What's more, other iron-related proteins, such as Heph, DMT1, and TfR, are relatively unchanged. Interestingly, even when exposed to high amounts of holo-Tf, the levels of Fpn do not decrease beyond 50%, suggesting there is a plateaued effect of holo-Tf within the 8-hour experimental time window. The holo-Tf-mediated internalization of Fpn is blocked when the ubiquitination of Fpn is inhibited. Furthermore, incubation of 0.25 μM holo-Tf starts to induce Fpn ubiquitination within 1 hour and peaks at about 3 hours. Taken together, these data suggest that holo-Tf exerts its effect through the established degradation pathway, similar to hepcidin. Interestingly, the binding of hepcidin to Fpn immediately results in Fpn ubiquitination[123], whereas the binding of holo-Tf to Fpn seems to have a delayed ubiquitin response. We hypothesize that holo-Tf physically blocks the function of Fpn, causing an internal cellular mechanism to tag a seemingly faulty Fpn for degradation.

To complete the process of iron export from the endothelial cells, Fpn interacts with a complex of proteins, including Heph[76,223]. Heph is a ferroxidase primarily expressed in barrier cells, such as ECs and enterocytes[236], that converts the Fpn-exported ferrous (Fe2+) to ferric (Fe3+) that can bind to apo-Tf and be utilized by cells. Numerous studies have shown that Heph

is required to stabilize Fpn in the plasma membrane and to enable iron export[76,223,237,238]. We have replicated these findings, by demonstrating that Fpn and Heph can be co-immunoprecipitated from ECs. Furthermore, we demonstrate the novel finding that both apo- and holo-Tf independently are co-immunoprecipitated with Fpn and Heph. These results suggest that apo- and holo-Tf bind to Fpn and Heph in a complex of iron export proteins. In order to narrow down which protein holo-Tf bound to in the membrane that resulted in decreasing Fpn, we employed PLA. We found that holo-Tf directly interacts with Fpn, while apo-Tf does not. On the other hand, apo-Tf interacts with Heph, while holo-Tf does not, a finding that is supported in the literature[103,104,107]. It is hypothesized that apo-Tf binds to Heph to accept the ferric iron that Heph converts from ferrous iron. This stimulates the release of more iron as long as there is apo-Tf to accept it. Taken together these data suggest that apo- and holo-Tf differentially interact with iron export proteins, likely due to their structural differences[239]. The exact binding sites, conformation changes, and catalysts for these interactions are an exciting unexplored area that could pave the way for clinical manipulation. For example, as has been done experimentally[17], Tf could be infused to modulate iron accumulation in diseases in which it is dysregulated. Additionally, pharmaceuticals could be designed to facilitate or inhibit the endogenous protein interactions in an effort to correct brain iron accumulation.

Prior to the discovery that elevated holo-Tf could suppress iron release, hepcidin was the primary focus of iron release regulation[126]. Hepcidin is a pro inflammatory hormone peptide primarily secreted by the liver and upregulated in environments of inflammation and high iron levels[113]. Astrocytes[114,115] and the choroid plexus[116,117] have also been shown to secrete hepcidin, though in much smaller amounts that cannot account for total brain hepcidin levels[117,118], suggesting much of the brain hepcidin comes from systemic levels when pathologically necessary, though this has not yet been proven. A number of groups have shown that astrocytic hepcidin reduces Fpn levels and subsequent iron release[101,125,240]. However, we have previously

demonstrated that pathophysiological levels of hepcidin are not capable of blocking iron release from ECs[18,98]. These data suggest that hepcidin cannot be the sole regulator of iron release in the brain. In support of this notion, Enculescu *et al.* modeled iron levels, and when compared to their experimental results, the study found that hepcidin control over iron uptake was necessary, but not sufficient[132]. Once a secondary regulatory mechanism was added to the model, their experimental results aligned with the model[132]. Thus, our data directly support that hepcidin is not the sole regulator of iron release and indicate the additional regulators are apo- and holo-Tf.

Our data offer an opportunity to explore the concept of regulation of iron uptake in general by hepcidin. We found that hepcidin competes with holo-Tf for binding to Fpn at low holo-Tf and high, pathophysiological hepcidin concentrations. However, when there was more holo-Tf or less hepcidin present, this effect was reduced. Notably, when hepcidin was only present at physiological levels[224], there was no interruption of the interaction between holo-Tf and Fpn. These findings suggest that hepcidin is only effective at controlling Fpn at levels consistent with inflammation or high iron. In observing competition between holo-Tf and hepcidin for Fpn binding, the internalization of Fpn was inhibited to determine if the competition was for binding site availability or rate of internalization. By preventing the internalization of Fpn, hepcidin had no impact on the interaction between holo-Tf and Fpn. This suggests that hepcidin internalizes Fpn faster than holo-Tf, which was confirmed by isolating membrane Fpn. Hepcidin reduces membrane Fpn by nearly 50% in 5 minutes, whereas holo-Tf only reduces membrane Fpn by 20% after 60 minutes. This finding is supported by Wallace *et al.* that showed hepcidin internalizes 50% of Fpn within 10 minutes[124]. On the other hand, no amount of hepcidin impacts the interaction between apo-Tf and Heph. These data offer the intriguing suggestion that if apo-Tf is present, it will bind to Heph even in pathophysiological states and may be an explanation for iron accumulation in neurodegenerative disease. It has been postulated that in Alzheimer's disease[241] and Parkinson's disease[178] the brain may start as functionally iron deficient, along with

elevated levels of apo-Tf, which triggers increased iron uptake until the excess iron detrimentally damages the BBB and surrounding cells. The question remains however, if the binding of apo-Tf to Heph will continue to stimulate iron release in the presence of hepcidin.

The model of apo- and holo-Tf regulation of iron release from ECs is a feedback loop. As cells, such as neurons or astrocytes, need iron for metabolic processes, myelin synthesis, or dopamine synthesis, they take up holo-Tf through TfR[95]. Once endocytosed, the iron is removed and the resulting apo-Tf is released[95]. The communication of brain iron status via apo- and holo-Tf allows cells to signal their iron needs based on their iron consumption. Numerous studies have shown higher regional iron uptake that correspond to areas with higher iron needs[67,96,97]. Our pervious data suggest that as the apo- to holo-Tf ratio changes in the extracellular fluid, more iron is released locally from the BBB. In support of this notion are data showing CSF from iron deficient monkeys and iron chelated astrocytes increase iron release from cultured BRECs, while iron loaded biological samples resulted in decreased iron release[16]. These data have been replicated when cells are exposed to apo- or holo-Tf directly[16,18,98] or when apo- or holo-Tf is directly infused into the brain[17]. In all studies mentioned here, apo-Tf increased iron release while holo-Tf decreased iron release.

The data in this study expand the model for brain iron uptake by suggesting that apo-Tf stimulates iron release by binding to Heph to access exported free iron (Figure 3-9A). Once loaded with iron, the now holo-Tf becomes available to surrounding cells. If the levels of holo-Tf in the extracellular fluid rise, holo-Tf binds to Fpn to suppress more iron release (Figure 3-9B). The internalization of Fpn by holo-Tf is not rapid, unlike hepcidin. When upregulated and present in high amounts, hepcidin can rapidly internalize Fpn (Figure 3-9C). Thus, we propose that hepcidin is likely used as a fast acting, immediate stop to iron release in environments of inflammation and very high iron. However, for moment-by-moment regional control of iron release, holo-Tf may be a better candidate to regulate regional iron supply.

Figure 3-9

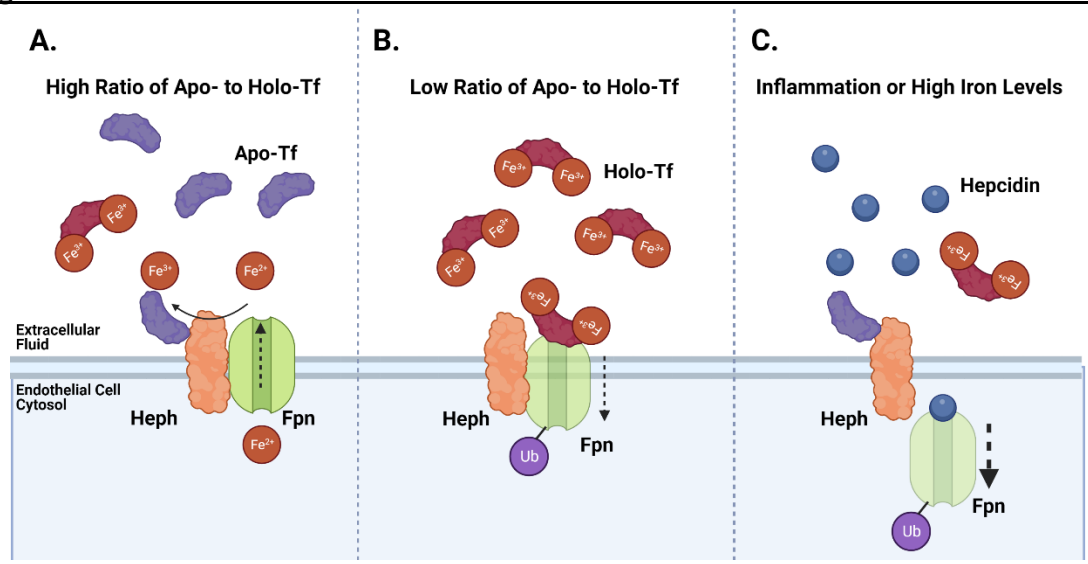

Model of Iron Release Regulation. In our proposed model, in areas that have higher ratios of apo- to holo-Tf (**A**), apo-Tf binds to Heph in order to accept the exported free iron and further stimulates iron release through Fpn. Alternatively, areas of lower ratios of apo- to holo-Tf (**B**), excessive holo-Tf binds to Fpn to facilitate the ubiquitination, internalization, and degradation of Fpn, and thus suppressing iron release through Fpn. In environments of inflammation or high iron levels, hepcidin production is upregulated (**C**). Hepcidin binds to Fpn and rapidly triggers Fpn's internalization and abruptly stop free iron release.

The regulation of brain iron uptake is not influenced by systemic levels[58], thus the regulation appears to come from the brain. Moreover, there are regional differences in the amount of iron in the brain. The data herein provide insights into a local regulatory process. This study is the first demonstration that apo- and holo-Tf differentially interact with Fpn and Heph to regulate iron release from ECs of the BBB. Moreover, we have identified a physiologically relevant dynamic between hepcidin and holo-Tf and their influence on membrane Fpn levels. Hepcidin interrupts the interaction between holo-Tf and Fpn by internalizing Fpn much faster than holo-Tf. Furthermore, we show that hepcidin does not interrupt the interaction between apo-Tf and

hepcidin. These data suggest the mechanism of free iron release from ECs at the BBB that is likely relevant to cellular iron release in general. These results provide guidelines for further studies in neurological disease models where the iron regulatory mechanism may be disrupted and may provide additional insights of iron regulation beyond the BBB.

Chapter 4

Amyloid-β exposed astrocytes induce iron transport from endothelial cells at the blood-brain barrier by altering the ratio of apo- and holo-transferrin

This work has been previously submitted as:

Baringer, S.L., Lukacher, A.S., Palsa, K., Kim, H., Lippmann, E.S., Spiegelman, V.S., Simpson, I.A., Connor, J.R. *Amyloid-β exposed astrocytes induce iron transport from endothelial cells at the blood-brain barrier by altering the ratio of apo- and holo-transferrin*. Journal of Neurochemistry. In revision

4.1 Abstract:

Excessive brain iron accumulation is observed in early in the onset of Alzheimer's disease, notably prior to widespread proteinopathy. These findings suggest that increases in brain iron levels are due to a dysregulation of the iron transport mechanism at the blood-brain barrier. Astrocytes release signals (apo- and holo-transferrin) that communicate brain iron needs to endothelial cells in order to modulate iron transport. Here we use iPSC-derived astrocytes and endothelial cells to investigate how early-disease levels of amyloid-β disrupt iron transport signals secreted by astrocytes to stimulate iron transport from endothelial cells. We demonstrate that conditioned media from astrocytes treated with amyloid-β stimulates iron transport from endothelial cells and induces changes in iron transport pathway protein levels. The mechanism underlying this response begins with increased iron uptake and mitochondrial activity by the astrocytes which in turn increases levels of apo-transferrin in the amyloid-β conditioned astrocyte media leading to increased iron transport from endothelial cells. These novel findings offer a

potential explanation for the initiation of excessive iron accumulation in early stages of Alzheimer's disease. What's more, these data provide the first example of how the mechanism of iron transport regulation by apo- and holo-transferrin becomes misappropriated in disease to detrimental ends. The clinical benefit from understanding early dysregulation in brain iron transport in AD cannot be understated. If therapeutics can target this early process, they could possibly prevent the detrimental cascade that occurs with excessive iron accumulation

4.2 Background:

Alzheimer's disease (AD) is a progressive neurodegenerative disease that is characterized clinically by memory impairment and cognitive decline and pathologically by amyloid-β (Aβ) plaques and neurofibrillary tau tangles. In addition to these hallmark pathologies, excessive brain iron accumulation is repeatedly observed in AD patients[10,133,135,141]. Unique patterns of regional brain iron accumulation[133,136] correlate with disease progression and can reliably predict cognitive impairment in AD patients[10]. Recently, Ayton *et al.* have shown that brain iron accumulation occurs early in AD and prior to widespread Aβ or tau pathology distribution[133], suggesting iron uptake dysfunction occurs independent from the vascular damage Aβ can inflict in later stages of the disease[145]. Anemic and iron transport processes are also upregulated in AD patient brain tissue[242], proposing the hypothesis that the AD brain may operate in functional iron deficiency.

Brain iron uptake is tightly regulated by endothelial cells (ECs) of the blood-brain barrier (BBB)[16–19]. Our group and others have shown that astrocytes release signals that modulate iron release from ECs[16,101]. Importantly, the iron status of astrocytes modulates iron release from ECs based on astrocytic iron needs: iron depleted astrocytes stimulate iron release whereas iron saturated astrocytes suppress iron release[16]. A mechanism for regulating iron release is the ratio of apo- (iron free) to holo- (iron bound) transferrin (Tf) in the extracellular fluid to increase and

decrease iron release, respectively[17,18,98]. We have also demonstrated this mechanism *in vivo* in healthy mice[17]. In this study we address if the model of apo- and holo-Tf ratio regulating iron release can be misappropriated in a disease setting. Numerous neurological diseases display alterations in brain iron levels that lead or contribute to pathology and symptoms[6], but it has remained unknown if altered iron levels were due to a dysregulation of iron transport mechanisms.

The majority of iron and AD research has focused on how iron can accelerate and contribute to Aβ and tau pathology deposition[243]. Despite the clear correlation between AD progression and brain iron accumulation, there has been a lack of attention in deciphering causes for increased iron uptake into the brain. In the present study, we offer a model for iron uptake initiation by the way of dysregulation in iron release signals. We demonstrate that astrocytes treated with low levels of Aβ increase their iron uptake, resulting in an increased release of apo-Tf which is a signal of iron deficiency and thus stimulates iron release from ECs. These results provide significant insight into mechanism of iron uptake regulation in response to early AD pathology.

4.3 Methods:

4.3.1 Cell Culture

Human brain endothelial-like cells (ECs) were differentiated from ATCC-DYS0100 human iPSCs as described previously[90,226]. Briefly, iPSCs were seeded onto a Matrigel-coated plate in E8 medium (Thermo Fisher Scientific, 05990) containing 10 μM ROCK inhibitor (Y-27632, R&D Systems, 1254) at a density of 15,000 cells/cm^2. The iPSC differentiation was initiated by changing the E8 medium to E6 medium (Thermo Fisher Scientific, A1516401) after

24 hours seeding. E6 medium was changed every 24 hours and cells were maintained in E6 medium up to 4 days. After 4 days, cells were switched to human endothelial serum free medium (hESFM) (Thermo Fisher Scientific, 11111) supplemented with 10nM bFGF (Fibroblast growth factor, Peprotech, 100-18B) and 10 μM all-trans retinoic acid (RA, Sigma, R2625) and 1% B27 (Thermo Fisher Scientific, 17504-044). Medium was not changed for 48 hours. After 48 hours, cells were collected and replated onto Transwell filters coated with collagen IV and fibronectin. Twenty-four hours after replating, bFGF and RA were removed from the medium to induce barrier phenotype.

iPSC-derived astrocytes were generated using the CC3 iPSC line as described perviously[244]. The undifferentiated iPSCs were cultured in E8 medium on 6-well plates coated with growth factor-reduced Matrigel (Corning). When the iPSCs reached 60-80% confluency, they were subcultured using Versene (Thermo Fisher Scientific). For differentiation, the iPSCs were dissociated using Versene and seeded in low-attachment plates to form embryoid bodies (EBs) with a density of $4x10^5$ cells/well in E6 medium supplemented with 100x N2 and 10 μM Y27632. Neural differentiation in the EBs was achieved through dual inhibition of SMAD signaling for 7 days. Subsequently, the EBs were seeded onto Matrigel-coated plates and cultured for another 7 days. During this time, NPCs were manually isolated and expanded as neurospheres in suspension culture for 7 days. The neurospheres were then dissociated into single cells and seeded onto Matrigel-coated plates for directed astroglial differentiation for 30 days. Medium changes were done every 48 hours with astroglia medium containing 10 ng/mL BMP-4 (PeproTech, 120-05ET), 10% N2 supplement (ThermoFisher, 17502-048), 20% B27 supplement (ThermoFisher, 12587-010), 20 ng/mL bFGF (PeproTech, 100-18B), and 10% penicillin-streptomycin (Hyclone, SV30010), and the cells were passaged at approximately 80% confluency.

4.3.2 Aβ Peptide Preparation and Treatment

$A\beta_{42}$ was prepared as previously described[245,246]. Briefly, chilled hexafluoroisopropanol (HFIP) was added to $A\beta_{42}$ peptide (Alfa Aesar, J66387) to obtain a concentration of 1 mM. The peptide solution was sonicated for 5 minutes and incubated at room temperature for 30 minutes. The solution was divided into single use aliquots. HFIP was removed via overnight evaporation and further exsiccated in vacuo in a lyophilizer. The tubes were stored at -80 °C. To use, the peptide film was reconstituted in corresponding cell culture media with sonication for 10 minutes. Cells were treated with 50 nM $A\beta_{42}$ for all experiments.

4.3.3 Radiolabeling

^{55}Fe (Perkin Elmer) was complexed with 1 mM nitrilotriacetic acid (NTA), 6 mM ferric chloride ($FeCl_3$), and 0.5 M sodium bicarbonate ($NaHCO_3$) at a ratio of 100 µL NTA: 6.7µL $FeCl_3$: 23.3 µL $NaHCO_3$: 50 µCi $^{55}FeCl_3$ to form the ^{55}Fe-NTA complex[17]. After complexing, ^{55}Fe-NTA was either used immediately or incubated with apo-Tf (Sigma) for 30 minutes to allow for iron loading. Unbound iron was separated from the total complex using PD midiTrap-G25 columns following manufacturer's instructions (GE Healthcare Bio-Sciences).

4.3.4 ^{55}Fe-Tf Transport Studies

The radiolabeled iron transport studies were described previously[90]. Initially, the apical chamber of 12-well Transwell plates (Costar Transwell, 0.4 µm pore, Corning) was coated with collagen IV (Sigma) and fibronectin (Sigma) at a ratio of 5:4:1 of ddH2O, 1 mg/ml collagen IV, and 1 mg/ml fibronectin respectively. A total of 200 µl was used to coat plates 4 h at 37 °C. Following coating, the differentiated ECs were replated onto the coated filters. The basal chamber

was filled with 1.5 mL of the same media. After allowing the cells to attach overnight at 37 °C, the media was changed in both chambers to hESFM, supplemented with 1% B27, but lacking bFGF and RA. Cells were incubated at 37 °C overnight to allow growth and tight junction formation, after which all transport studies were performed. Before experimental media addition, trans endothelial electrical resistance (TEER) measurements were taken using an Epithelial Volt/Ohm Meter (EVOM2, STX2, World Precision Instruments). Blank (media only) TEER readings were obtained and subtracted from all other TEER measurements. Across all experimental conditions, we report an average TEER value of $3800 \pm 126\ \Omega \times cm^2$. At the beginning of the experiment, all media was removed. 500 µl of serum-free media were added to the apical chamber containing,10 µCi of ^{55}Fe-Tf (1 mg/ml) and 1 mg/ml RITC-Dextran (70 kD, Sigma) – to monitor tight junction formation and barrier. In the basal chamber, 1.8 mL of the experimental media was placed. At hours 0, 4, 8, and 24, 100 µl was removed from the basal chamber and added to scintillation vials along with 10 mL CytoScint scintillation cocktail (MP Biosciences). Samples were counted using the Hidex 300 SL (LabLogic) for three minutes each. Blank tube values were subtracted from final counts to correct for background counts. At hours 0, 4, 8, and 24, an additional 100 µl was removed from the basal chamber to measure RITC fluorescence (excitation: 555 nm, emission: 580 nm) on a SpectraMax Gemini EM plate reader (Molecular Devices).

4.3.5 Protein Detection in Media

Frozen aliquoted media samples were thawed for protein detection. $A\beta_{42}$ levels were measured by enzyme-linked immunosorbent assay (Invitrogen, KHB3441). Soluble amyloid precursor protein α (sAPP-α) levels were measured by enzyme-linked immunosorbent assay (IBL, 27734). Interleukin-6 (IL-6) levels were measured by enzyme-linked immunosorbent assay

(R&D Systems, D6050). Lactate dehydrogenase (LDH) levels were measured using Cytotoxicity Detection Kit (Roche, 11644793001) according to manufacturer's directions.

The ratio of apo- to holo-Tf was determined using a urea gel shift assay similar to previously described methods[247]. Briefly, urea binds to the unoccupied iron binding sites on apo-Tf, which results in apo-Tf running slower through a gel and separating from holo-Tf. Conditioned media was concentrated 10x using Amicon Ultra-15 centrifugal filter units 10kD (Millipore, UFC901024). To pull down Tf from the media, 10 µl of anti-transferrin antibody (Abcam, ab82411) was incubated with 100 µl Dynabeads Protein A (Thermo, 10001D). After washing, 100 µl of concentrated media sample was added and allowed to incubate with rotation overnight. The next day, after washing, Tf was eluted from the magnetic beads using 200 µl urea-based elution buffer (8 M urea, 20 mM Tris, pH 7.5, and 100 mM NaCl) with gentle agitation three times. The eluted solution was then concentrated 20x using Amicon Ultra-0.5 centrifugal filer units 50 kD (Millipore, UFC505024). The resulting concentrate was mixed in equal part with TBE urea sample buffer (Bioworld 10530025-1) and loaded on a 10% 15-well TBE urea gel (Biorad 4566036). The gel was run at 170V for 5 hours, after which the gels was washed with water and all protein was stained using RAPIDstain (Calbiochem, 553215) for 1 hour. After additional washing, the stained gel was imaged on an Amersham Imager 600 (GE Amersham). To quantify the percentage of apo-Tf present in samples, a standard curve was made with percentages of apo- and holo-Tf totaling 5 µg of protein. The band intensities of apo- and holo-Tf were determined and the ratio of apo:holo was calculated. The ratio value was plotted against the percentage of apo-Tf to create the standard curve (Figure 4-1).

Figure 4-1

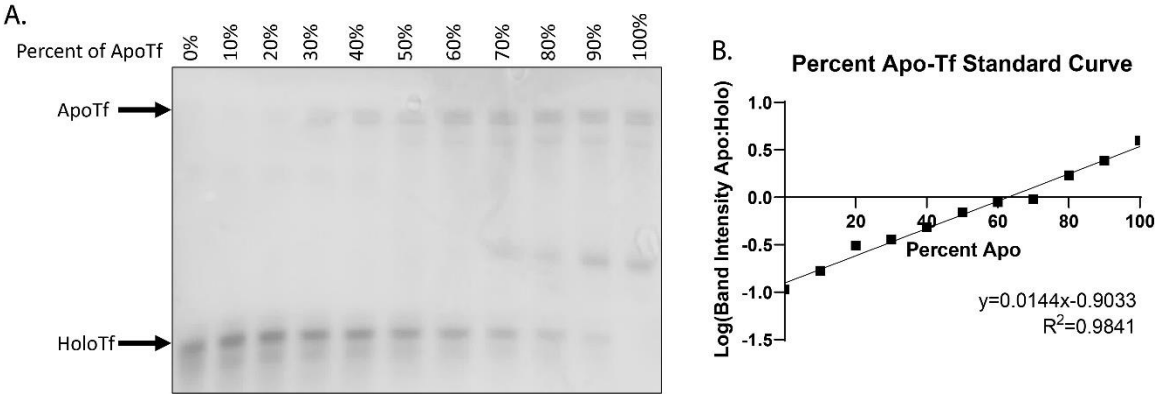

Urea Gel Shift Tf Standard Curve. In order to more accurately determine the percentage of apo-Tf present in experimental CM samples, a standard curve was created (**A**). Set percentages of apo- and holo-Tf were mixed together. Five µg of protein was run on TBE-urea gels and Tf bands were visualized using total protein stain. Because urea binds to the available iron binding sites on apo-Tf, apo-Tf runs slower through the gel compared to holo-Tf. This results in apo- and holo-Tf reliably separating as shown here (**A**). The band intensity of both apo- and holo-Tf were determined and the ratio of apo:holo was calculated. After performing the experiment three times, the ratios were averaged together. The log of the band intensity ratio was plotted against the known percent of apo-Tf in the solution to create the standard curve (**B**). The equation of the linear regression was used to determine the unknown percent of apo-Tf in CM samples based on the experimentally determined band intensity ratio.

4.3.6 Iron content

Astrocyte media iron concentrations were measured by the ICP-AES method. Briefly, 1:1 volumes of media and 70% ultrapure nitric acid were added to glass tubes and incubated at 60 °C for 18 hours. Digested media was centrifuged at 10,000 g for 10 minutes at room temperature, and the supernatant fraction was collected and diluted with metal-free water. Iron concentration

was determined ICP-AES against internal standards. Results were expressed as µg Fe/ml of media.

4.3.7 ^{55}Fe Uptake

Astrocytes were plated 20,000 cells/cm^2 on Matrigel-coated plates. The following day, cells were co-incubated with either 50 nM Aβ or untreated control and 5 µCi of ^{55}Fe-NTA. After 72 hours of incubation, the cells were washed x3 with PBS and then dissolved in 100 µl 0.2 M NaOH for 30 minutes. Once fully dissolved, the solution was collected and added to scintillation vials along with 10 mL CytoScint scintillation cocktail (MP Biosciences). Samples were counted using the Hidex 300 SL (LabLogic) for three minutes each. Blank tube values were subtracted from final counts to correct for background counts. Blank Matrigel-coated wells were simultaneously incubated with either 50 nM Aβ or untreated control and 5 µCi of ^{55}Fe-NTA and further processed to subtract any Matrigel-captured ^{55}Fe.

4.3.8 Mitochondrial Activity

Astrocytes were plated 20,000 cells/cm^2 on Matrigel-coated plates. The following day, cells were co-incubated with either 50 nM Aβ or untreated control and 1:50 CCK8 reagent (Abcam, ab228554) and astroglial media. CCK8 uses a tetrazolium salt that is reduced in the presence of active mitochondria; thus it was used as a measure of metabolic activity. After 72 hours of incubation, media was collected and absorbance was read at 460 nm. To normalize the results to cell count, the cells were washed with PBS and lifted using TrypLE Express Enzyme (Thermo, 12604013). The cell solution was spun down and the pellet resuspended. Cell count was

obtained using trypan blue and the Countess II Cell Counter (Thermo). There was no change to cell count with control or Aβ treatment.

As an addition measure of mitochondrial activity, citrate synthase activity was measured by Citrate Synthase Activity Assay Kit (ab119692). Astrocytes were plated 20,000 cells/cm^2 on Matrigel-coated plates. The following day, cells were co-incubated with either 50 nM Aβ or untreated control in astroglial media After 72 hours of incubation, the cells were collected and assayed per the manufacture's instruction. Results are reported as the change in mean absorbance per μg of protein in each sample.

4.3.9 Immunoblotting

Samples were loaded onto a 4-20% Criterion TGX Precast Protein Gel (Bio-Rad)[17]. Protein was transferred onto a nitrocellulose membrane and probed for Fpn (Alpha Diagnostics, MTP11-S, 1:1000), DMT1 (Millipore, ABS983, 1:1000), Heph (Santa Cruz, SC-365365, 1:1000), TfR (Santa Cruz, sc-65882, 1:250), NEP-1 (ProteinTech, 18008-1-AP, 1:1000), APP (ProteinTech, 60342-1-Ig, 1:1000), IRP1 (Cell Signaling, 20272, 1:1000), IRP2 (Cell Signaling, 37135, 1:1000), FTH (Cell Signaling, 4393 1:1000), FTL (Abcam, ab69090 1:1000), Cytochrome C (ProteinTech, 66264-1-Ig, 1:1000), TOM20 (ProteinTech, 66777-1-Ig, 1:1000), and beta-actin (Sigma, a5441, 1:1000) or cyclophilin B (Abcam, ab16045, 1:1000) as a loading control. Corresponding secondary antibody conjugated to HRP was used (1:5000, GE Amersham) and bands were visualized using ECL reagents (Perkin-Elmer) on an Amersham Imager 600 (GE Amersham). Cellular lysate samples were normalized to cyclophilin B protein as a loading control, and then subsequently normalized to an untreated control sample within each experiment. Membrane protein samples were stained with Ponceau S and normalized to total protein as a loading control.

4.3.10 Statistical Analysis

Statistical analyses were performed using Prism 9.5 software (Graphpad Software Inc.). Data from at least three independent biological replicates were averaged and are expressed as the mean ± standard error of the mean (SEM). One-way ANOVA with Tukey post-hoc analysis, two-way ANOVA with Sidak's post hoc analysis, or unpaired t-tests were used to evaluate for statistical significance. A p-value <0.05 was considered significant. For each experiment, n indicates 2-3 wells of cells pooled together for one replicate and a different passage of cells per n.

4.4 Results:

4.4.1 Media from Aβ-treated astrocytes increases iron transport from ECs

To first determine if Aβ-treated astrocytes could stimulate the transport of iron from ECs, astrocytes were treated with 50 nM Aβ for 72 hours to simulate the chronic nature of Aβ exposure. The control condition was no Aβ exposure. The conditioned media (CM) was collected from both control and Aβ-treated astrocytes. ECs were cultured onto Transwell inserts and control CM or Aβ CM was placed in the basal chamber to represent the brain-side. In the apical chamber, ^{55}Fe-Tf and RITC-dextran were added, and at various intervals, aliquots were taken from the basal chamber to measure the transport of ^{55}Fe-Tf and the leakage of RITC-dextran. ECs incubated with Aβ CM displayed a significant 3-fold increase of ^{55}Fe-Tf transport over 24 hours (**$p<0.01$, Figure 4-2A). Neither Control CM nor Aβ CM induced any barrier leakage (Figure 4-2B).

To further investigate changes in iron regulatory proteins resulting in an increase of iron transport, ECs were collected for immunoblotting after basal incubation of control CM and Aβ CM for 8 hours. Ferroportin (Fpn), the only known iron exporter protein, was increased by nearly

3-fold in ECs incubated with Aβ CM (**p<0.01, Figure 4-2C). Divalent metal transporter (DMT1), which transports from the endosome into the cytosol was also increased (*p<0.05, Figure 4-2C). Hephaestin (Heph) and transferrin receptor (TfR) were unchanged (Figure 4-2C).

Figure 4-2

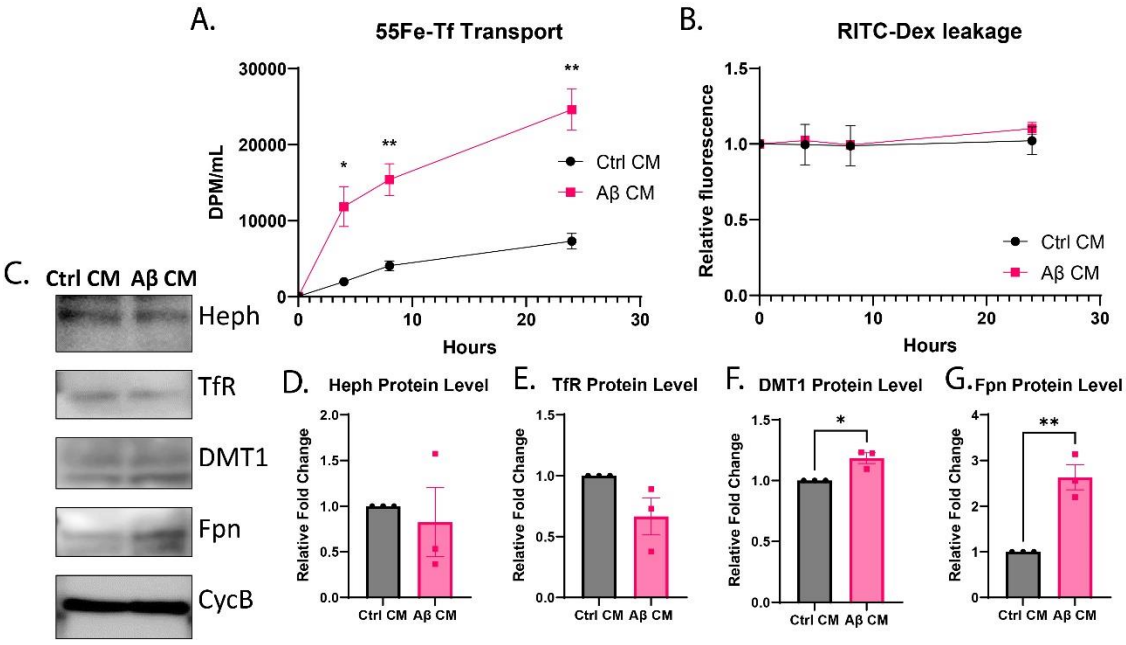

Modulation of iron transport from ECs by Aβ conditioned media from astrocytes. iPSC-derived astrocytes were treated with nothing (control) or 50 nM Aβ and the respective control (Ctrl) conditioned media (CM) and Aβ CM were collected after 72 hours. iPSC-derived ECs were cultured on bi-chamber plates and incubated with Ctrl CM or Aβ CM in the basal chamber and 10 μCi 55Fe-Tf and 1mg/ml RITC-dextran in the apical chamber. Aliquots were taken from the basal chamber to measure 55Fe-Tf transport and RITC-dextran leakage. ECs incubated with Aβ CM had a 3-fold increase of 55Fe-Tf transport (**A**) with no change to monolayer permeability (**B**) compared to ECs exposed to Ctrl CM. ECs incubated with Ctrl CM and Aβ CM for 8 hours were collected for immunoblotting with all proteins normalized to cyclophilin B (CycB) (**C**). Hephaestin (Heph) (**D**) and transferrin receptor (TfR) (**E**) levels were unchanged in either condition. Divalent metal transporter (DMT1) (**F**) and ferroportin (Fpn) (**G**) levels were increased

in ECs exposed to Aβ CM. n=3 for all experiments, means of biological replicates ± SEM were evaluated for statistical significance using two- way ANOVA with Sidak's posttest for significance (A-B) or using unpaired t-test (D-G). *p<0.05, **p<0.01

4.4.2 Aβ-conditioned media contains known iron transport stimulators

In observing increased iron transport from ECs and corresponding changes to iron transport proteins after Aβ CM incubation, we examined multiple components of the control CM and Aβ CM previously demonstrated to have an impact on iron transport in ECs[16,148,151,248]. First, the levels of $A\beta_{42}$[148] were measured in control CM, Aβ CM, and media alone (never exposed to cells) with 50 nM Aβ added to determine how much Aβ remained in the CM after incubation with astrocytes. Aβ CM contained about 10% less Aβ than the media where 50 nM Aβ was added (*p<0.05, Figure 4-3A), which is consistent with literature suggesting that astrocytes participate in Aβ clearance[249]. Iron levels[16] in the control CM, Aβ CM, and media alone were determined using ICP-MS. Aβ CM contained 50% less iron than control CM (**p<0.01) and was below media without cells (Figure 4-3B), indicating an increase of iron uptake by the astrocytes. To accompany the decrease of media iron content, we hypothesized the percentage of apo-Tf (iron free) would be similarly increased. To determine the percentage of apo-Tf in the media samples, we used a urea gel shift assay (Figure 4-3C). The band intensity of both apo- and holo-Tf were determined and the ratio was compared to the standard curve (Figure 4-1) to determine the percentage of apo-Tf. Aβ CM contained twice as much apo-Tf compared to control CM (****p<0.0001, Figure 4-3D). Additional suspected iron stimulators were measured by ELISA. Soluble amyloid precursor protein-α (sAPP-α)[248] in control CM and Aβ CM were measured and found to be elevated 2-fold in Aβ CM (**p<0.01, Figure 4-3E). As a measure of general cytokine

production, IL-6[151] was elevated 1.5-fold in Aβ CM compared to control CM (****p<0.0001, Figure 4-3F).

Figure 4-3

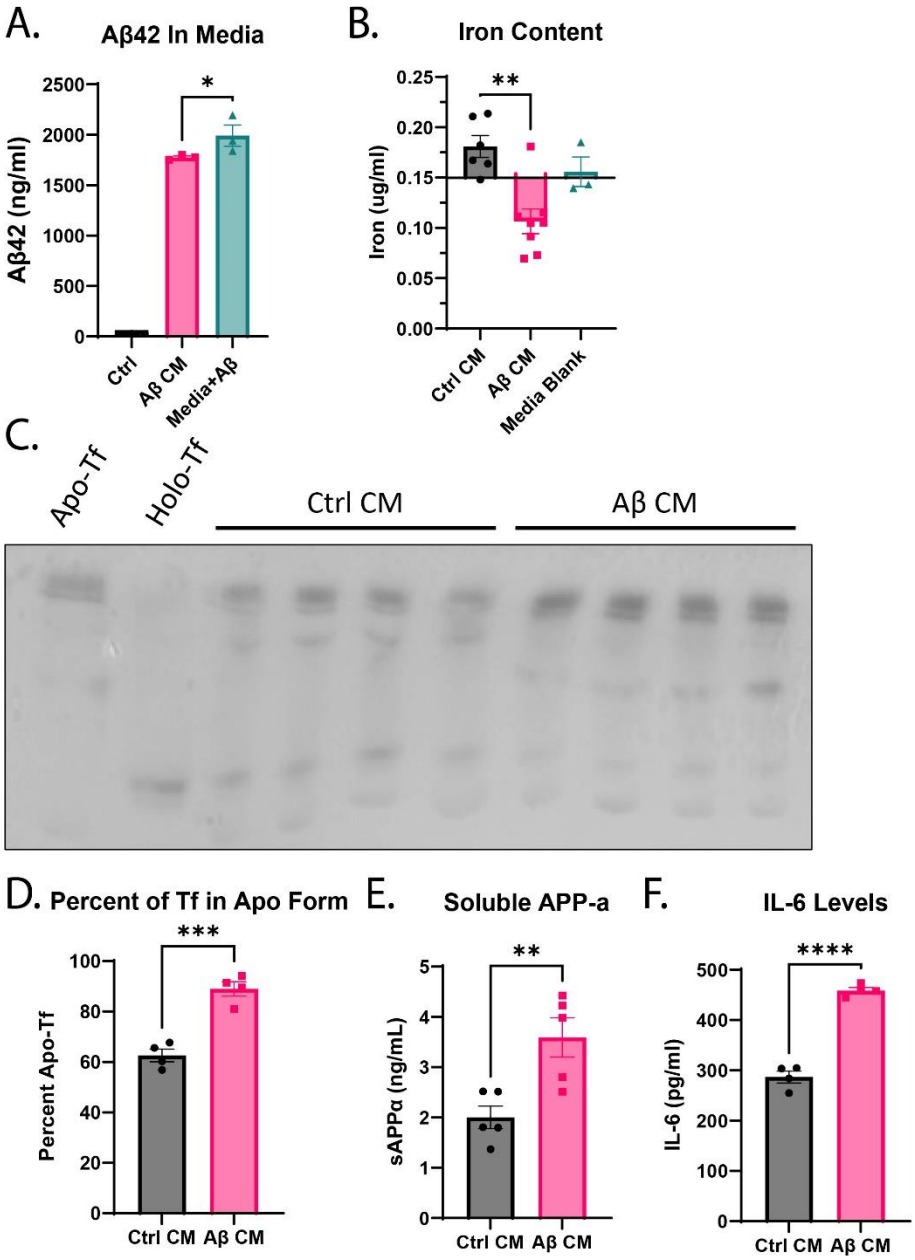

Potential iron transport stimulators found in conditioned media. iPSC-derived astrocytes were treated with control or 50 nM Aβ and the respective control (Ctrl) conditioned media (CM) and Aβ CM were collected after 72 hours for further analysis. The amount of $A\beta_{42}$ still present in

the media was assessed using ELISA (**A**). 50 nM Aβ was added to astrocyte media and incubated in an empty 6-well plate for 72 hours to compare. In the Aβ CM, about 10% of the Aβ has been degraded by the astrocytes, though a large amount remains present in the Aβ CM (**A**). Iron content of the media was determined using ICP-MS (**B**). Astrocyte media not exposed to cells was used as a blank measurement. Aβ CM contained about 50% less iron than Ctrl CM and less than the baseline media (**B**). The percentage of apo-Tf in the media was determined using a urea gel shift assay. The band intensity of both apo- and holo-Tf bands were measured and the ratio of apo:holo was calculated. Using the standard curve made with known ratios of apo:holo, the percentage of Tf in the apo form was calculated (**C**). Aβ CM contains about 30% more apo-Tf than Ctrl CM (**D**). Levels of soluble amyloid precusor protein-α (sAPP-α) were measured using ELISA (**E**). Aβ CM contained almost 2-fold more sAPP- α than Ctrl CM (**E**). Levels of IL-6 as a marker of general inflammatory response were measured using ELSIA (**F**). Aβ CM contained 50% more IL-6 than Ctrl CM (**D**). n=3 to 8 for all experiments, means of biological replicates ± SEM were evaluated for statistical significance using one- way ANOVA with Tukey's posttest for significance (A-B) or using unpaired t-test (C, D, F). *p<0.05, **p<0.01, ****p<0.0001

4.4.3 Astrocytes treated with Aβ display increased iron uptake and mitochondrial activity

After observing decreased iron content and increased percentage of apo-Tf in Aβ CM, we tested the hypothesis that the decrease in media iron content was due to increased iron uptake and mitochondrial activity[250] after exposure to Aβ. Astrocytes plated in equal densities were incubated with ^{55}Fe-NTA with or without 50 nM Aβ and collected after 72 hours to measure ^{55}Fe uptake. Astrocytes treated with Aβ took up nearly double the amount of ^{55}Fe than control (**p<0.01, Figure 4-4A). In order to test mitochondrial activity, we employed two assays: CCK8

and citrate synthase activity. The CCK8 reagent contains a tetrazolium salt that is reduced by active mitochondria resulting in a colorimetric change. Astrocytes were incubated with CCK8 reagent with or without 50 nM Aβ, and after 72 hours, the media was analyzed and number of adherent cells was counted to normalize CCK8 absorbance. CCK8 absorbance increased by almost 2-fold after astrocytes were treated with Aβ (**$p<0.01$, Figure 4-4B), indicating an increase of mitochondrial activity. Because the CCK8 assay is often used to measure cell viability we wanted to confirm no change in cell viability with or without Aβ treatment. We measured LDH levels in the control CM and Aβ CM, and there was no change in control CM or Aβ CM (Figure 4-4C), indicating no increase of cell death. Citrate synthase is the first enzymatic step of the citric acid cycle within mitochondria. As such, we measured enzyme activity in astrocytes after incubation with 50 nM Aβ or untreated control for 72 hours. Similar to CCK8, citrate synthase activity increased by 2-fold over the course of 30 minutes (*$p<0.05$, Figure 4-4D), further implicating increased mitochondrial activity.

To confirm our functional findings, astrocytes incubated with 50 nM Aβ or control media for 72 hours were collected to assess various protein level changes via immunoblotting. Neprilysin (NEP-1) is an astrocytic Aβ-degrading enzyme and is upregulated in response to $A\beta^{251}$ compared to control (*$p<0.05$, Figure 4-4F). Additionally, APP, the precursor to sAPP-α, was decreased after Aβ treatment (*$p<0.05$, Figure 4-4G). When intracellular iron levels increase, either Iron response protein (IRP) 1 or IRP2 is reduced in order to regulate iron export and storage, though rarely both[252]. In astrocytes after Aβ treatment, while not statistically significant, IRP1 decreased by 20% (Figure 4-4H) and IRP2 was unchanged (Figure 4-4I). Consistent with these findings, ferritin heavy chain (FTH) and ferritin light chain (FTL), both proteins that form ferritin to store intracellular iron, are increased by 2-fold in astrocytes treated with Aβ, though only FTL reaches statistical significance (*$p<0.05$, Figure 4-4J-K). Cytochrome C is an iron complex protein used in the electron transport chain within mitochondria, and TOM20 is a receptor found on the outer

mitochondrial membrane. Both cytochrome C and TOM20 are often used as mitochondrial markers, and both are increased in astrocytes after Aβ treatment (*p<0.05, Figure 4-4L-M).

Figure 4-4

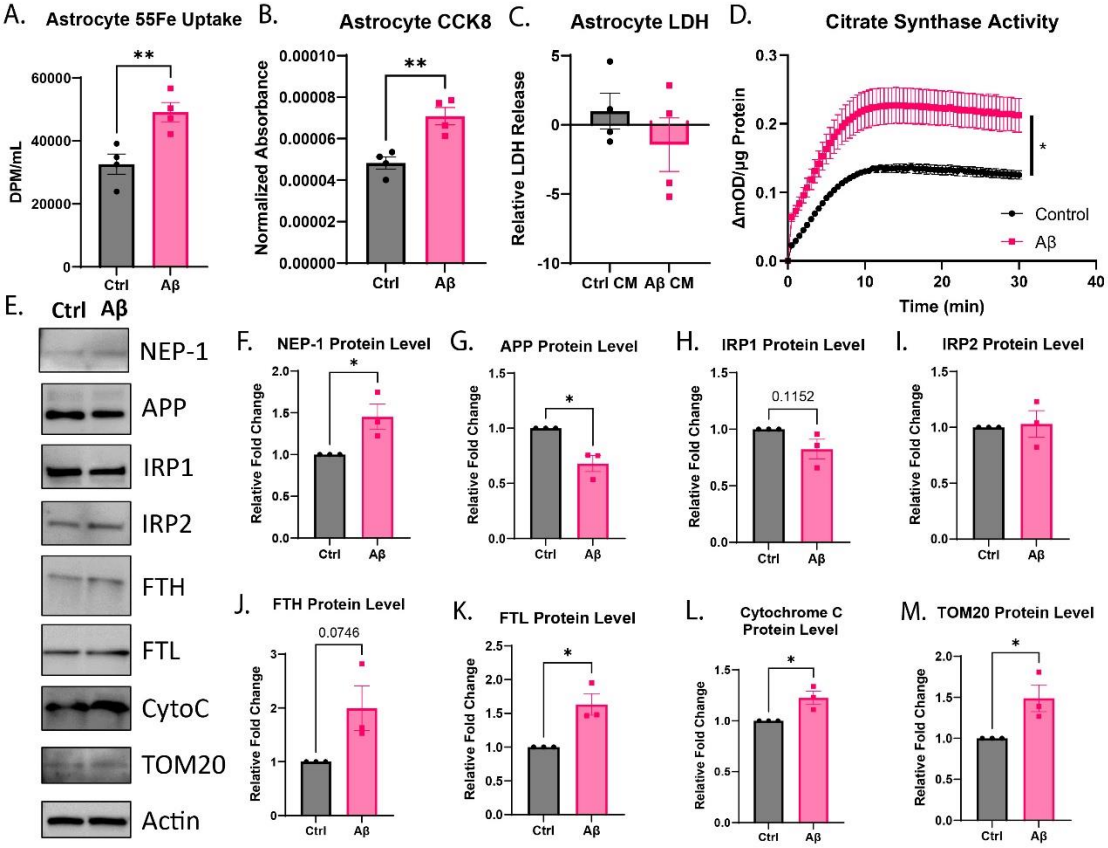

Aβ-induced changes in astrocytes.

iPSC-derived astrocytes were treated with nothing (control, Ctrl) or 50 nM Aβ for 72 hours. To measure iron uptake, cells were co-incubated with 5 μCi of ^{55}Fe-NTA and Aβ, and after 72 hours, the cells were dissolved and collected for liquid scintilation counting (**A**). Astrocytes treated with Aβ had a significant increase of ^{55}Fe uptake (**A**). To measure mitochondrial activity, cells were co-incubated with CCK8 reagent and Aβ, and after 72 hours, the media was collected to measure CCK8 reduction and the cells were collected for cell count (**B**). Astrocytes treat with Aβ had a signiciant increase of mitochondrial activity normailized to cell count (**B**). To measure cell viability after Aβ treatment, LDH was measured in the control (Ctrl) CM and Aβ CM and found

to have no change (**C**). Citrate synthase activity, another marker of mitochondrial activity, was measured and found to be increased after Aβ exposure (**D**). To determine molecular changes to confirm the functional findings, cells were collected for immunoblotting after Aβ treatment (**E**). NEP-1 levels were increased with Aβ treatment, supporting astrocytic response to Aβ (**F**). APP levels were decreased supporting the increase of sAPP-α in the Aβ CM (**G**). Changes to IRP1, FTH, and FTL levels supported increased cellular iron content (**H, J, K**). Increases of cytochrome C and TOM20 levels supported increased mitochondrial activity with Aβ treatment (**L, M**). n=3 to 4 for all experiments, means of biological replicates ± SEM were evaluated for statistical significance using unpaired t-test or two-way ANOVA. *p<0.05, **p<0.01

4.4.4 sAPP-α alone does not increase iron transport from ECs

Our group has previously demonstrated that iron deficient conditions and apo-Tf stimulate iron transport from ECs[16–18], and sAPP-α has been reported to increase iron release from ECs[248]. To determine if either apo-Tf or sAPP-α could mimic the iron transport stimulation by Aβ CM, ECs were cultured onto Transwell inserts and 0.25 μM apo-Tf (physiological in CSF[229]), 0.1 nM sAPP-α (concentration in Aβ CM), apo-Tf and sAPP-α, or control was placed in the basal chamber. Again, the apical chamber contained ^{55}Fe-Tf and RITC-dextran, and at hourly intervals, aliquots were taken from the basal chamber to measure the transport of ^{55}Fe-Tf and assess the integrity of the tight junctions with RITC-dextran. As previously shown, apo-Tf stimulated ^{55}Fe-Tf transport compared to control (**p<0.01, Figure 4-5A), however, sAPP-α failed to stimulate iron transport alone (Figure 4-5A). The combination of sAPP-α and apo-Tf did not further increase ^{55}Fe-Tf transport than apo-Tf alone (*p<0.05, Figure 4-5A), indicating that apo-Tf was driving the response. Neither apo-Tf nor sAPP-α increased RITC-dextran leakage (Figure 4-5B).

Fpn levels were examined to determine if either apo-Tf or sAPP-α altered the levels of Fpn in ECs similar to Aβ CM did, and Fpn levels remained consistent across experimental conditions (Figure 4-5C-D).

Figure 4-5

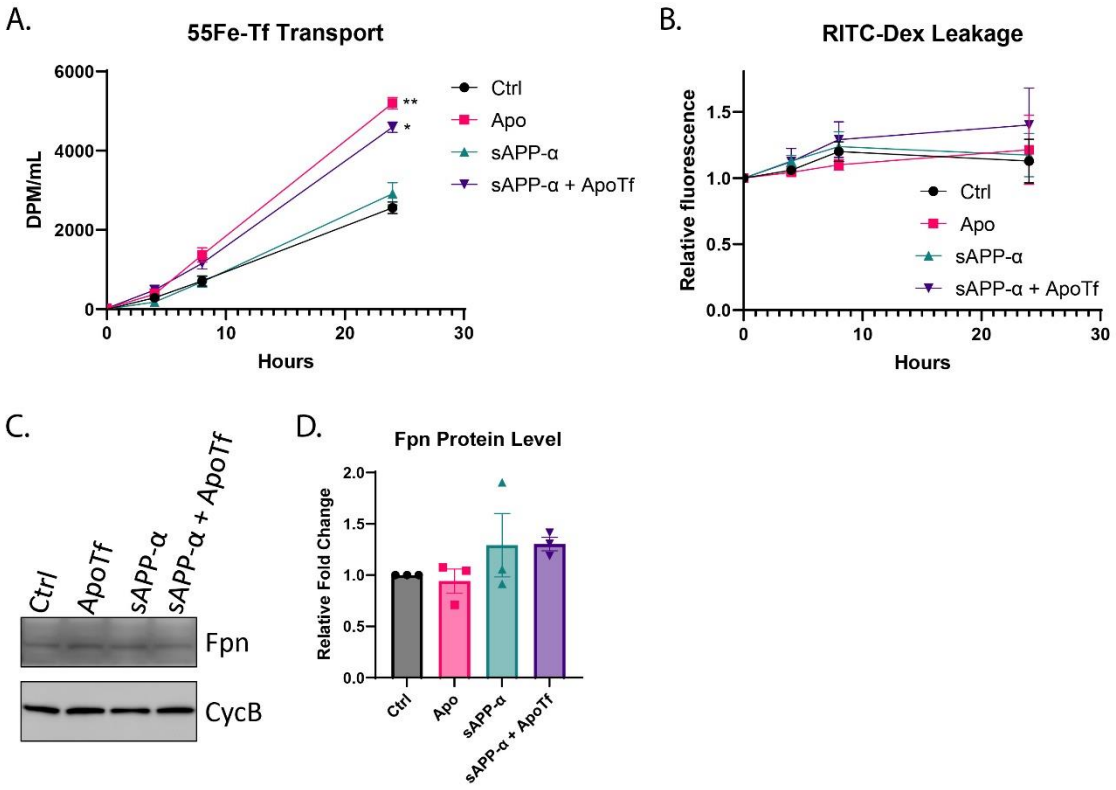

Lack of effect by soluble APP-α on iron transport from ECs. iPSC-derived ECs were cultured on bi-chamber plates and incubated with 0.25 μM apo-Tf and/or 0.1 nM sAPP-α in the basal chamber and 10 μCi ^{55}Fe-Tf and 1mg/ml RITC-dextran in the apical chamber. Aliquotes were taken from the basal chamber to measure ^{55}Fe-Tf transport and RITC-dextran leakage. Apo-Tf and the combination of apo-Tf and sAPP-α increased ^{55}Fe-Tf transport but sAPP-α alone did not (**A**). All conditions did not impact monolayer permieability (**B**). ECs incubated with apo-Tf and/or sAPP-α for 8 hours were collected for immunoblotting for Fpn levels, which were normailized to cyclophilin B (CycB) (**C**). No experimental condition increased ferroportin (Fpn) (**D**) levels. n=3 for all experiments, means of biological replicates ± SEM were evaluated for

statistical significance using two- way ANOVA with Sidak's posttest for significance (A-B) or using one-way ANOVA with Tukey's posttest for significance (D). *p<0.05, **p<0.01

4.4.5 Traditional inflammatory cytokines do not elicit changes in iron transport from ECs

Numerous studies have shown cytokine-induced EC monolayer integrity dysfunction[151,253–255] and that cytokines or neuroinflammation can impact iron uptake in the brain[130,154]. To determine if classically AD-elevated cytokines[256] could mimic the iron transport stimulation of Aβ CM, ECs were cultured on Transwell inserts and combinations of 50 nM Aβ, 100 ng/mL IL-6, 50 ng/ml tumor necrosis factor α (TNF-α), and/or 100 ng/ml interleukin-1β (IL-1β), or control were placed in the basal chamber, and ^{55}Fe-Tf and RITC-dextran were placed in the apical chamber. Aliquots were taken from the basal chamber to measure the transport of ^{55}Fe-Tf and the leakage of RITC-dextran. Neither solo exposures of Aβ, IL-6, TNF-α, or IL-1β nor combinations increased ^{55}Fe-Tf transport (Figure 4-6A and C) or RITC-Dextran leakage (Figure 4-6B and D). Fpn levels were examined to determine if any cytokine treatment or Aβ increased EC Fpn, and Fpn levels remained consistent across experimental conditions (Figure 4-6E-F).

Figure 4-6

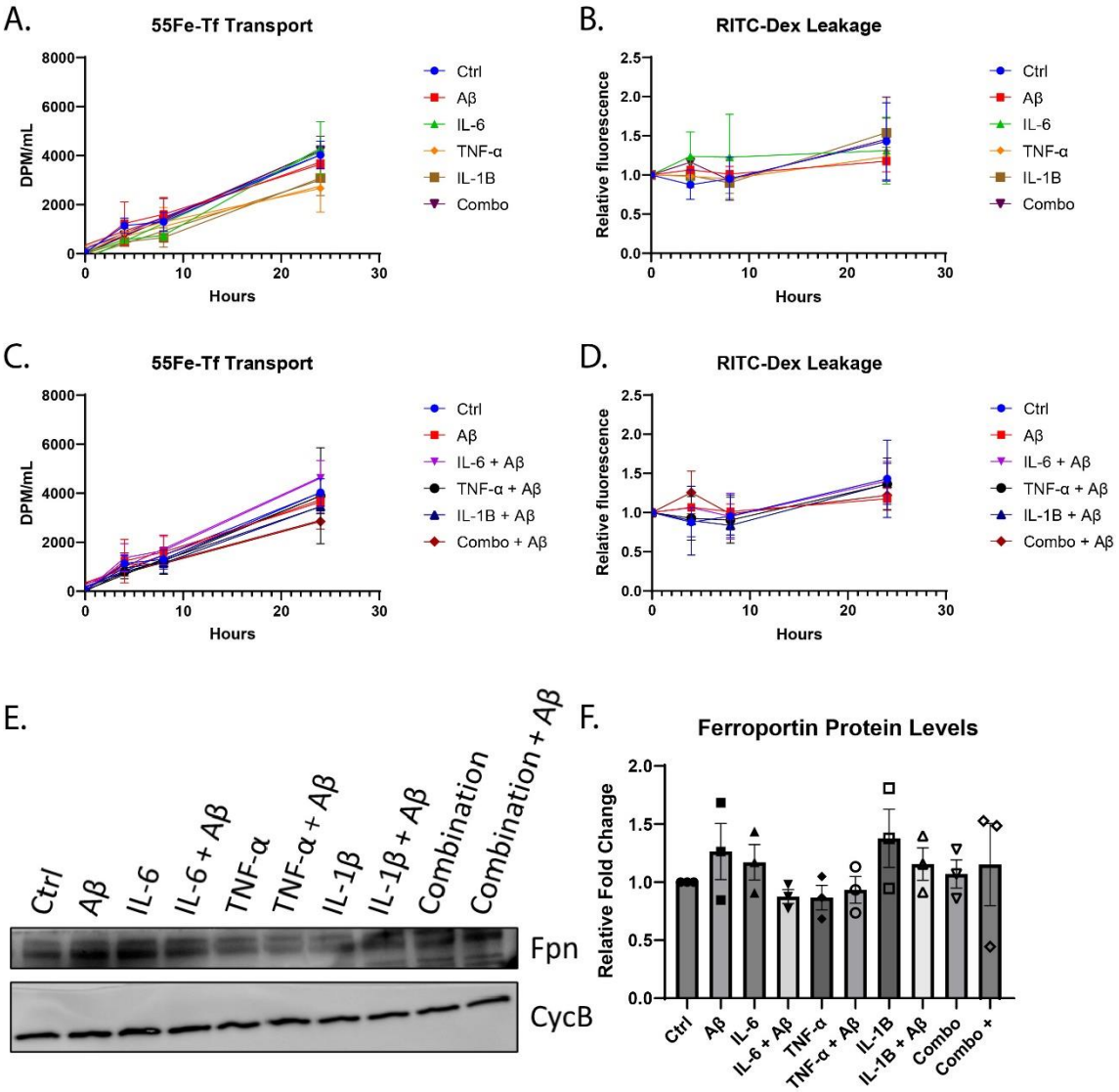

Lack of effect by cytokines on iron transport from ECs. iPSC-derived ECs were cultured on bi-chamber plates and incubated with combinations of 50 nM Aβ, 100 ng/mL IL-6, 50 ng/ml TNF-α, and/or 100 ng/ml IL-1β in the basal chamber and 10 μCi ^{55}Fe-Tf and 1mg/ml RITC-dextran in the apical chamber. Aliquotes were taken from the basal chamber to measure ^{55}Fe-Tf transport and RITC-dextran leakage. None of the cytokines nornor Aβalone or in combination impacted ^{55}Fe-Tf transport (**A and C**) or to monolayer permieability (**B and D**). ECs incubated with Aβ and cytokines for 8 hours were collected for immunoblotting to for Fpn levels normailized to cyclophilin B (CycB) (**E**). Noexperimental condition increased ferroportin (Fpn)

(**F**) levels. n=3 for all experiments, means of biological replicates ± SEM were evaluated for statistical significance using two- way ANOVA with Sidak's posttest for significance (A-D) or using one-way ANOVA with Tukey's posttest for significance (F).

4.5 Discussion:

This study suggests a possible mechanism for excessive iron accumulation in response to early AD Aβ deposition. Herein, we demonstrate that astrocytes treated with low levels of Aβ, consistent with early AD pathology, stimulate the transport of iron from ECs at the BBB (Figure 4-7). An investigation into the media components for known stimulators of iron release found that Aβ CM from astrocytes contained less iron and a higher percentage of apo-Tf than control CM. Additionally, levels of sAPP-α and inflammatory cytokines such as IL-6 were elevated in Aβ CM. In response to Aβ exposure, astrocytes increased their mitochondrial activity which was consistent with increased iron uptake. The increase iron need by the astrocytes is accompanied with increased release of apo-Tf. When ECs were incubated with apo-Tf, iron transport was increased, as previously demonstrated[16–18]. Other reported iron release stimulators, such as sAPP-α, Aβ, and inflammatory cytokines, did not mimic the effects of Aβ CM on iron transport in ECs. These findings suggest the mechanism for the initiation of excessive brain iron accumulation in AD starts with Aβ creating an iron deficient environment that promotes iron uptake mechanisms, leading to misappropriation of the astrocyte-EC iron regulatory signally and subsequent iron accumulation.

Figure 4-7

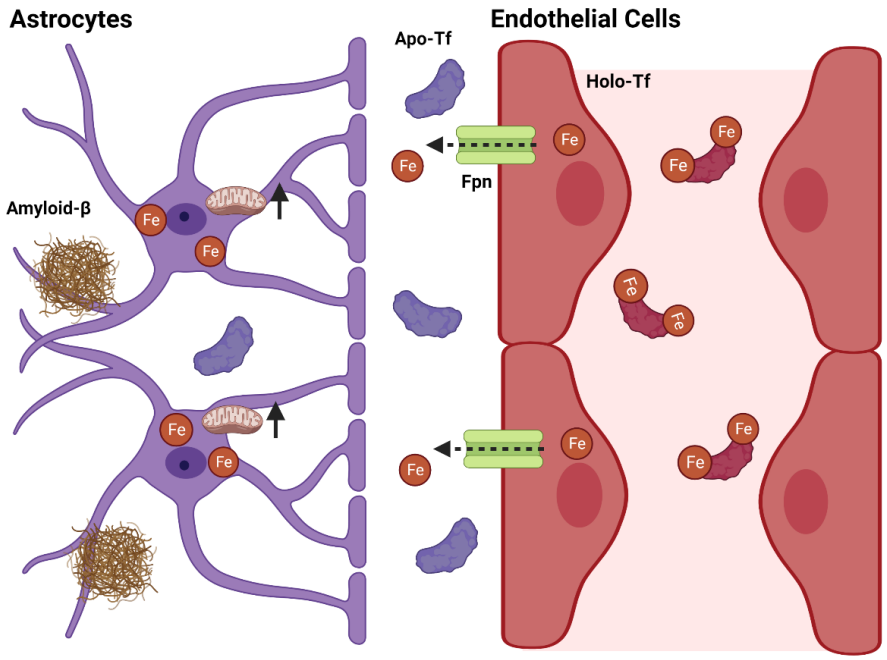

Summary Model. In response to amyloid-β (Aβ), astrocytes increase their mitochondrial activity, partially in response to an increase of energetic needs due to Aβ clearance. This is accompanied by an increase of iron uptake and consumption, leaving an iron deficient enviornment in the extracellular space and elevated levels of apo (iron free)- transferrin (Tf). Apo-Tf stimulates iron release from endothelial cells (ECs), resulting in an increase of iron transport across the blood-brain barrier.

The process of iron transport at ECs is highly regulated, which allows for proper neural functioning[257]. In order to cross the BBB, holo-Tf binds to TfR on the luminal membrane (blood side). The complex is endocytosed and the iron is reduced and transported out of the endosome by DMT1. Once free in the cell, iron is either used in the labile iron pool, stored in ferritin or exported via Fpn. Fpn is the major focus for most studies on iron release regulators. Heph stabilizes Fpn and aids in iron export by oxidizing the free iron released into the extracellular fluid and enables binding to apo-Tf[258]. In the present study, ECs exposed to Aβ CM significantly

increased iron transport with no change to EC monolayer permeability. These data suggest that the ECs themselves were not damaged or leaky, but rather the process of iron transport was engaged. When proteins involved in iron transport were examined, DMT1 and Fpn were found to be increased in ECs exposed to Aβ CM, which is consistent with an increase of iron transport and release. TfR was unchanged, but it is noteworthy that TfR is found on both the luminal and basolateral membranes[16] and our technique does not differentiate between the two TfR populations. Taken together, these data suggest that a component in Aβ CM signals to ECs to increase iron transport.

Our group has studied at length how apo- and holo-Tf act as signals of brain iron status in order to modulate iron release from ECs with corresponding molecular changes[16,18,98,258]. Apo-Tf signals an iron deficient environment and stimulates iron release from ECs, whereas holo-Tf signals an iron saturated environment and suppresses iron release. In line with reduced iron release, we have shown that ECs incubated with holo-Tf have reduced Fpn levels[16,258]. Recently, LeVine *et al.* found that iron deficiency, iron transport, and mitochondrial related processes were all upregulated in AD patient tissue[242]. Here, we found that Aβ CM contained significantly less iron than control CM. In line with this finding, we also discovered that of the Tf present in Aβ CM, the larger percentage of it was apo-Tf compared to control CM. Furthermore, when ECs were incubated with apo-Tf in the basal chamber, iron transport was increased, supporting our previous demonstration[16,18] and suggesting that an increase of apo-Tf in Aβ CM is a substantial contributor to the observed increase in iron transport.

One possible explanation for a decrease of iron in Aβ CM from astrocytes would be increased iron uptake due to metabolic activity. Astrocytes take up large amounts of iron and can increase their iron content by 9-fold before viability is affected[259]. Once iron is taken up by astrocytes, the iron is either stored in ferritin or incorporated into iron-sulfur clusters, which are crucial electron transfer molecules in mitochondrial respiration such as cytochrome C[260]. Studies

have shown higher amounts of Aβ can negatively impact astrocytic metabolism[249,250]. Here, we found that astrocytes treated with 50 nM Aβ (widely considered physiological[261]) display increased iron uptake and mitochondrial activity compared to control. Additionally, there was no change in cell viability with or without Aβ treatment, suggesting the increased iron content is not yet detrimental to the cells. An examination of molecular changes in the astrocytes corroborated our functional findings. Proteins associated with increased iron storage (FTH and FTL) and mitochondria density (TOM20 and cytochrome C) were increased in astrocytes treated with 50 nM Aβ. While there are multiple possibilities for increased energetic needs in response to Aβ, two measured here were APP and NEP-1. Decreased APP levels suggest an increase of APP cleavage, and increased NEP-1 levels suggest an increase of Aβ clearance. Taken together, these data suggest that, in response to low levels of Aβ, astrocytes increase their mitochondrial activity, leading to increased iron consumption and an iron deficient extracellular environment. All of these processes are functions of normal debris clearance and iron transport regulatory mechanisms; however, the chronic nature of AD likely leads to chronic iron build-up and damage over time.

sAPP-α is another potential iron release stimulator secreted by astrocytes. APP is a transmembrane protein most commonly known for its role in Aβ formation, though also plays an important role in iron release from ECs[76,262]. Amyloidogenic processing occurs when Aβ-secretase incorrectly cleaves APP, thus producing insoluble pathogenic Aβ[263]. Non-amyloidogenic processing occurs when α-secretase cleaves APP and produces sAPP-α[263]. Numerous groups have shown that APP is required for Fpn function and stability in the plasma membrane[262] through direct binding to Fpn[76]. The Fpn targeting peptide sequence present within APP is also present in sAPP-α[248]. McCarthy *et al.* demonstrated that sAPP-α similarly binds to Fpn and 10 nM treatment of sAPP-α induces iron release from ECs, though not due to ferroxidase activity like Heph[248]. In our present study, we found that treatment with 50 nM Aβ increased

levels of sAPP-α secreted from astrocytes. This observation combined with reduced levels of membrane APP in astrocytes treated with Aβ suggests that Aβ stimulates non-amyloidogenic processing of APP leading to increased sAPP-α production. Our study did not find an increase of iron transport from ECs associated with sAPP-α alone, but the Aβ CM only contained 0.1 nM of sAPP-α compared to the 10 nM required to induce iron efflux[248], suggesting that sAPP-α is not a cause for the Aβ CM-induced increase in iron transport from ECs seen in this study.

Another potential inducer of iron release at the BBB following activation of astrocytes is the release of inflammatory cytokines which has been shown in response to Aβ exposure with both *in vitro*[155] and *in vivo* models[156]. In AD patient CSF, increases of inflammatory cytokines, IL-6 and TNF-α, positively correlate with AD pathology[264] and with worsening cognitive impairment[265,266]. Numerous studies have shown dysfunction in BBB permeability after exposure to inflammatory cytokines[151,253–255]. Notably, de Vries *et al.* found that IL-6, TNF-α, and IL-1β reduced EC monolayer integrity by about 60% in rat cerebral ECs[151]. Other studies have shown increases of Fpn and TfR, which are indicative of increase iron transport, in response to Aβ *in vivo*[159]. Contrary to these previous studies, Kim *et al* showed that, in order to negatively impact EC monolayer permeability, reactive astrocytes needed direct contact with the ECs and that single doses of various inflammatory cytokines did not impact ECs alone[244]. In our present study, IL-6, TNF-α, and IL-1β in single doses and combination doses with 50 nM Aβ do not have any impact on iron transport or monolayer permeability compared to control. In addition, none of these experimental conditions influenced Fpn levels in ECs. Our findings support those of Kim *et al.* and indicate that IL-6, TNF-α, IL-1β, or Aβ cannot account for the increased iron transport from ECs after incubation with Aβ CM.

The narrative of iron in AD has long focused on how iron contributes to mid-stage disease pathology and iron overload. Our data uniquely point to an early-stage disease initiation of excessive iron accumulation. This study is the first to start to decipher the process of how the

normal communication between astrocytes and ECs can be misappropriated by a toxin to initiate dysregulation of brain iron acquisition. We show that in response to Aβ, astrocytes increase their mitochondrial activity and iron consumption, resulting in the secretion of iron release signals (apo-Tf) to ECs. These data build on our demonstration of the role of apo- and holo-Tf in regulating brain iron uptake and expand it into a pathological setting. Understanding how this normal response to a pathological substance result in excessive brain iron accumulation in AD may provide a possible therapeutic intervention point to mitigate the downstream damage of unchecked brain iron accumulation.

Chapter 5

Apo- and Holo-Tf as the Primary Iron Release Regulators: It Works

5.1 Introduction: Summary of the Main Findings of Dissertation

The main findings from this dissertation have demonstrated brain iron acquisition is regulated by apo (iron free)- and holo (iron bound)- transferrin (Tf) through protein-protein interactions at endothelial cells (ECs) of the blood-brain barrier (BBB). In the first chapter of this dissertation, I outlined the three steps of brain iron acquisition – uptake, transcytosis, and release – and both the intrinsic and extrinsic factors that play a role in the regulation of iron movement at each step. Additionally, I explored how this process may be dysregulated due to a misalignment of iron release signals in three diseases – Alzheimer's disease, Parkinson's disease, and Restless legs syndrome.

In my second chapter, I built upon previous *in vitro* findings that apo- and holo-Tf modulated iron release from ECs of the BBB[16,18,98] to examine *in vivo* effects of manipulating the ratio of apo- and holo-Tf in the brain on iron delivery in both male and female mice. I demonstrated that ratios of apo- and holo-Tf in the brain modulate iron uptake when bound to Tf as a delivery protein, but not when bound to H-ferritin (FTH). Furthermore, stark sex differences are present in both the regulatory response to brain ratios of apo- and holo-Tf and baseline iron uptake when delivered via Tf or FTH. This work reveals that the regulation of iron uptake is dependent on both the delivery protein (Tf or FTH) and sex, which is crucial information in order to apply these mechanisms of iron uptake regulation to a clinical setting.

In my third chapter, I investigated the molecular mechanism of apo- and holo-Tf mediated influence of iron release that occurs on the basolateral membrane of ECs. I

demonstrated that apo-Tf directly interacts with hephaestin (Heph), a ferroxidase that aids ferroportin (Fpn) to export iron and converts Fe^{2+} to Fe^{3+} immediately upon export. Additionally, holo-Tf interacts with Fpn, resulting in the ubiquitination and subsequent internalization of Fpn. What's more, hepcidin, which has long been thought to be the sole iron release regulator, interrupted the protein interaction of holo-Tf and Fpn only at levels consistent with pathological states. This body of work offers a dynamic model of iron release regulation in which apo- and holo-Tf exert primary control over the process but when hepcidin is deployed, as is the case in systemic inflammation or high iron levels, hepcidin halts iron release faster than holo-Tf.

Lastly, in my fourth chapter, I explored how the process of iron transport at ECs may be misappropriated in Alzheimer's disease in an *in vitro* model. I discovered that, in response to amyloid-β (Aβ), astrocytes increase their mitochondrial activity and iron consumption, resulting in a surrounding iron deficient environment and elevated levels of apo-Tf. The elevated levels of apo-Tf in astrocyte media can stimulate iron transport from ECs. The importance of this study cannot be understated as it offers a mechanistic cause for excessive iron accumulation in early AD prior to widespread proteinopathy distribution[133] and BBB breakdown[186]. The concept that the AD brain may start as iron starved, leading to a need for iron, iron that can propagate AD pathologies, is novel to the field with increasing evidence pointing to the idea[242] and offers early therapeutic targets in hopes of slowing disease progression.

In this final chapter, I will explore the theme of apo- and holo-Tf as cellular iron release regulating molecules. To begin with, I will describe the theoretical feedback loop of cellular iron needs and consumption and the consistent evidence to support the hypothesis. I will focus on how this process is employed in the brain and then suggest the presence of apo- and holo-Tf as iron release regulators at other organ barriers, such as the intestine, and at the site of cells throughout the body. Additionally, I will discuss how the theory of hepcidin being the sole iron release regulator lacks sound rationale, a gap that is bridged by apo- and holo-Tf. Taken together, I will

position the reader to understand the foremost question raised by my dissertation work: are apo- and holo-Tf better candidates for the primary cellular iron release regulators?

5.2 Apo- and Holo-Tf as Iron Release Regulators

Iron is essential to cellular health, thus there are a number of uptake methods employed to meet iron needs of the cell: FTH delivery, free iron transport, and Tf-bound uptake. First, iron can be delivered via FTH and Tim-1 (Tim-2 in mouse) receptor or transferrin receptor (TfR) endocytosis[212,267]; however, FTH iron delivery does not seem to be as dominant as Tf iron delivery nor is it subjected to the same regulation at Tf-bound iron delivery *in vivo*[17]. Next, free iron can be transported directly into the cell via divalent metal transporter (DMT1)[234], but free iron is uncommon in extracellular fluid, due to the over-abundance of apo-Tf present[268], prepared to bind any free iron it may encounter. Thus, cellular iron needs are primarily met via Tf and TfR endocytosis on the plasma membrane.

Once holo-Tf binds to TfR, the complex is endocytosed and ferrireductases lower the pH within the endosome to convert Fe^{3+} to Fe^{2+} and inducing the iron to detach from Tf[257]. The iron is transported into the intracellular cytosol via DMT1 on the endosome membrane, and the resulting apo-Tf is released back into the extracellular space[257]. The more iron a cell needs, the more holo-Tf it will take up, and thus the more apo-Tf it will release once acquiring the iron carried[257]. The presence of apo-Tf indicates an iron deficient environment, whereas the presence of holo-Tf indicates an iron saturated environment. Thus, apo- and holo-Tf can be used as signaling molecules to various cell types to alter the availability of iron. Cells can signal their iron needs based on their own iron consumption to stimulate real-time changes to the locally available iron supply, and thus creating a feedback loop (Figure 5-1).

Figure 5-1:

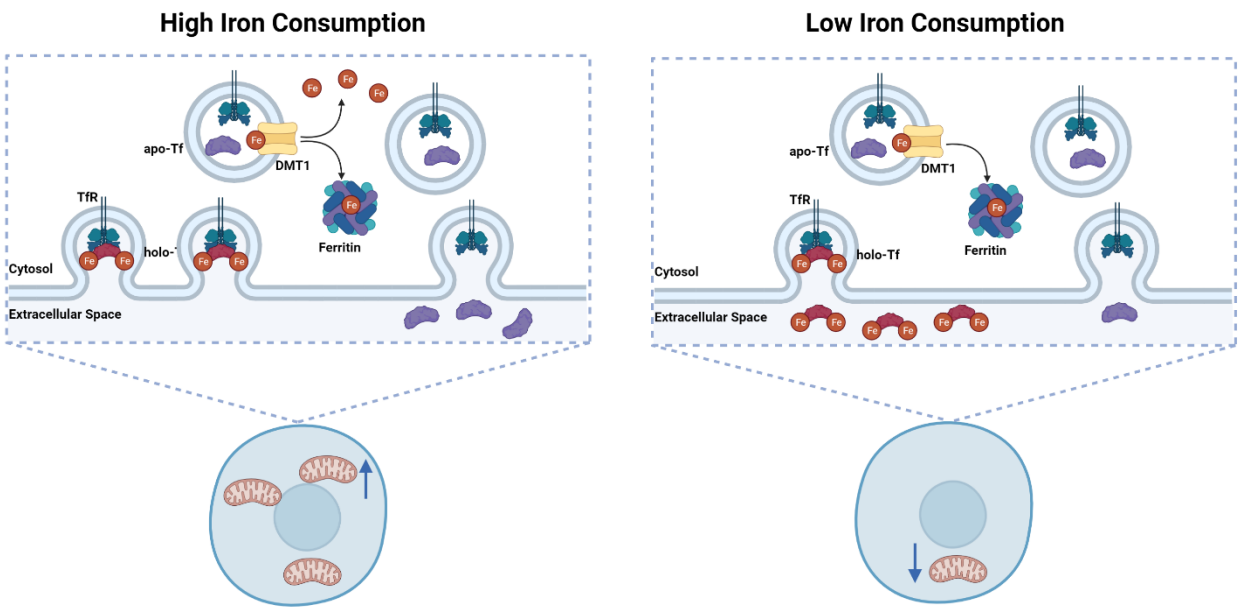

Model of Iron Signals Based on Iron Consumption. When cells have increased iron needs, as is the case with increased mitochondrial activity, the cells increase their iron consumption. Holo-Tf is taken up via TfR to meet the cellular iron needs. Once the iron is removed, the resulting apo-Tf is released back into the extracellular fluid. This results in an elevated ratio of apo- to holo-Tf. When cells have decreased iron needs, the cells decrease their iron consumption and take up less holo-Tf. This results in a lower ratio of apo- to holo-Tf.

5.2.1 Evidence at the Blood-Brain Barrier

Much of our work understanding the regulation of iron release via apo- and holo-Tf has focused at the BBB. Fluctuations in brain iron can have detrimental effects on neurological health[6,257]. An influx of free iron without apo-Tf available to bind to and render the iron useable can wreak havoc on cellular structures. Because iron is a transition metal and gains and loses electrons with ease, unbound iron can cause lipid peroxidation to phospholipids within the plasma

membrane of cells and trigger ferroptosis, iron-mediated cell death. If iron were able to cross the BBB without resistance, any influx of dietary iron would result in permanent brain damage. Thus, it only makes sense that the brain needs the ability to control iron transport across the BBB. The cells that form the first layer of the BBB moving from blood- to brain-side are ECs. ECs are highly polarized and exclusively express a number of proteins, such as Fpn and Heph, on the basolateral membrane[226,235]. This polarization positions the brain to relay iron release signals to ECs, which are themselves reservoirs of iron[17].

The model of apo- and holo-Tf as regulators of iron release fits logically with the region specific and temporally demanding iron needs in the brain (Figure 5-2). As neural cells utilize holo-Tf in the interstitial fluid of the brain and subsequently release apo-Tf, this allows the ECs to only release more iron as needed. This form of regulated release prevents over saturation of iron in the brain while ensuring adequate supply when required. Furthermore, this model explains the occurrence of regional iron uptake in the brain[67,96,97]. Overall, areas of the brain that have higher iron needs – metabolic activity, myelination, and certain neurotransmitter synthesis – have higher rates of iron uptake[96,269].

Our group has shown that, when ECs are incubated with conditioned media from iron deficient and iron treated astrocytes, iron release increases and decreases respectively[16]. Moreover, these effects are mimicked by apo- and holo-Tf in numerous *in vitro* and *in vivo* studies in which apo-Tf stimulates iron release and holo-Tf suppresses iron release from ECs[16–18,98]. The mechanism of apo- and holo-Tf's control over iron release was recently deciphered. We found that apo-Tf directly interacts with Heph, presumably to accept the newly exported iron, while holo-Tf directly interacts with Fpn and causes the ubiquitination and subsequent degradation of Fpn[258]. Given our findings over the years, there is no denying that apo- and holo-Tf are regulators of iron release from ECs at the BBB, but what about other cellular barriers?

5.2.2 Possibility at Other Barriers

The intestinal tract is one of the most prominent cellular barriers in the human body. Upon dietary iron consumption, the iron must be transported across enterocytes within the duodenum, which is the first part of the small intestine[270]. Briefly, free iron is transported into the cell via DMT1 on the apical membrane, and from there, the iron can be exported across the basolateral membrane into the blood via Fpn[270]. As it exists the enterocyte, the iron can bind to Tf and be transported to be used by cells throughout the body. The parallels between enterocytes and ECs are abundant. Both cell types are highly polarized with proteins designated to their respective membranes[271], are reservoirs of iron with high levels of ferritin for iron storage[272], and require regulation of iron release[273]. The importance of the regulation of brain iron uptake was outline above, but regulation is equally important at enterocytes. The human body does not possess a mechanism for iron excretion once in circulation[270], thus enterocytes must have a similar mechanism to regulate iron release into the blood as the brain does.

In order to prevent iron overload in the blood and the body in general, it becomes clear that apo- and holo-Tf are good candidates for this important task (Figure 5-2). As is hypothesized in the brain, elevated levels of apo-Tf would indicate the availability of Tf to bind iron and carry to other cells, while elevated levels of holo-Tf would indicate too much Tf-bound iron in circulation and more iron transport could be damaging. Evidence of iron signaling to enterocytes is present in the adipose-gut axis in which iron depleted and iron overloaded adipocytes stimulated and suppressed, respectively, iron transport from enterocytes[274]. In line with our work demonstrating that apo-Tf directly induces iron release from ECs, apo-Tf has been shown to similarly induce iron release from Caco-2 cells, colon epithelial cells that share many properties with enterocytes[110]. Enterocytes, like ECs, express Heph and Fpn on the basolateral membrane, though Heph can be found transcellularly before being trafficked to the membrane. When

intestinal cells were incubated with apo-Tf in the basal chamber, Heph was localized to the basolateral membrane[275], suggesting apo-Tf requires Heph availability to exert control over iron release. Our work proposes apo-Tf requires direct interact with Heph. In HEK293 cells, we showed that apo-Tf and Heph interact at the cell surface[258] and others have suggested this interaction using cell-free proteins[103,104,106]. Based on existing literature, it is likely that, similar to the BBB, 1) locally available apo- and holo-Tf directly regulate iron release from enterocytes, 2) apo- and holo-Tf interact with Heph and Fpn respectively in enterocytes, and 3) holo-Tf induces Fpn internalization in enterocytes.

5.2.3 Generalization to Cells Throughout the Body

Tf-bound iron is a substantial source of iron for nearly all cells, thus apo- and holo-Tf occupy the extracellular space of organs throughout the body. Most cell types are primarily focused on iron uptake via TfR, which is controlled by intracellular iron levels[257], but iron efflux is equally important. All cells express Fpn to export iron in the event of excess intracellular iron. Systemic iron homeostasis requires maintenance of a balance of iron inflow and outflow from the circulation[276]. If cells release more iron than localized Tf can bind to, free iron could be released to wreak havoc and free radicals. Logic dictates that there be something regulating this process. The need for iron efflux regulation throughout the body additionally explains why of all circulating Tf, only 30% is saturated with iron (holo-Tf). In fact, circulating Tf levels remain constant in healthy and disorders such as iron deficiency, but Tf saturation (ratio of apo- to holo-Tf) changes based on iron availability.

Apo- and holo-Tf are poised to be comprehensive regulators of iron release (Figure 5-2). Our previous work shows that holo-Tf binds to Fpn, resulting in Fpn internalization and reduced iron release, in both ECs and HEK293 cells[258]. The use of two cell types, the latter of which are

embryonic kidney cells, strongly indicates that these protein-protein interactions are omnipresent. It is worth noting that Fpn exists in two isoforms: 1a and 1b; however the only difference between them is the presence of an iron response element (IRE) to allow intracellular iron levels to control protein translation[93]. Fpn1b, which lacks an IRE, has only been found in enterocytes[93] and ECs[94]. Thus our experiments likely indirectly tested the ability of holo-Tf to bind to both Fpn1a and Fpn1b, with seemingly no difference. As for the interaction between apo-Tf and Heph, our use of different cell types[258] and others use of cell-free recombinant protein experiments[103,104], again suggests this interaction persists in all cell types. The caveat is that Heph is not ubiquitously expressed in all cells and is most highly expressed in enterocytes and the nervous system[277]. Ceruloplasmin (Cp) is the homologous ferroxidase found in circulation to convert newly released Fe^{2+} to Fe^{3+} to be picked up by apo-Tf. While Cp and Heph are homologous, they do have distinct roles[78], and studies examining the potential interaction between Cp and apo-Tf are conflicting[106]. Overall, literature and theory would indicate that elevated holo-Tf prevents iron release from other cells throughout the body, while apo-Tf may not have Heph to interact with to stimulate iron release in places other than the intestine and BBB.

Figure 5-2

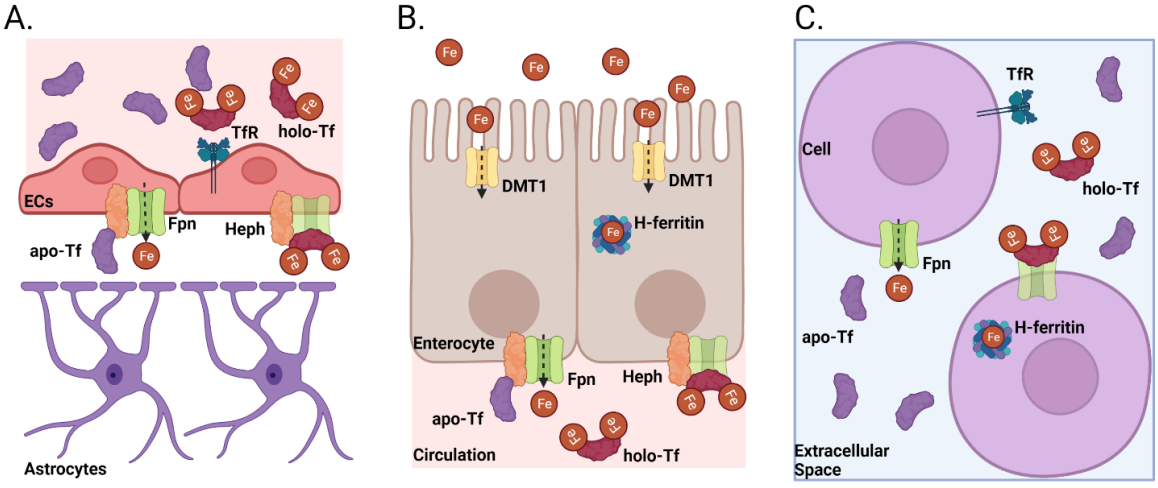

Parallels in Cellular Iron Release. At the site of ECs of the BBB, apo-Tf is released from astrocytes and interacts with Heph on the basolateral membrane to stimulate iron release (**A**).

Excessive levels of holo-Tf in the interstitial fluid interact with Fpn to suppress iron release. On the basal membrane of enterocytes, we hypothesize that apo- and holo-Tf participate in identical protein interactions to similarly regulate iron release in the circulation (**B**). The universal expression of Fpn on cellular membranes and the importance of controlling efflux of free iron into the extracellular space suggest holo-Tf binds to Fpn on all cells to suppress iron release (**C**).

5.3 The Role of Hepcidin

5.3.1 At Physiological Levels Consistent with Homeostasis

The conventional regulator of iron release from cells has long been attributed to hepcidin, an inflammatory hormone peptide primarily secreted by hepatocytes in the liver. To control iron release from cells, hepcidin binds to Fpn and causes its rapid internalization and degradation[120]. Studies have shown a negative correlation with hepcidin and brain iron[71,72,101], however, the concept of hepcidin being the primary iron regulator requires a constant level of expression and extracellular concentration of this protein that has not been demonstrated. In addition to hepatocytes, hepcidin is also expressed in astrocytes[114,115] and the choroid plexus[116,117]; however, in the central nervous system, the expression of hepcidin is much less than in the liver[117,118]. Hepcidin mRNA can be found near endothelium of blood vessels and the choroid plexus at low levels, yet hepcidin protein is highly expressed on the luminal membrane of blood vessels in the brain, suggesting the protein found in the brain originates from a different source[117], likely the liver. The transport of liver-produced hepcidin from circulation to the brain is an understudied and unknown mechanism. Similar peptides to hepcidin, defensins and amphipathic peptide cations, cross the BBB via diffusion[115], but it is unconfirmed if hepcidin has a similar

mechanism. Even with crossing the BBB, the idea of systemic hepcidin controlling brain iron uptake is further problematic. Due to the high metabolic activity of the brain and the specialized neural processes that iron participates in, brain iron needs and thus levels differ greatly from systemic iron. In fact, brain iron levels and systemic iron levels rarely correlate, especially in certain neurological diseases[6]. As such, upon critical reflection, the notion that systemic hepcidin would adequately regulate brain iron uptake has multiple limitations.

Hepcidin as the primary regulator of iron transport in the intestine also has flaws as a theoretical model. The upregulation of hepcidin production in response to systemically high iron levels and inflammation occurs rapidly and is then circulated throughout the body[278]. This mechanism results in hepcidin being reactive to damaging stimuli rather than controlling iron levels in daily maintenance. On the other hand, apo- and holo-Tf are ever-present at the site of iron release and can inform of real time iron status and regulate iron transport accordingly. In our experiments studying the protein-protein interactions in which apo- and holo-Tf participate, we found that at physiological levels that are consistent with systemic homeostasis, hepcidin did not disrupt the protein interactions[258]. These data suggest that at these levels, hepcidin would not be influential enough to impact iron release. Our hypothesis is consistent with recent work that created a mathematical model of systemic iron regulation based on hepcidin[132]. When *in vivo* measurements of iron levels were taken, the model could not account for the experimental results until an additional mechanism of iron regulation was added[132].

5.3.2 At Pathophysiological Levels Consistent with Disease

Rather than a day-to-day, minute-to-minute iron release regulator, hepcidin fits more as a metaphorical panic button to halt iron release in times of systemic stress. Hepcidin production is upregulated in response to high iron levels and inflammation, a mechanism that likely developed

to protect the body from iron overload and pathogens[115]. Both increased levels of circulation iron induce the BMP-SMAD pathway and the expression of interleukin-6 (IL-6) in the liver directly increase hepcidin production to counter high iron and inflammation respectively[278]. In line with this evolutionary theory, the upregulation of hepcidin is common in disease, ranging from hemochromatosis to neuroinflammation[225], further emphasizing its vital role in iron homeostasis during pathophysiological challenges.

Once deployed and in circulation, hepcidin will bind to Fpn and induce the rapid internalization and subsequent degradation of Fpn[120,122,279]. We and others have shown that hepcidin will reduce membrane Fpn levels by nearly 50% within 10 minutes[124,258]. On the other hand, holo-Tf reduces membrane Fpn levels by about 20% after 60 minutes[258]. These data highlight the prompt action of hepcidin to immediately slow and/or stop iron release once hepcidin is present near cells. In addition to the speed of hepcidin-induced Fpn internalization, our data show that only pathophysiological levels of hepcidin that are consistent with disease[225] can disrupt the protein-protein interaction of holo-Tf and Fpn, while levels more consistent with physiological baseline do not[258]. This finding suggests that in a homeostatic environment, hepcidin does not have as much influence over Fpn than holo-Tf, but when hepcidin production is upregulated in response to harmful stimuli, hepcidin does have more influence over Fpn and can swiftly reduce Fpn presence on the cellular membrane and render it inactive.

Hepcidin and holo-Tf share the goal to suppress iron release from cells by acting on Fpn and may even work in cooperation when both are elevated. However, apo-Tf stimulates iron release by interaction with Heph[18,258]. In physiological conditions, apo- and holo-Tf are both present. In serum, iron occupies about 30% of the circulating Tf, and in in the brain extracellular fluid, most Tf is in the holo-Tf form. In our recent *in vivo* study, a small infusion of apo-Tf into the lateral ventricle significantly increased brain iron uptake[17], suggesting that the slightest change in the presence of apo-Tf stimulates iron transport regardless of surrounding holo-Tf. As

for hepcidin, we have shown that the protein-protein interaction between apo-Tf and Heph is not disrupted by even pathophysiological levels of hepcidin[258]. While no direct testing of this hypothesis has been performed, these studies ask the question: which regulator has the greater influential pull-on iron release, apo-Tf or hepcidin?

While it may seem unlikely that apo-Tf and hepcidin would both be present in the local environment of cells, it is very possible to be the case in Alzheimer's disease (AD), the most common progressive neurodegenerative disease. AD displays excessive iron accumulation that occurs prior to widespread proteinopathies that are hallmarks of the disease[10,133] or BBB breakdown that would allow unimpeded iron flow[145]. An emerging hypothesis is that the AD brain is functionally iron deficient. Gene expression of both iron deficiency and iron transport related processes are upregulated in AD brain tissue[242]. Recently, we have shown that, in response to amyloid-β (Aβ), a core pathology in AD, astrocytes increase their iron consumption, resulting in elevated levels of apo-Tf[280]. Similarly, AD patient cerebrospinal fluid contains less iron but no change in Tf levels, indicating increased amount of apo-Tf[281]. In conjunction with apo-Tf, hepcidin expression is increased in response to Aβ in *in vivo* studies[159] and serum hepcidin is increased in AD patients[282]. Taken together, these studies paint a picture of apo-Tf and hepcidin co-existing and likely working against each other to exert control of iron transport in the brain. Given that excessive iron accumulation persists in AD, apo-Tf appears to win out to stimulate iron release.

5.4 Conclusions

To summarize, the body of work produced by this dissertation has established how local iron regulation in the brain may occur while challenging long-held beliefs about the regulation of cellular iron release. In particular it asks the question: are apo- and holo-Tf the primary regulators

of iron release? The hypothetical model is simple, yet elegant. As outlined above, apo- and holo-Tf can create a self-regulating feedback loop, a common phenomenon in biology, all centered around iron availability. My work opens the door for the entire iron biology field to reexamine previously held beliefs about the mechanism of cellular iron release in homeostatic environment and the relative importance of hepcidin to regulate iron release in pathophysiological conditions. Moreover, my research reveals how, unlike our traditional thinking about how iron dysregulation contributes to diseases, there is less of a dysregulation but rather a misappropriation of the mechanism of apo- and holo-Tf regulation. In the case of neurological diseases, theories of iron regulation falling by the wayside may need replaced with theories of disease pathology misappropriating iron release signals from cells functioning in a manner necessary to deal with the said pathology. In general, the ironclad paradigm of apo- and holo-Tf as the primary iron release regulators simply works as a better model.

References

1. Dev, S. & Babitt, J. L. Overview of Iron Metabolism in Health and Disease. *Hemodial Int* **21**, S6–S20 (2017).
2. Connor, J. R. *et al.* Neuropathological examination suggests impaired brain iron acquisition in restless legs syndrome. *Neurology* **61**, 304–309 (2003).
3. O'Keeffe, S. T., Gavin, K. & Lavan, J. N. Iron status and restless legs syndrome in the elderly. *Age Ageing* **23**, 200–203 (1994).
4. Bartzokis, G. *et al.* Gender and iron genes may modify associations between brain iron and memory in healthy aging. *Neuropsychopharmacology* **36**, 1375–1384 (2011).
5. Earley, C. J., B Barker, P., Horská, A. & Allen, R. P. MRI-determined regional brain iron concentrations in early- and late-onset restless legs syndrome. *Sleep Med* **7**, 458–461 (2006).
6. Kim, Y. & Connor, J. R. The roles of iron and HFE genotype in neurological diseases. *Mol Aspects Med* **75**, 100867 (2020).
7. Wang, J.-Y. *et al.* Meta-analysis of brain iron levels of Parkinson's disease patients determined by postmortem and MRI measurements. *Sci Rep* **6**, (2016).
8. Ci, Y.-Z. *et al.* Iron overload induced by IRP2 gene knockout aggravates symptoms of Parkinson's disease. *Neurochemistry International* **134**, 104657 (2020).
9. Gajowiak, A., Styś, A., Starzyński, R. R., Staroń, R. & Lipiński, P. Misregulation of iron homeostasis in amyotrophic lateral sclerosis. *Postepy Hig Med Dosw (Online)* **70**, 709–721 (2016).
10. Ayton, S. *et al.* Brain iron is associated with accelerated cognitive decline in people with Alzheimer pathology. *Molecular Psychiatry* 1–10 (2019) doi:10.1038/s41380-019-0375-7.
11. Liu, J.-L., Fan, Y.-G., Yang, Z.-S., Wang, Z.-Y. & Guo, C. Iron and Alzheimer's Disease: From Pathogenesis to Therapeutic Implications. *Front Neurosci* **12**, (2018).
12. Daneman, R. & Prat, A. The Blood–Brain Barrier. *Cold Spring Harb Perspect Biol* **7**, (2015).

13. Menaceur, C., Gosselet, F., Fenart, L. & Saint-Pol, J. The Blood-Brain Barrier, an Evolving Concept Based on Technological Advances and Cell-Cell Communications. *Cells* **11**, 133 (2021).

14. Gordon, G. R. J., Howarth, C. & MacVicar, B. A. Bidirectional control of arteriole diameter by astrocytes. *Exp Physiol* **96**, 393–399 (2011).

15. Attwell, D. *et al.* Glial and neuronal control of brain blood flow. *Nature* **468**, 232–243 (2010).

16. Simpson, I. A. *et al.* A novel model for brain iron uptake: introducing the concept of regulation. *J Cereb Blood Flow Metab* **35**, 48–57 (2015).

17. Baringer, S. L., Neely, E. B., Palsa, K., Simpson, I. A. & Connor, J. R. Regulation of brain iron uptake by apo- and holo-transferrin is dependent on sex and delivery protein. *Fluids Barriers CNS* **19**, 49 (2022).

18. Chiou, B. *et al.* Endothelial cells are critical regulators of iron transport in a model of the human blood-brain barrier. *J. Cereb. Blood Flow Metab.* **39**, 2117–2131 (2019).

19. Burdo, J. R., Antonetti, D. A., Wolpert, E. B. & Connor, J. R. Mechanisms and regulation of transferrin and iron transport in a model blood-brain barrier system. *Neuroscience* **121**, 883–890 (2003).

20. McCarthy, R. C. & Kosman, D. J. Mechanisms and regulation of iron trafficking across the capillary endothelial cells of the blood-brain barrier. *Front Mol Neurosci* **8**, 31 (2015).

21. Campos-Escamilla, C. *et al.* X-ray Characterization of Conformational Changes of Human Apo- and Holo-Transferrin. *Int J Mol Sci* **22**, 13392 (2021).

22. Yersin, A., Osada, T. & Ikai, A. Exploring transferrin-receptor interactions at the single-molecule level. *Biophys J* **94**, 230–240 (2008).

23. Gammella, E., Buratti, P., Cairo, G. & Recalcati, S. The transferrin receptor: the cellular iron gate. *Metallomics* **9**, 1367–1375 (2017).

24. Harrison, P. M. & Arosio, P. The ferritins: molecular properties, iron storage function and cellular regulation. *Biochim Biophys Acta* **1275**, 161–203 (1996).

25. Fisher, J. *et al.* Ferritin: a novel mechanism for delivery of iron to the brain and other organs. *Am J Physiol Cell Physiol* **293**, C641-649 (2007).

26. Chiou, B., Neely, E. B., Mcdevitt, D. S., Simpson, I. A. & Connor, J. R. Transferrin and H-ferritin involvement in brain iron acquisition during postnatal development: impact of sex and genotype. *Journal of Neurochemistry* **152**, 381–396 (2020).

27. Fiandra, L. *et al.* In Vitro Permeation of FITC-loaded Ferritins Across a Rat Blood-brain Barrier: a Model to Study the Delivery of Nanoformulated Molecules. *J Vis Exp* (2016) doi:10.3791/54279.

28. Montemiglio, L. C. *et al.* Cryo-EM structure of the human ferritin-transferrin receptor 1 complex. *Nat Commun* **10**, 1121 (2019).

29. Li, L. *et al.* Binding and uptake of H-ferritin are mediated by human transferrin receptor-1. *Proc Natl Acad Sci U S A* **107**, 3505–3510 (2010).

30. Johnsen, K. B., Burkhart, A., Thomsen, L. B., Andresen, T. L. & Moos, T. Targeting the transferrin receptor for brain drug delivery. *Prog Neurobiol* **181**, 101665 (2019).

31. Friden, P. M. *et al.* Anti-transferrin receptor antibody and antibody-drug conjugates cross the blood-brain barrier. *Proc Natl Acad Sci U S A* **88**, 4771–4775 (1991).

32. Friden, P. M. *et al.* Drug delivery to the brain using an anti-transferrin receptor antibody. *NIDA Res Monogr* **120**, 202–217 (1992).

33. Friden, P. M. *et al.* Blood-brain barrier penetration and in vivo activity of an NGF conjugate. *Science* **259**, 373–377 (1993).

34. Johnsen, K. B. & Moos, T. Revisiting nanoparticle technology for blood-brain barrier transport: Unfolding at the endothelial gate improves the fate of transferrin receptor-targeted liposomes. *J Control Release* **222**, 32–46 (2016).

35. Okuyama, T. *et al.* Iduronate-2-Sulfatase with Anti-human Transferrin Receptor Antibody for Neuropathic Mucopolysaccharidosis II: A Phase 1/2 Trial. *Mol Ther* **27**, 456–464 (2019).

36. Okuyama, T. *et al.* A Phase 2/3 Trial of Pabinafusp Alfa, IDS Fused with Anti-Human Transferrin Receptor Antibody, Targeting Neurodegeneration in MPS-II. *Mol Ther* **29**, 671–679 (2021).

37. Ullman, J. C. *et al.* Brain delivery and activity of a lysosomal enzyme using a blood-brain barrier transport vehicle in mice. *Science Translational Medicine* **12**, (2020).

38. Arguello, A. *et al.* Molecular architecture determines brain delivery of a transferrin receptor-targeted lysosomal enzyme. *J Exp Med* **219**, e20211057 (2022).

39. Cerghet, M. *et al.* Proliferation and death of oligodendrocytes and myelin proteins are differentially regulated in male and female rodents. *J Neurosci* **26**, 1439–1447 (2006).

40. McDermott, J. L., Liu, B. & Dluzent, D. E. Sex Differences and Effects of Estrogen on Dopamine and DOPAC Release from the Striatum of Male and Female CD-1 Mice. *Experimental Neurology* **125**, 306–311 (1994).

41. Munro, C. A. *et al.* Sex Differences in Striatal Dopamine Release in Healthy Adults. *Biological Psychiatry* **59**, 966–974 (2006).

42. Lord, M. N. *et al.* Sexually Dimorphic Effects of a Western Diet on Brain Mitochondrial Bioenergetics and Neurocognitive Function. *Nutrients* **13**, 4222 (2021).

43. Cheli, V. T., Correale, J., Paez, P. M. & Pasquini, J. M. Iron Metabolism in Oligodendrocytes and Astrocytes, Implications for Myelination and Remyelination. *ASN Neuro* **12**, 1759091420962681 (2020).

44. Khan, F. H., Ahlberg, C. D., Chow, C. A., Shah, D. R. & Koo, B. B. Iron, dopamine, genetics, and hormones in the pathophysiology of restless legs syndrome. *J Neurol* **264**, 1634–1641 (2017).

45. Uchino, E., Tsuzuki, T. & Inoue, K. The effects of age and sex on seven elements of Sprague-Dawley rat organs. *Lab Anim* **24**, 253–264 (1990).

46. Hahn, P. *et al.* Age-dependent and gender-specific changes in mouse tissue iron by strain. *Experimental Gerontology* **44**, 594–600 (2009).

47. Duck, K. A., Neely, E. B., Simpson, I. A. & Connor, J. R. A role for sex and a common HFE gene variant in brain iron uptake. *J. Cereb. Blood Flow Metab.* **38**, 540–548 (2018).

48. Dacks, P. A. Estrogens iron out the details: a novel direct pathway for estrogen control of iron homeostasis. *Endocrinology* **153**, 2942–2944 (2012).

49. Yang, Q., Jian, J., Katz, S., Abramson, S. B. & Huang, X. 17β-Estradiol inhibits iron hormone hepcidin through an estrogen responsive element half-site. *Endocrinology* **153**, 3170–3178 (2012).

50. Shin, J. A., Kim, H.-S., Lee Kang, J. & Park, E.-M. Estrogen deficiency is associated with brain iron deposition via upregulation of hepcidin expression in aged female mice. *Neurobiol Aging* **96**, 33–42 (2020).

51. Hou, Y. *et al.* Estrogen regulates iron homeostasis through governing hepatic hepcidin expression via an estrogen response element. *Gene* **511**, 398–403 (2012).

52. Qian, Y. *et al.* Estrogen contributes to regulating iron metabolism through governing ferroportin signaling via an estrogen response element. *Cell Signal* **27**, 934–942 (2015).

53. Bajbouj, K. *et al.* Estrogen signaling differentially alters iron metabolism in monocytes in an Interleukin 6-dependent manner. *Immunobiology* **225**, 151995 (2020).

54. Xu, M. *et al.* Differential regulation of estrogen in iron metabolism in astrocytes and neurons. *J Cell Physiol* **234**, 4232–4242 (2019).

55. Qu, Y. *et al.* Estrogen Up-Regulates Iron Transporters and Iron Storage Protein Through Hypoxia Inducible Factor 1 Alpha Activation Mediated by Estrogen Receptor β and G Protein Estrogen Receptor in BV2 Microglia Cells. *Neurochem Res* (2022) doi:10.1007/s11064-022-03658-1.

56. Ikeda, Y. *et al.* Estrogen regulates hepcidin expression via GPR30-BMP6-dependent signaling in hepatocytes. *PLoS One* **7**, e40465 (2012).

57. Crowe, A. & Morgan, E. H. Iron and copper interact during their uptake and deposition in the brain and other organs of developing rats exposed to dietary excess of the two metals. *J Nutr* **126**, 183–194 (1996).

58. Felt, B. T. & Lozoff, B. Brain iron and behavior of rats are not normalized by treatment of iron deficiency anemia during early development. *J Nutr* **126**, 693–701 (1996).

59. Piñero, D. J., Li, N. Q., Connor, J. R. & Beard, J. L. Variations in dietary iron alter brain iron metabolism in developing rats. *J Nutr* **130**, 254–263 (2000).

60. Prado, E. L. & Dewey, K. G. Nutrition and brain development in early life. *Nutr Rev* **72**, 267–284 (2014).

61. Georgieff, M. K. The role of iron in neurodevelopment: fetal iron deficiency and the developing hippocampus. *Biochem Soc Trans* **36**, 1267–1271 (2008).

62. Taylor, E. M. & Morgan, E. H. Developmental changes in transferrin and iron uptake by the brain in the rat. *Brain Res Dev Brain Res* **55**, 35–42 (1990).

63. Morgan, E. H. & Moos, T. Mechanism and developmental changes in iron transport across the blood-brain barrier. *Dev Neurosci* **24**, 106–113 (2002).

64. McCarthy, R. C. & Kosman, D. J. Iron transport across the blood-brain barrier: development, neurovascular regulation and cerebral amyloid angiopathy. *Cell. Mol. Life Sci.* **72**, 709–727 (2015).

65. Moos, T. & Rosengren Nielsen, T. Ferroportin in the postnatal rat brain: implications for axonal transport and neuronal export of iron. *Semin Pediatr Neurol* **13**, 149–157 (2006).

66. Carlson, E. S., Stead, J. D. H., Neal, C. R., Petryk, A. & Georgieff, M. K. Perinatal iron deficiency results in altered developmental expression of genes mediating energy metabolism and neuronal morphogenesis in hippocampus. *Hippocampus* **17**, 679–691 (2007).

67. Erikson, K. M., Pinero, D. J., Connor, J. R. & Beard, J. L. Regional Brain Iron, Ferritin and Transferrin Concentrations during Iron Deficiency and Iron Repletion in Developing Rats. *The Journal of Nutrition* **127**, 2030–2038 (1997).

68. Beard, J. Iron deficiency alters brain development and functioning. *J Nutr* **133**, 1468S–72S (2003).

69. Grubić Kezele, T. & Ćurko-Cofek, B. Age-Related Changes and Sex-Related Differences in Brain Iron Metabolism. *Nutrients* **12**, E2601 (2020).

70. Yang, A. C. *et al.* Physiological blood-brain transport is impaired with age by a shift in transcytosis. *Nature* **583**, 425–430 (2020).

71. Mezzanotte, M., Ammirata, G., Boido, M., Stanga, S. & Roetto, A. Activation of the Hepcidin-Ferroportin1 pathway in the brain and astrocytic-neuronal crosstalk to counteract iron dyshomeostasis during aging. *Sci Rep* **12**, 11724 (2022).

72. Sato, T., Shapiro, J. S., Chang, H.-C., Miller, R. A. & Ardehali, H. Aging is associated with increased brain iron through cortex-derived hepcidin expression. *Elife* **11**, e73456 (2022).

73. Finger, C. E., Moreno-Gonzalez, I., Gutierrez, A., Moruno-Manchon, J. F. & McCullough, L. D. Age-related immune alterations and cerebrovascular inflammation. *Mol Psychiatry* **27**, 803–818 (2022).

74. Mayle, K. M., Le, A. M. & Kamei, D. T. The Intracellular Trafficking Pathway of Transferrin. *Biochim Biophys Acta* **1820**, 264–281 (2012).

75. De Domenico, I. *et al.* The molecular mechanism of hepcidin-mediated ferroportin down-regulation. *Mol Biol Cell* **18**, 2569–2578 (2007).

76. Dlouhy, A. C., Bailey, D. K., Steimle, B. L., Parker, H. V. & Kosman, D. J. Fluorescence resonance energy transfer links membrane ferroportin, hephaestin but not ferroportin, amyloid precursor protein complex with iron efflux. *J. Biol. Chem.* **294**, 4202–4214 (2019).

77. McCarthy, R. C. & Kosman, D. J. Ferroportin and exocytoplasmic ferroxidase activity are required for brain microvascular endothelial cell iron efflux. *J. Biol. Chem.* **288**, 17932–17940 (2013).

78. Jiang, R. *et al.* Hephaestin and Ceruloplasmin Play Distinct but Interrelated Roles in Iron Homeostasis in Mouse Brain. *The Journal of Nutrition* **145**, 1003–1009 (2015).

79. Fishman, J. B., Rubin, J. B., Handrahan, J. V., Connor, J. R. & Fine, R. E. Receptor-mediated transcytosis of transferrin across the blood-brain barrier. *J Neurosci Res* **18**, 299–304 (1987).

80. Pardridge, W. M., Buciak, J. L. & Friden, P. M. Selective transport of an anti-transferrin receptor antibody through the blood-brain barrier in vivo. *J Pharmacol Exp Ther* **259**, 66–70 (1991).

81. Zhang, Y. & Pardridge, W. M. Neuroprotection in transient focal brain ischemia after delayed intravenous administration of brain-derived neurotrophic factor conjugated to a blood-brain barrier drug targeting system. *Stroke* **32**, 1378–1384 (2001).

82. Stocki, P. *et al.* Blood-brain barrier transport using a high affinity, brain-selective VNAR antibody targeting transferrin receptor 1. *FASEB J* **35**, e21172 (2021).

83. Kariolis, M. S. *et al.* Brain delivery of therapeutic proteins using an Fc fragment blood-brain barrier transport vehicle in mice and monkeys. *Science Translational Medicine* **12**, (2020).

84. Pardridge, W. M. Kinetics of Blood-Brain Barrier Transport of Monoclonal Antibodies Targeting the Insulin Receptor and the Transferrin Receptor. *Pharmaceuticals (Basel)* **15**, 3 (2021).

85. Villaseñor, R., Schilling, M., Sundaresan, J., Lutz, Y. & Collin, L. Sorting Tubules Regulate Blood-Brain Barrier Transcytosis. *Cell Rep* **21**, 3256–3270 (2017).

86. Tian, X. *et al.* On the shuttling across the blood-brain barrier via tubule formation: Mechanism and cargo avidity bias. *Sci Adv* **6**, eabc4397 (2020).

87. Virgintino, D. *et al.* Plasma membrane-derived microvesicles released from tip endothelial cells during vascular sprouting. *Angiogenesis* **15**, 761–769 (2012).

88. András, I. E. & Toborek, M. Extracellular vesicles of the blood-brain barrier. *Tissue Barriers* **4**, e1131804 (2016).

89. Saint-Pol, J., Gosselet, F., Duban-Deweer, S., Pottiez, G. & Karamanos, Y. Targeting and Crossing the Blood-Brain Barrier with Extracellular Vesicles. *Cells* **9**, E851 (2020).

90. Palsa, K. *et al.* Exosomes are involved in iron transport from human blood-brain barrier endothelial cells and are modified by endothelial cell iron status. *J Biol Chem* **299**, 102868 (2023).

91. Pantopoulos, K. Iron metabolism and the IRE/IRP regulatory system: an update. *Ann N Y Acad Sci* **1012**, 1–13 (2004).

92. Wang, J. & Pantopoulos, K. Regulation of cellular iron metabolism. *Biochem J* **434**, 365–381 (2011).

93. Zhang, D.-L., Hughes, R. M., Ollivierre-Wilson, H., Ghosh, M. C. & Rouault, T. A. A ferroportin transcript that lacks an iron-responsive element enables duodenal and erythroid precursor cells to evade translational repression. *Cell Metab* **9**, 461–473 (2009).

94. Wu, L. J. *et al.* Expression of the iron transporter ferroportin in synaptic vesicles and the blood-brain barrier. *Brain Res* **1001**, 108–117 (2004).

95. Ji, C. & Kosman, D. J. Molecular mechanisms of non-transferrin-bound and transferring-bound iron uptake in primary hippocampal neurons. *J Neurochem* **133**, 668–683 (2015).

96. Beard, J. L., Wiesinger, J. A., Li, N. & Connor, J. R. Brain iron uptake in hypotransferrinemic mice: influence of systemic iron status. *J Neurosci Res* **79**, 254–261 (2005).

97. Connor, J. R., Snyder, B. S., Beard, J. L., Fine, R. E. & Mufson, E. J. Regional distribution of iron and iron-regulatory proteins in the brain in aging and Alzheimer's disease. *Journal of Neuroscience Research* **31**, 327–335 (1992).

98. Duck, K. A., Simpson, I. A. & Connor, J. R. Regulatory mechanisms for iron transport across the blood-brain barrier. *Biochem. Biophys. Res. Commun.* **494**, 70–75 (2017).

99. Patel, B. N. & David, S. A novel glycosylphosphatidylinositol-anchored form of ceruloplasmin is expressed by mammalian astrocytes. *J Biol Chem* **272**, 20185–20190 (1997).

100. Li, Z.-D. *et al.* The divergent effects of astrocyte ceruloplasmin on learning and memory function in young and old mice. *Cell Death Dis* **13**, 1006 (2022).

101. McCarthy, R. C. & Kosman, D. J. Glial cell ceruloplasmin and hepcidin differentially regulate iron efflux from brain microvascular endothelial cells. *PLoS One* **9**, e89003 (2014).

102. Patel, B. N. *et al.* Ceruloplasmin regulates iron levels in the CNS and prevents free radical injury. *J Neurosci* **22**, 6578–6586 (2002).

103. Ha-Duong, N.-T., Eid, C., Hémadi, M. & El Hage Chahine, J.-M. In vitro interaction between ceruloplasmin and human serum transferrin. *Biochemistry* **49**, 10261–10263 (2010).

104. Eid, C., Hémadi, M., Ha-Duong, N.-T. & El Hage Chahine, J.-M. Iron uptake and transfer from ceruloplasmin to transferrin. *Biochim Biophys Acta* **1840**, 1771–1781 (2014).

105. Hudson, D. M., Krisinger, M. J., Griffiths, T. A. M. & Macgillivray, R. T. A. Neither human hephaestin nor ceruloplasmin forms a stable complex with transferrin. *J Cell Biochem* **103**, 1849–1855 (2008).

106. Sokolov, A. V. *et al.* Comparison of Interaction between Ceruloplasmin and Lactoferrin/Transferrin: to Bind or Not to Bind. *Biochemistry (Mosc)* **82**, 1073–1078 (2017).

107. Sakajiri, T. *et al.* Zinc mediates the interaction between ceruloplasmin and apo-transferrin for the efficient transfer of Fe(III) ions. *Metallomics* **13**, mfab065 (2021).

108. Bédard, Y. C., Pinkerton, P. H. & Simon, G. T. Uptake of circulating iron by the duodenum of normal mice and mice with altered iron stores, including sex-linked anemia: high resolution radioautographic study. *Lab Invest* **34**, 611–615 (1976).

109. Donovan, A. *et al.* The iron exporter ferroportin/Slc40a1 is essential for iron homeostasis. *Cell Metab* **1**, 191–200 (2005).

110. Alvarez-Hernandez, X., Smith, M. & Glass, J. The effect of apotransferrin on iron release from Caco-2 cells, an intestinal epithelial cell line. *Blood* **91**, 3974–3979 (1998).

111. Alvarez-Hernandez, X., Smith, M. & Glass, J. Apo-transferrin is internalized and routed differently from Fe-transferrin by caco-2 cells: a confocal microscopy study of vesicular transport in intestinal cells. *Blood* **95**, 721–723 (2000).

112. Moriya, M. & Linder, M. C. Vesicular transport and apotransferrin in intestinal iron absorption, as shown in the Caco-2 cell model. *Am J Physiol Gastrointest Liver Physiol* **290**, G301-309 (2006).

113. Collins, J. F., Wessling-Resnick, M. & Knutson, M. D. Hepcidin regulation of iron transport. *J Nutr* **138**, 2284–2288 (2008).

114. Hänninen, M. M. *et al.* Expression of iron-related genes in human brain and brain tumors. *BMC Neurosci* **10**, 36 (2009).

115. Vela, D. Hepcidin, an emerging and important player in brain iron homeostasis. *J Transl Med* **16**, 25 (2018).

116. Yanase, K. *et al.* Immunoreactivities for hepcidin, ferroportin, and hephaestin in astrocytes and choroid plexus epithelium of human brains. *Neuropathology* **40**, 75–83 (2020).

117. Raha-Chowdhury, R. *et al.* Expression and cellular localization of hepcidin mRNA and protein in normal rat brain. *BMC Neurosci* **16**, 24 (2015).

118. Zechel, S., Huber-Wittmer, K. & von Bohlen und Halbach, O. Distribution of the iron-regulating protein hepcidin in the murine central nervous system. *J Neurosci Res* **84**, 790–800 (2006).

119. Poli, M., Asperti, M., Ruzzenenti, P., Regoni, M. & Arosio, P. Hepcidin antagonists for potential treatments of disorders with hepcidin excess. *Front Pharmacol* **5**, 86 (2014).

120. Nemeth, E. *et al.* Hepcidin regulates cellular iron efflux by binding to ferroportin and inducing its internalization. *Science* **306**, 2090–2093 (2004).

121. Pan, Y. *et al.* Structural basis of ion transport and inhibition in ferroportin. *Nat Commun* **11**, 5686 (2020).

122. Nemeth, E. *et al.* The N-terminus of hepcidin is essential for its interaction with ferroportin: structure-function study. *Blood* **107**, 328–333 (2006).

123. Qiao, B. *et al.* Hepcidin-induced endocytosis of ferroportin is dependent on ferroportin ubiquitination. *Cell Metab* **15**, 918–924 (2012).

124. Wallace, D. F. *et al.* The dynamics of hepcidin-ferroportin internalization and consequences of a novel ferroportin disease mutation. *Am J Hematol* **92**, 1052–1061 (2017).

125. You, L. *et al.* Astrocyte-derived hepcidin controls iron traffic at the blood-brain-barrier via regulating ferroportin 1 of microvascular endothelial cells. *Cell Death Dis* **13**, 667 (2022).

126. Lin, L. *et al.* Iron transferrin regulates hepcidin synthesis in primary hepatocyte culture through hemojuvelin and BMP2/4. *Blood* **110**, 2182–2189 (2007).

127. Ramos, E. *et al.* Evidence for distinct pathways of hepcidin regulation by acute and chronic iron loading in mice. *Hepatology* **53**, 1333–1341 (2011).

128. Sangkhae, V. & Nemeth, E. Regulation of the Iron Homeostatic Hormone Hepcidin. *Adv Nutr* **8**, 126–136 (2017).

129. Nemeth, E. *et al.* IL-6 mediates hypoferremia of inflammation by inducing the synthesis of the iron regulatory hormone hepcidin. *J Clin Invest* **113**, 1271–1276 (2004).

130. Urrutia, P. *et al.* Inflammation alters the expression of DMT1, FPN1 and hepcidin, and it causes iron accumulation in central nervous system cells. *J Neurochem* **126**, 541–549 (2013).

131. You, L.-H. *et al.* Astrocyte hepcidin is a key factor in LPS-induced neuronal apoptosis. *Cell Death Dis* **8**, e2676 (2017).

132. Enculescu, M. *et al.* Modelling Systemic Iron Regulation during Dietary Iron Overload and Acute Inflammation: Role of Hepcidin-Independent Mechanisms. *PLoS Comput Biol* **13**, e1005322 (2017).

133. Ayton, S. *et al.* Regional brain iron associated with deterioration in Alzheimer's disease: A large cohort study and theoretical significance. *Alzheimers Dement* (2021) doi:10.1002/alz.12282.

134. Langkammer, C., Ropele, S., Pirpamer, L., Fazekas, F. & Schmidt, R. MRI for Iron Mapping in Alzheimer's Disease. *NDD* **13**, 189–191 (2014).

135. Bulk, M. *et al.* Postmortem MRI and histology demonstrate differential iron accumulation and cortical myelin organization in early- and late-onset Alzheimer's disease. *Neurobiology of Aging* **62**, 231–242 (2018).

136. Moon, Y., Han, S.-H. & Moon, W.-J. Patterns of Brain Iron Accumulation in Vascular Dementia and Alzheimer's Dementia Using Quantitative Susceptibility Mapping Imaging. *Journal of Alzheimer's Disease* **51**, 737–745 (2016).

137. Rogers, J. *et al.* Iron and the translation of the amyloid precursor protein (APP) and ferritin. *Biochem Soc Trans* **36**, 1282–1287 (2008).

138. Rogers, J. T. *et al.* An Iron-responsive Element Type II in the 5′-Untranslated Region of the Alzheimer's Amyloid Precursor Protein Transcript. *Journal of Biological Chemistry* **277**, 45518–45528 (2002).

139. Cho, H.-H. *et al.* Selective Translational Control of the Alzheimer Amyloid Precursor Protein Transcript by Iron Regulatory Protein-1. *Journal of Biological Chemistry* **285**, 31217–31232 (2010).

140. Telling, N. D. *et al.* Iron Biochemistry is Correlated with Amyloid Plaque Morphology in an Established Mouse Model of Alzheimer's Disease. *Cell Chemical Biology* **24**, 1205-1215.e3 (2017).

141. Gong, N.-J., Dibb, R., Bulk, M., van der Weerd, L. & Liu, C. Imaging beta amyloid aggregation and iron accumulation in Alzheimer's disease using quantitative susceptibility mapping MRI. *Neuroimage* **191**, 176–185 (2019).

142. Joppe, K., Roser, A.-E., Maass, F. & Lingor, P. The Contribution of Iron to Protein Aggregation Disorders in the Central Nervous System. *Front Neurosci* **13**, (2019).

143. Meadowcroft, M. D., Connor, J. R. & Yang, Q. X. Cortical iron regulation and inflammatory response in Alzheimer's disease and APPSWE/PS1ΔE9 mice: a histological perspective. *Front Neurosci* **9**, 255 (2015).

144. Meadowcroft, M. D., Peters, D. G., Dewal, R. P., Connor, J. R. & Yang, Q. X. The effect of iron in MRI and transverse relaxation of amyloid-beta plaques in Alzheimer's disease. *NMR Biomed* **28**, 297–305 (2015).

145. Erickson, M. A. & Banks, W. A. Blood-brain barrier dysfunction as a cause and consequence of Alzheimer's disease. *J Cereb Blood Flow Metab* **33**, 1500–1513 (2013).

146. Yamazaki, Y. & Kanekiyo, T. Blood-Brain Barrier Dysfunction and the Pathogenesis of Alzheimer's Disease. *Int J Mol Sci* **18**, (2017).

147. Montagne, A. *et al.* APOE4 leads to blood–brain barrier dysfunction predicting cognitive decline. *Nature* 1–6 (2020) doi:10.1038/s41586-020-2247-3.

148. Parodi-Rullán, R., Ghiso, J., Cabrera, E., Rostagno, A. & Fossati, S. Alzheimer's amyloid β heterogeneous species differentially affect brain endothelial cell viability, blood-brain barrier integrity, and angiogenesis. *Aging Cell* e13258 (2020) doi:10.1111/acel.13258.

149. del Valle, J. *et al.* Cerebral amyloid angiopathy, blood-brain barrier disruption and amyloid accumulation in SAMP8 mice. *Neurodegener Dis* **8**, 421–429 (2011).

150. Kinney, J. W. *et al.* Inflammation as a central mechanism in Alzheimer's disease. *Alzheimers Dement (N Y)* **4**, 575–590 (2018).

151. de Vries, H. E. *et al.* The influence of cytokines on the integrity of the blood-brain barrier in vitro. *J Neuroimmunol* **64**, 37–43 (1996).

152. Wong, D., Dorovini-Zis, K. & Vincent, S. R. Cytokines, nitric oxide, and cGMP modulate the permeability of an in vitro model of the human blood-brain barrier. *Exp Neurol* **190**, 446–455 (2004).

153. Pan, W. *et al.* Cytokine Signaling Modulates Blood-Brain Barrier Function. *Curr Pharm Des* **17**, 3729–3740 (2011).

154. Thomsen, M. S. *et al.* Neurodegeneration with inflammation is accompanied by accumulation of iron and ferritin in microglia and neurons. *Neurobiol Dis* **81**, 108–118 (2015).

155. Montoliu-Gaya, L. *et al.* Aβ-oligomer uptake and the resulting inflammatory response in adult human astrocytes are precluded by an anti-Aβ single chain variable fragment in combination with an apoE mimetic peptide. *Molecular and Cellular Neuroscience* **89**, 49–59 (2018).

156. García-Matas, S. *et al.* In vitro and in vivo activation of astrocytes by amyloid-beta is potentiated by pro-oxidant agents. *J Alzheimers Dis* **20**, 229–245 (2010).

157. Sofroniew, M. V. Molecular dissection of reactive astrogliosis and glial scar formation. *Trends Neurosci* **32**, 638–647 (2009).

158. Park, J.-C. & Mook-Jung, S.-H. H. & I. Peripheral inflammatory biomarkers in Alzheimer's disease: a brief review. *BMB Reports* **53**, 10–19 (2020).

159. Zhang, X. *et al.* Hepcidin overexpression in astrocytes alters brain iron metabolism and protects against amyloid-β induced brain damage in mice. *Cell Death Discovery* **6**, 1–14 (2020).

160. Cherny, R. A. *et al.* Treatment with a copper-zinc chelator markedly and rapidly inhibits beta-amyloid accumulation in Alzheimer's disease transgenic mice. *Neuron* **30**, 665–676 (2001).

161. Adlard, P. A. *et al.* Metal ionophore treatment restores dendritic spine density and synaptic protein levels in a mouse model of Alzheimer's disease. *PLoS One* **6**, e17669 (2011).

162. Lannfelt, L. *et al.* Safety, efficacy, and biomarker findings of PBT2 in targeting Abeta as a modifying therapy for Alzheimer's disease: a phase IIa, double-blind, randomised, placebo-controlled trial. *Lancet Neurol* **7**, 779–786 (2008).

163. Fawzi, S. F., Menze, E. T. & Tadros, M. G. Deferiprone ameliorates memory impairment in Scopolamine-treated rats: The impact of its iron-chelating effect on β-amyloid disposition. *Behav Brain Res* **378**, 112314 (2020).

164. Rao, S. S. *et al.* The Iron Chelator Deferiprone Improves the Phenotype in a Mouse Model of Tauopathy. *J Alzheimers Dis* **77**, 753–771 (2020).

165. Belaidi, A. A. & Bush, A. I. Iron neurochemistry in Alzheimer's disease and Parkinson's disease: targets for therapeutics. *J. Neurochem.* **139 Suppl 1**, 179–197 (2016).

166. Zarow, C., Lyness, S. A., Mortimer, J. A. & Chui, H. C. Neuronal loss is greater in the locus coeruleus than nucleus basalis and substantia nigra in Alzheimer and Parkinson diseases. *Arch Neurol* **60**, 337–341 (2003).

167. Genoud, S., Senior, A. M., Hare, D. J. & Double, K. L. Meta-Analysis of Copper and Iron in Parkinson's Disease Brain and Biofluids. *Mov Disord* **35**, 662–671 (2020).

168. Riederer, P. *et al.* Transition metals, ferritin, glutathione, and ascorbic acid in parkinsonian brains. *J Neurochem* **52**, 515–520 (1989).

169. Dexter, D. T. *et al.* Increased nigral iron content in postmortem parkinsonian brain. *Lancet* **2**, 1219–1220 (1987).

170. Pyatigorskaya, N. *et al.* High nigral iron deposition in LRRK2 and Parkin mutation carriers using R2* relaxometry. *Mov Disord* **30**, 1077–1084 (2015).

171. Oestreicher, E. *et al.* Degeneration of nigrostriatal dopaminergic neurons increases iron within the substantia nigra: a histochemical and neurochemical study. *Brain Res* **660**, 8–18 (1994).

172. Ma, L. *et al.* Parkinson's disease: Alterations in iron and redox biology as a key to unlock therapeutic strategies. *Redox Biol* **41**, 101896 (2021).

173. Hirsch, E. C. Biochemistry of Parkinson's disease with special reference to the dopaminergic systems. *Mol Neurobiol* **9**, 135–142 (1994).

174. Rao, K. S. J. *et al.* Amyloid beta and neuromelanin--toxic or protective molecules? The cellular context makes the difference. *Prog Neurobiol* **78**, 364–373 (2006).

175. Zecca, L. *et al.* Iron, neuromelanin and ferritin content in the substantia nigra of normal subjects at different ages: consequences for iron storage and neurodegenerative processes. *J Neurochem* **76**, 1766–1773 (2001).

176. Ayton, S., Lei, P., Mclean, C., Bush, A. I. & Finkelstein, D. I. Transferrin protects against Parkinsonian neurotoxicity and is deficient in Parkinson's substantia nigra. *Signal Transduct Target Ther* **1**, 16015 (2016).

177. Loeffler, D. A. *et al.* Transferrin and iron in normal, Alzheimer's disease, and Parkinson's disease brain regions. *J Neurochem* **65**, 710–724 (1995).

178. Du, G. *et al.* Dynamics of Nigral Iron Accumulation in Parkinson's Disease: From Diagnosis to Late Stage. *Mov Disord* (2022) doi:10.1002/mds.29062.

179. Devos, D. *et al.* Trial of Deferiprone in Parkinson's Disease. *N Engl J Med* **387**, 2045–2055 (2022).

180. Bjørklund, G., Hofer, T., Nurchi, V. M. & Aaseth, J. Iron and other metals in the pathogenesis of Parkinson's disease: Toxic effects and possible detoxification. *J Inorg Biochem* **199**, 110717 (2019).

181. Hare, D. J. & Double, K. L. Iron and dopamine: a toxic couple. *Brain* **139**, 1026–1035 (2016).

182. Wise, R. M. *et al.* Interactions of dopamine, iron, and alpha-synuclein linked to dopaminergic neuron vulnerability in Parkinson's disease and Neurodegeneration with Brain Iron Accumulation disorders. *Neurobiol Dis* **175**, 105920 (2022).

183. Santiago, M., Matarredona, E. R., Granero, L., Cano, J. & Machado, A. Neurotoxic relationship between dopamine and iron in the striatal dopaminergic nerve terminals. *Brain Res* **858**, 26–32 (2000).

184. Dichtl, S. *et al.* Dopamine promotes cellular iron accumulation and oxidative stress responses in macrophages. *Biochem Pharmacol* **148**, 193–201 (2018).

185. Zhang, H.-Y. *et al.* 6-Hydroxydopamine promotes iron traffic in primary cultured astrocytes. *Biometals* **26**, 705–714 (2013).

186. Sweeney, M. D., Sagare, A. P. & Zlokovic, B. V. Blood–brain barrier breakdown in Alzheimer disease and other neurodegenerative disorders. *Nat Rev Neurol* **14**, 133–150 (2018).

187. Fujita, K. *et al.* Blood-brain barrier permeability in Parkinson's disease patients with and without dyskinesia. *J Neurol* **268**, 2246–2255 (2021).

188. Song, T. *et al.* Nigral Iron Deposition Is Associated With Levodopa-Induced Dyskinesia in Parkinson's Disease. *Front Neurosci* **15**, 647168 (2021).

189. Ben-Shachar, D., Livne, E., Spanier, I., Leenders, K. L. & Youdim, M. B. Typical and atypical neuroleptics induce alteration in blood-brain barrier and brain 59FeCl3 uptake. *J Neurochem* **62**, 1112–1118 (1994).

190. Arreguin, S., Nelson, P., Padway, S., Shirazi, M. & Pierpont, C. Dopamine complexes of iron in the etiology and pathogenesis of Parkinson's disease. *J Inorg Biochem* **103**, 87–93 (2009).

191. Alhassen, S., Senel, M. & Alachkar, A. Surface Plasmon Resonance Identifies High-Affinity Binding of l-DOPA to Siderocalin/Lipocalin-2 through Iron-Siderophore Action: Implications for Parkinson's Disease Treatment. *ACS Chem Neurosci* **13**, 158–165 (2022).

192. Nordlander, N. B. Therapy in restless legs. *Acta Med Scand* **145**, 453–457 (1953).

193. Berger, K. *et al.* Iron metabolism and the risk of restless legs syndrome in an elderly general population--the MEMO-Study. *J Neurol* **249**, 1195–1199 (2002).

194. Zhou, X. *et al.* The Efficacy and Safety of Pharmacological Treatments for Restless Legs Syndrome: Systemic Review and Network Meta-Analysis. *Front Neurosci* **15**, 751643 (2021).

195. Godau, J., Klose, U., Di Santo, A., Schweitzer, K. & Berg, D. Multiregional brain iron deficiency in restless legs syndrome. *Mov Disord* **23**, 1184–1187 (2008).

196. Allen, R. P. *et al.* MRI measurement of brain iron in patients with restless legs syndrome. *Neurology* **56**, 263–265 (2001).

197. Connor, J. R. *et al.* Profile of altered brain iron acquisition in restless legs syndrome. *Brain* **134**, 959–968 (2011).

198. Connor, J. R. *et al.* Altered dopaminergic profile in the putamen and substantia nigra in restless leg syndrome. *Brain* **132**, 2403–2412 (2009).

199. Connor, J. R., Patton, S. M., Oexle, K. & Allen, R. P. Iron and restless legs syndrome: treatment, genetics and pathophysiology. *Sleep Med* **31**, 61–70 (2017).

200. Connor, J. R. *et al.* Evidence for communication of peripheral iron status to cerebrospinal fluid: clinical implications for therapeutic strategy. *Fluids Barriers CNS* **17**, 28 (2020).

201. Wade, Q. W., Chiou, B. & Connor, J. R. Iron uptake at the blood-brain barrier is influenced by sex and genotype. *Adv Pharmacol* **84**, 123–145 (2019).

202. Chiou, B. *et al.* Pharmaceutical iron formulations do not cross a model of the human blood-brain barrier. *PLoS One* **13**, e0198775 (2018).

203. Sousa, L., Oliveira, M. M., Pessôa, M. T. C. & Barbosa, L. A. Iron overload: Effects on cellular biochemistry. *Clin Chim Acta* **504**, 180–189 (2020).

204. Pivina, L., Semenova, Y., Doşa, M. D., Dauletyarova, M. & Bjørklund, G. Iron Deficiency, Cognitive Functions, and Neurobehavioral Disorders in Children. *J Mol Neurosci* **68**, 1–10 (2019).

205. Goldstein, G. W. & Betz, A. L. The blood-brain barrier. *Sci Am* **255**, 74–83 (1986).

206. Hladky, S. B. & Barrand, M. A. Mechanisms of fluid movement into, through and out of the brain: evaluation of the evidence. *Fluids Barriers CNS* **11**, 26 (2014).

207. Aldred, A. R., Dickson, P. W., Marley, P. D. & Schreiber, G. Distribution of transferrin synthesis in brain and other tissues in the rat. *J Biol Chem* **262**, 5293–5297 (1987).

208. Moos, T. Brain iron homeostasis. *Dan Med Bull* **49**, 279–301 (2002).

209. Siddappa, A. J. M. *et al.* Iron Deficiency Alters Iron Regulatory Protein and Iron Transport Protein Expression in the Perinatal Rat Brain. *Pediatr Res* **53**, 800–807 (2003).

210. Moos, T. & Morgan, E. H. The metabolism of neuronal iron and its pathogenic role in neurological disease: review. *Ann N Y Acad Sci* **1012**, 14–26 (2004).

211. Beard, J. L., Wiesinger, J. A., Li, N. & Connor, J. R. Brain iron uptake in hypotransferrinemic mice: influence of systemic iron status. *J Neurosci Res* **79**, 254–261 (2005).

212. Chiou, B., Lucassen, E., Sather, M., Kallianpur, A. & Connor, J. Semaphorin4A and H-ferritin utilize Tim-1 on human oligodendrocytes: A novel neuro-immune axis. *Glia* **66**, 1317–1330 (2018).

213. Moos, T. & Morgan, E. H. Kinetics and distribution of [59Fe-125I]transferrin injected into the ventricular system of the rat. *Brain Res* **790**, 115–128 (1998).

214. Moos, T. Delivery of transferrin and immunoglobulins to the ventricular system of the rat. *Front Biosci* **8**, a102-109 (2003).

215. Brightman, M. W. The distribution within the brain of ferritin injected into cerebrospinal fluid compartments. I. Ependymal distribution. *J Cell Biol* **26**, 99–123 (1965).

216. Brightman, M. W. The intracerebral movement of proteins injected into blood and cerebrospinal fluid of mice. *Prog Brain Res* **29**, 19–40 (1968).

217. Iliff, J. J. *et al.* A paravascular pathway facilitates CSF flow through the brain parenchyma and the clearance of interstitial solutes, including amyloid β. *Sci Transl Med* **4**, 147ra111 (2012).

218. Pardridge, W. M. CSF, blood-brain barrier, and brain drug delivery. *Expert Opin Drug Deliv* **13**, 963–975 (2016).

219. Hino, K., Otsuka, S., Ichii, O., Hashimoto, Y. & Kon, Y. Strain differences of cerebral ventricles in mice: can the MRL/MpJ mouse be a model for hydrocephalus? *Jpn J Vet Res* **57**, 3–11 (2009).

220. Khan, F. H. Iron, dopamine, genetics, and hormones in the pathophysiology of restless legs syndrome. *J Neurol* 8 (2017).

221. Martin, J. *et al.* Weak correlations between serum and cerebrospinal fluid levels of estradiol, progesterone and testosterone in males. *BMC Neurosci* **20**, 53 (2019).

222. Kenealy, B. P. *et al.* Neuroestradiol in the hypothalamus contributes to the regulation of gonadotropin releasing hormone release. *J Neurosci* **33**, 19051–19059 (2013).

223. Ji, C., Steimle, B. L., Bailey, D. K. & Kosman, D. J. The Ferroxidase Hephaestin But Not Amyloid Precursor Protein is Required for Ferroportin-Supported Iron Efflux in Primary Hippocampal Neurons. *Cell. Mol. Neurobiol.* **38**, 941–954 (2018).

224. Bergamaschi, G. & Villani, L. Serum hepcidin: a novel diagnostic tool in disorders of iron metabolism. *Haematologica* **94**, 1631–1633 (2009).

225. Girelli, D., Nemeth, E. & Swinkels, D. W. Hepcidin in the diagnosis of iron disorders. *Blood* **127**, 2809–2813 (2016).

226. Neal, E. H. *et al.* A Simplified, Fully Defined Differentiation Scheme for Producing Blood-Brain Barrier Endothelial Cells from Human iPSCs. *Stem Cell Reports* **12**, 1380–1388 (2019).

227. Nwogu, N., Ortiz, L. E. & Kwun, H. J. Surface charge of Merkel cell polyomavirus small T antigen determines cell transformation through allosteric FBW7 WD40 domain targeting. *Oncogenesis* **9**, 53 (2020).

228. Kondaiah, P., Aslam, M. F., Mashurabad, P. C., Sharp, P. A. & Pullakhandam, R. Zinc induces iron uptake and DMT1 expression in Caco-2 cells via a PI3K/IRP2 dependent mechanism. *Biochem J* **476**, 1573–1583 (2019).

229. Patton, S. M. *et al.* Cerebrospinal fluid (CSF) biomarkers of iron status are associated with CSF viral load, antiretroviral therapy, and demographic factors in HIV-infected adults. *Fluids Barriers CNS* **14**, 11 (2017).

230. Arena, T. A., Harms, P. D. & Wong, A. W. High Throughput Transfection of HEK293 Cells for Transient Protein Production. *Methods Mol Biol* **1850**, 179–187 (2018).

231. Hu, J. *et al.* Human Embryonic Kidney 293 Cells: A Vehicle for Biopharmaceutical Manufacturing, Structural Biology, and Electrophysiology. *Cells Tissues Organs* **205**, 1–8 (2018).

232. Pulix, M., Lukashchuk, V., Smith, D. C. & Dickson, A. J. Molecular characterization of HEK293 cells as emerging versatile cell factories. *Curr Opin Biotechnol* **71**, 18–24 (2021).

233. Viveiros, A. *et al.* Reduced iron export associated with hepcidin resistance can explain the iron overload spectrum in ferroportin disease. *Liver Int* **40**, 1941–1951 (2020).

234. Jiang, L., Garrick, M. D., Garrick, L. M., Zhao, L. & Collins, J. F. Divalent metal transporter 1 (Dmt1) mediates copper transport in the duodenum of iron-deficient rats and when overexpressed in iron-deprived HEK-293 cells. *J Nutr* **143**, 1927–1933 (2013).

235. Katt, M. E., Xu, Z. S., Gerecht, S. & Searson, P. C. Human Brain Microvascular Endothelial Cells Derived from the BC1 iPS Cell Line Exhibit a Blood-Brain Barrier Phenotype. *PLoS One* **11**, e0152105 (2016).

236. Petrak, J. & Vyoral, D. Hephaestin--a ferroxidase of cellular iron export. *Int J Biochem Cell Biol* **37**, 1173–1178 (2005).

237. Jiang, R. *et al.* Hephaestin and ceruloplasmin play distinct but interrelated roles in iron homeostasis in mouse brain. *J Nutr* **145**, 1003–1009 (2015).

238. Yeh, K.-Y., Yeh, M. & Glass, J. Interactions between ferroportin and hephaestin in rat enterocytes are reduced after iron ingestion. *Gastroenterology* **141**, 292–299, 299.e1 (2011).

239. Wally, J. *et al.* The crystal structure of iron-free human serum transferrin provides insight into inter-lobe communication and receptor binding. *J Biol Chem* **281**, 24934–24944 (2006).

240. Xu, Y. *et al.* Astrocyte hepcidin ameliorates neuronal loss through attenuating brain iron deposition and oxidative stress in APP/PS1 mice. *Free Radical Biology and Medicine* **158**, 84–95 (2020).

241. Lane, D. J. R., Ayton, S. & Bush, A. I. Iron and Alzheimer's Disease: An Update on Emerging Mechanisms. *Journal of Alzheimer's Disease* **64**, S379–S395 (2018).

242. LeVine, S. M., Tsau, S. & Gunewardena, S. Exploring Whether Iron Sequestration within the CNS of Patients with Alzheimer's Disease Causes a Functional Iron Deficiency That Advances Neurodegeneration. *Brain Sci* **13**, 511 (2023).

243. Liu, J.-L., Fan, Y.-G., Yang, Z.-S., Wang, Z.-Y. & Guo, C. Iron and Alzheimer's Disease: From Pathogenesis to Therapeutic Implications. *Front Neurosci* **12**, 632 (2018).

244. Kim, H. *et al.* Reactive astrocytes transduce inflammation in a blood-brain barrier model through a TNF-STAT3 signaling axis and secretion of alpha 1-antichymotrypsin. *Nat Commun* **13**, 6581 (2022).

245. Stine, W. B., Jungbauer, L., Yu, C. & LaDu, M. J. Preparing synthetic Aβ in different aggregation states. *Methods Mol Biol* **670**, 13–32 (2011).

246. Stine, W. B., Dahlgren, K. N., Krafft, G. A. & LaDu, M. J. In vitro characterization of conditions for amyloid-beta peptide oligomerization and fibrillogenesis. *J Biol Chem* **278**, 11612–11622 (2003).

247. Ekaputri, S. *et al.* A small molecule redistributes iron in ferroportin-deficient mice and patient-derived primary macrophages. *Proc Natl Acad Sci U S A* **119**, e2121400119 (2022).

248. McCarthy, R. C., Park, Y.-H. & Kosman, D. J. sAPP modulates iron efflux from brain microvascular endothelial cells by stabilizing the ferrous iron exporter ferroportin. *EMBO Rep* **15**, 809–815 (2014).

249. Fleeman, R. M., Kuhn, M. K., Chan, D. C. & Proctor, E. A. Apolipoprotein E ε4 modulates astrocyte neuronal support functions in the presence of amyloid-β. *J Neurochem* (2023) doi:10.1111/jnc.15781.

250. Andersen, J. V. *et al.* Hippocampal disruptions of synaptic and astrocyte metabolism are primary events of early amyloid pathology in the 5xFAD mouse model of Alzheimer's disease. *Cell Death Dis* **12**, 954 (2021).

251. Liu, R.-X., Huang, C., Bennett, D. A., Li, H. & Wang, R. The characteristics of astrocyte on Aβ clearance altered in Alzheimer's disease were reversed by anti-inflammatory agent (+)-2-(1-hydroxyl-4-oxocyclohexyl) ethyl caffeate. *Am J Transl Res* **8**, 4082–4094 (2016).

252. Bouton, C., Oliveira, L. & Drapier, J. C. Converse modulation of IRP1 and IRP2 by immunological stimuli in murine RAW 264.7 macrophages. *J Biol Chem* **273**, 9403–9408 (1998).

253. Lee, J. *et al.* Interaction of IL-6 and TNF-α contributes to endothelial dysfunction in type 2 diabetic mouse hearts. *PLoS One* **12**, e0187189 (2017).

254. Montgomery, A. *et al.* Overlapping and distinct biological effects of IL-6 classic and trans-signaling in vascular endothelial cells. *American Journal of Physiology-Cell Physiology* **320**, C554–C565 (2021).

255. O'Carroll, S. J. *et al.* Pro-inflammatory TNFα and IL-1β differentially regulate the inflammatory phenotype of brain microvascular endothelial cells. *Journal of Neuroinflammation* **12**, 131 (2015).

256. Taipa, R. *et al.* Proinflammatory and anti-inflammatory cytokines in the CSF of patients with Alzheimer's disease and their correlation with cognitive decline. *Neurobiol Aging* **76**, 125–132 (2019).

257. Baringer, S. L., Simpson, I. A. & Connor, J. R. Brain iron acquisition: An overview of homeostatic regulation and disease dysregulation. *J Neurochem* (2023) doi:10.1111/jnc.15819.

258. Baringer, S. L., Palsa, K., Spiegelman, V. S., Simpson, I. A. & Connor, J. R. Apo- and holo-transferrin differentially interact with hephaestin and ferroportin in a novel mechanism of cellular iron release regulation. *J Biomed Sci* **30**, (2023).

259. Dang, T. N., Bishop, G. M., Dringen, R. & Robinson, S. R. The putative heme transporter HCP1 is expressed in cultured astrocytes and contributes to the uptake of hemin. *Glia* **58**, 55–65 (2010).

260. Hohnholt, M. C. & Dringen, R. Uptake and metabolism of iron and iron oxide nanoparticles in brain astrocytes. *Biochem Soc Trans* **41**, 1588–1592 (2013).

261. Ovod, V. *et al.* Amyloid β concentrations and stable isotope labeling kinetics of human plasma specific to central nervous system amyloidosis. *Alzheimers Dement* **13**, 841–849 (2017).

262. Wong, B. X. *et al.* β-Amyloid precursor protein does not possess ferroxidase activity but does stabilize the cell surface ferrous iron exporter ferroportin. *PLoS One* **9**, e114174 (2014).

263. O'Brien, R. J. & Wong, P. C. Amyloid Precursor Protein Processing and Alzheimer's Disease. *Annu Rev Neurosci* **34**, 185–204 (2011).

264. Ayton, S. *et al.* Acute phase markers in CSF reveal inflammatory changes in Alzheimer's disease that intersect with pathology, APOE ε4, sex and age. *Prog Neurobiol* **198**, 101904 (2021).

265. Lyra E Silva, N. M. *et al.* Pro-inflammatory interleukin-6 signaling links cognitive impairments and peripheral metabolic alterations in Alzheimer's disease. *Transl Psychiatry* **11**, 251 (2021).

266. Zhao, M. *et al.* The induction of the TNFalpha death domain signaling pathway in Alzheimer's disease brain. *Neurochem Res* **28**, 307–318 (2003).

267. Han, J. *et al.* Iron uptake mediated by binding of H-ferritin to the TIM-2 receptor in mouse cells. *PLoS One* **6**, e23800 (2011).

268. Kasvosve, I. & Delanghe, J. Total iron binding capacity and transferrin concentration in the assessment of iron status. *Clin Chem Lab Med* **40**, 1014–1018 (2002).

269. Kleinridders, A. *et al.* Regional differences in brain glucose metabolism determined by imaging mass spectrometry. *Mol Metab* **12**, 113–121 (2018).

270. Duck, K. A. & Connor, J. R. Iron uptake and transport across physiological barriers. *Biometals* **29**, 573–591 (2016).

271. Massey-Harroche, D. Epithelial cell polarity as reflected in enterocytes. *Microsc Res Tech* **49**, 353–362 (2000).

272. Turiel-Fernández, D., Bettmer, J. & Montes-Bayón, M. Evaluation of the uptake, storage and cell effects of nano-iron in enterocyte-like cell models. *J Trace Elem Med Biol* **49**, 98–104 (2018).

273. Vogt, A.-C. S. *et al.* On Iron Metabolism and Its Regulation. *Int J Mol Sci* **22**, 4591 (2021).

274. Zhang, Z. *et al.* Adipocyte iron levels impinge on a fat-gut crosstalk to regulate intestinal lipid absorption and mediate protection from obesity. *Cell Metab* **33**, 1624-1639.e9 (2021).

275. Lee, S.-M. *et al.* Iron repletion relocalizes hephaestin to a proximal basolateral compartment in polarized MDCK and Caco2 cells. *Biochem Biophys Res Commun* **421**, 449–455 (2012).

276. Ganz, T. Cellular iron: ferroportin is the only way out. *Cell Metab* **1**, 155–157 (2005).

277. Hudson, D. M. *et al.* Human hephaestin expression is not limited to enterocytes of the gastrointestinal tract but is also found in the antrum, the enteric nervous system, and pancreatic {beta}-cells. *Am J Physiol Gastrointest Liver Physiol* **298**, G425-432 (2010).

278. Sangkhae, V. & Nemeth, E. Regulation of the Iron Homeostatic Hormone Hepcidin. *Adv Nutr* **8**, 126–136 (2017).

279. De Domenico, I., Lo, E., Ward, D. M. & Kaplan, J. Hepcidin-induced internalization of ferroportin requires binding and cooperative interaction with Jak2. *Proc Natl Acad Sci U S A* **106**, 3800–3805 (2009).

280. Baringer, S. L. *et al.* Amyloid-β exposed astrocytes induce iron transport from endothelial cells at the blood-brain barrier by altering the ratio of apo- and holo-transferrin. 2023.05.15.540795 Preprint at https://doi.org/10.1101/2023.05.15.540795 (2023).

281. Hare, D. J. *et al.* Decreased Plasma Iron in Alzheimer's Disease Is Due to Transferrin Desaturation. *ACS Chem. Neurosci.* **6**, 398–402 (2015).

282. Sternberg, Z. *et al.* Serum Hepcidin Levels, Iron Dyshomeostasis and Cognitive Loss in Alzheimer's Disease. *Aging Dis* **8**, 215–227 (2017).

VITA

Stephanie L. Baringer

Education

2019-2023 Pennsylvania State University, Dual-title Ph.D. Candidate, Biomedical Sciences and Clinical/Translational Sciences

2014-2017 University of New Haven, B.A. Psychology

Awards

2022 Penn State Graduate Alumni Society Award

2022 Penn State Graduate Student Travel Award

2021 Translational Research Training Program TL1 Recipient

2019 Funds for Excellence in Graduate Recruitment Award

Selected Publications

Baringer SL, Lukacher AS, Palsa K, Kim H, Lippmann ES, Spiegelman VS, Simpson IA, Connor JR. Amyloid-β exposed astrocytes induce iron transport from endothelial cells at the blood-brain barrier by altering the ratio of apo- and holo-transferrin. Journal of Neurochemistry. *Under Review* 2023

Baringer SL, Palsa K, Spiegelman VS, Simpson IA, Connor JR. Apo- and holo- transferrin differentially interact with hephaestin and ferroportin in a novel mechanism of cellular iron release regulation. Journal of Biomedical Sciences. 2023 June 6. doi: 10.1186/s12929-023-00934-2

Baringer SL, Simpson IA, Connor JR. Brain iron acquisition: An overview of homeostatic regulation and disease dysregulation. Journal of Neurochemistry. 2023 Mar 31. doi: 10.1111/jnc.15819.

Baringer SL, Neely EB, Palsa K, Simpson IA, Connor JR. Regulation of brain iron uptake by apo- and holo-transferrin is dependent on sex and delivery protein. Fluids Barriers of the CNS. 2022 Jun 10;19(1):49. doi: 10.1186/s12987-022-00345-9.

Selected Presentations

Baringer SL, Neely EB, Palsa K. Simpson IA, Connor JR. Apo- and holo-Tf interact with hephaestin and ferroportin to regulate iron release at the blood-brain barrier. Poster Presentation at Brain Barrier at CSHL. Cold Spring Harbor, NY. March 28-April 1, 2023

Baringer SL, Neely EB, Palsa K, Simpson IA, Connor JR. Brain-side transferrin modulates iron uptake at the blood-brain barrier. Poster Presentation at Society for Neuroscience annual meeting. San Diego. November 10, 2022

Baringer SL, Neely EB, Palsa K. Simpson IA, Connor JR. Brain-side transferrin modulates iron uptake at the blood-brain barrier. Poster Presentation at 24th International Symposium of Signal Transduction at the Blood-Brain Barrier. Bari, Italy. September 21-23, 2022

Baringer SL, Neely EB, Palsa K, Simpson IA, Connor JR. Sex differences in the modulation of iron release via transferrin at the blood-brain barrier. Poster Presentation at Barriers of the CNS Gordan Research Seminar and Conference. New London, NH. June 11-17, 2022

Baringer SL. Establishment of hiPSC-derived Endothelial Cells to Investigate Iron Release Regulation. Oral Presentation at Institute for Translational Medicine Symposium: "Translational Science in a Pandemic World". Virtual. October 11, 2021

Baringer SL, Neely EB, Simpson IA, Connor JR. *Apo and Holo Transferrin Modulate Brain Iron Uptake In Vivo*. Poster Presentation at Blood-Brain Barrier Consortium annual meeting: "Cultivating the Next Generation of Translational Scientists", Virtual. March 11, 2021.